A Quantum Chemical Study of Grignard Reagent Formation and the Chemical Bond in C_2.

An investigation using magnetic shielding calculations and post-Hartree-Fock wave functions.

Josh John Mellor Kirsopp

Master of Science by Research

University of York

Chemistry

July, 2016

Abstract

This thesis presents a quantum chemical study of Grignard reagent formation and the effect modifying the chosen ether solvent has on Grignard reagent structure. Isotropic shielding calculations are used as one method of investigation for the first time in organometallic compounds. New interactions are discussed, including halogen bonding in transition states.

A second investigation has been performed into the nature of the chemical bond in dicarbon. Isotropic shielding calculations both along the molecular axis and in the molecular plane provide new insights into the order of the bond and the extent to which the centres are hybridised according to valence bond theory. Ionic species are discussed, with the N_2^{2+} ion displaying almost identical shielding patterns to dicarbon.

Contents

List of Tables

List of Figures

Acknowledgements

First and foremost, I would like to thank my supervisor, Dr Peter Karadakov, for his ongoing support and even more-so his patience in dealing with my questions and (often ludicrous) ideas with little direct relevance to the project. His friendly nature and extensive collection of travel tales have made my first experience of postgraduate study a real pleasure. For this, I could not be more grateful.

It would be inappropriate were I not to thank my family for their generous support over the last 24 years. My mother, father and brother in particular. 2015 was a difficult year for the Kirsopps (and Mellor), but making it to the other side without all three would have been infinitely more difficult. A very special thank you must be extended to my grandmother, without whom I would not have had a magical first five years on earth, and none of this would have been possible.

I am both incredibly grateful and fortunate to have stumbled across each member of the Karadakov group. Muntadar Al-Yassiri for the tales of his country and wonderful company, Will Drysdale for demonstrating how not to write a FORTRAN code, Make Di for saving the world, one computer code at a time, Julien Pacquier for the endless supply of coffee and agar, and Peter Hearnshaw for the interesting conversations on quantum mechanics and mathematics (and refreshing my interest in the latter).

Last but certainly not least, the sincerest of thanks to Holly Towell for being a driving force, confidante and support like no other over the last 2 years and for being the highlight of my week, every week. I wish her every success with her PhD and beyond.

Declaration

The work presented in this thesis was carried out between June, 2015 and July, 2016 in the Department of Chemistry at the University of York. To the best of my knowledge, this work is original and my own, except where reference is made to other authors, and has not been presented for any other award at this or any other institution.

1 Introduction

1.1 The Grignard Reagent

More than a century ago, Victor Grignard won a Nobel prize for his work "on some new organometallic compounds of magnesium". Since then, the Grignard reaction has become an invaluable part of the modern synthetic chemist's arsenal.[1] The flexibility of the reaction, together with its simple preparation and poorly understood mechanism has positioned it amongst the most debated topics in chemistry.

From organic chemistry, we know that providing a solution of organic halide in ether with a solid magnesium surface leads to the oxidative insertion of a magnesium atom between the halide and its adjacent carbon atom. It is also possible to generate a Grignard reagent from another Grignard reagent by deprotonating an alkyne.

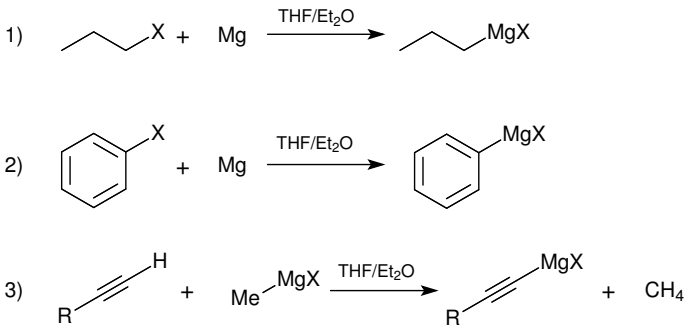

Figure 1.1: Grignard reagent formation, general reaction schemes (X=Cl, Br or I); 1) Alkyl Grignard formation, 2) Aryl Grignard formation, 3) Formation of a Grignard reagent by deprotonating an alkyne.

The product of Grignard reagent formation (GRF) is usually used to generate carbon-carbon bonds. The mechanism for this found in most organic chemistry textbooks is one in which the C-Mg bond is severed and the electrons from this bond then attack an electron deficient carbon in some other molecule. The other product being a positively charged magnesium mono-halide.

It is generally accepted that the mechanism of Grignard reagent formation (GRF) is of radical nature, thanks, in no small part to the early work of Walborsky and Garst among many others.[2,3] Walborsky's pioneering work had included data taken from optically active Grignard species. Under the assumption that complete racemization will only occur if the radicals are entirely free, Walborsky suggested that the reten-

tion of some optical character is evidence that they are not free in solution and so the reaction is taking place entirely at the magnesium surface (for any step which included the diffusion of a 3-coordinate carbon radical would result in racemization, and the radical would have to return to the surface in any case to pick up a magnesium atom).[4] Further evidence was provided by Walborsky to suggest that an observed decrease in optical purity as temperature is increased indicates a mechanism of surface nature.[5] This, when one considers the well-known behaviour of solid-liquid interfaces as temperature is altered, makes for a strong case. That is, as temperature is increased, the surface becomes more disordered and the exchange of substrates more rapid.

Garst is in favour of a diffusion based mechanism. Most of Garst's work was carried out at $>$30 °C. It had already been reported by Walborsky that at over 20 °C, the optical purity and hence the portion of the reaction occurring at the surface decreases. The work of Garst was mainly rooted in kinetic studies, in which he points out that the by products of GRF are in ratios one may expect of a free radical reaction. He also comments that the reaction pathway taken is not rigid, and for different systems one may expect entirely different routes. This is sensitive not only to solvent, but also to the R group in R-X, as is discussed shortly.[6]

While the pair differ in preference of model for GRF, both present definitive evidence of radical species at the magnesium surface. Disagreement arises in the interpretation of data suggesting that radicals may be diffusing away from the surface as GRF proceeds, both parties operate within the proposition that the radical species exist mainly as intermediates along pathway R.[6]

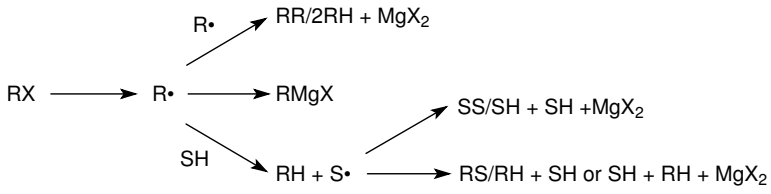

Figure 1.2: Pathway R, showing the reaction channels considered in the AAD/ADD/DDD models. Note that all reaction channels not included in these models have been omitted, including products of isomerisation, radical trapping and a variety of reduction products.

Within the above pathway, one may find a subset of possible mechanisms, where

over each reaction, the label D is given to a version which includes diffusion of the radical intermediates, and the label A is given to a version in which the radical intermediate remains adsorbed at the solid surface. A sequence of the two implies events of that order, for instance, ADA is Adsorption $\rightarrow$ Diffusion $\rightarrow$ Adsorption. Not unsurprisingly, the DDD model is favoured by Garst, and the AAD model is favoured by Walborsky.[6]

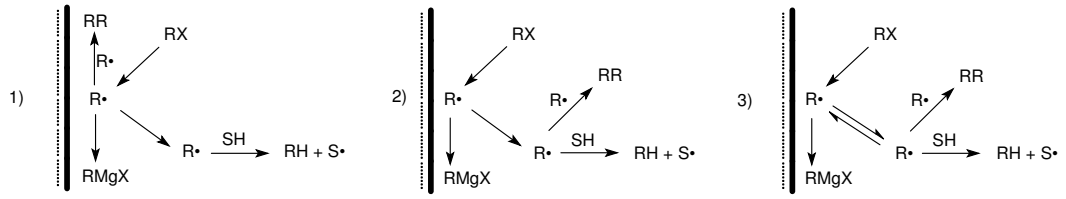

Figure 1.3: GRF Radical reaction mechanisms as reported by Garst; 1) AAD, 2) ADD, 3) DDD. A refers to adsorption and D to diffusion of the radical through the various reaction channels.

Garst comments on the viability of all of the mechanisms in figure 1.3, and in the case of the methyl radical, supports DDD and in the case of the phenyl radical admits that DDD fails.[6] This disparity in the proposed mechanisms for methyl and phenyl radicals (Garst also suggests that in the aryl case, the mechanism may not be radical at all) lends support to the argument that if one is to study GRF, one must venture beyond the simplest radical species and be ready to accept that a multitude of mechanisms may represent the real case equally well.

While this debate continued, computational facilities developed considerably. Since then, much of the work undertaken on GRF has been performed by theoretical chemists, most notably by Tulub et al.[7] To address the unreasonable demand a calculation involving a solid lattice would entail, the approximation of a Mg_4 cluster was taken, and seen to be reasonable later on, with an increasing stability of the cluster (and subsequently improved ability to catalyse the reaction by increasing the freedom of the lattice to change with reaction co-ordinate) as the cluster size was increased from Mg_4 to Mg_{10}, and significant in terms of energy but not in terms of transition state structures in the context of GRF.[8] Tulub was also able to incorporate radical reaction channels into the the cluster model.[9] Further work has been carried out in this area by Xu and co-workers, who consider an exhaustive range of transition states, but did not consider any halogen heavier than chlorine or any R group larger

than a methyl group.[10]

Despite ether solvent molecules being essential to Grignard reagent action, little computational work has been performed in this area. Tulub was able to show that the solvation of Grignard reagents is a barrierless reaction, but offered little else in his discussion. An unconsidered reaction channel thus far has been the known interaction between a Lewis base (ether solvent) and Lewis acid (halogen atom in a methyl halide) in the context of GRF.

1.2 The Nature of the Chemical bond in C_2

Among lanthanides, actinides and heavy transition metals, where the number of orbitals available and size of the orbitals is much greater than in the main group of the periodic table, bond order has recently been shown to reach as high as 5 or 6.[11–13] For the lighter elements of the main group, formal bond order has long been limited to 3.[14] The orbitals from which triple bonds form in the main group is straight forward, and involves a single σ bond, and two π bonds. There is an ongoing debate in chemistry about the nature of the bonding in a selection of homonuclear diatomics from the main group of the periodic table. Most notably concerning the nature of the chemical bond in C_2 and whether or not it is possible to describe it as a quadruple bond, or equivalently, as a bond of order 4.[15–21]

In the valence bond description, there are three bonds as described previously. There are two electrons in outward-facing lobes which, in the ground state, are singlet paired but do not form another bond. And so it has been said that, under this approximation, the interaction of these two should not be labelled as a new type of bond, given that this description has been known since the early 1970s.[22] Additionally, the C-C quadruple bond has been dismissed as being the product of naïvety, and a lesson in the way computational chemistry may breathe life into ideas which do not survive thorough scrutiny.[19] The arguments for the existence of the main group quadruple bond are equally compelling. The debate currently seems to have no conclusion in sight.

Despite the excellent work being done in this area, there has yet to be a study which allows one to visually examine the electronic environment between and around the nuclei. It is in this way that a study based on the calculations of isotropic shielding contour plots and curves in and along the molecular plane and axis, respectively, offers new insight. Isotropic shielding calculations are discussed in greater detail in the next section.

1.3 Investigating Chemical Bonds Using Magnetic Shielding Calculations

In experimental chemistry, when one measures magnetic shielding, the values reported are measurements taken at the very centre of the nucleus of each atom. Furthermore, experimental chemical shifts are measured relatively. That is, a reference nucleus R is used and the chemical shift of nucleus J is taken as being the difference between the isotropic shielding experienced by R and J (isotropic shielding σ_{iso} is one third of the trace of the shielding magnetic tensor, which is a $3\times$ 3 matrix). It is known from general NMR theory that any nucleus J in a molecule which finds itself in a magnetic field $\mathbf{B}_0$ experiences a modified magnetic field $\mathbf{B}_J$, which is usually not identical to $\mathbf{B}_0$. For a molecule in a solvent, this is as a result of solvent-substrate interactions and the immediate electronic environment. For an isolated, gaseous molecule this is as a result of the amount of shielding provided to nucleus J by the other electrons in the molecule. The modified magnetic field is given by

$$\mathbf{B}_J = (\mathbf{1} - \sigma_J)\,\mathbf{B}_0 \tag{1.1}$$

where σ_J is the magnetic shielding tensor of nucleus J. Of course, the positions of each atom in a molecule must be different, and so the electronic environment each nucleus experiences is different (ignoring the obvious caveat of isolated molecules of high symmetry having numerous nuclei experiencing exactly the same electronic environment), and so they exhibit different chemical shifts.

There is no requirement or restriction in the definition of magnetic shielding which states that is only possible for nuclei to experience it. In fact, any point in space where there happens to be electron density will be shielded, and experience the magnetic field $\mathbf{B}(\vec{x})$ rather than $\mathbf{B}_0$. Unfortunately, in experimental chemistry it is not possible to measure shielding at any point other than at the centre of nuclei and so any information to be gleaned from off-nucleus shielding is unavailable. It is, however, possible to calculate magnetic shieldings using modern quantum chemical codes by placing "ghost atoms", which are essentially atoms with no basis functions, charge or mass, at the point of interest and calculating the shieldings normally.

The earliest off-nucleus shieldings were reported by Johnson and Bovey who, based on Pauling's free electron model, began calculating ring current effects and eventually reported proton shieldings at various points around a benzene ring.[23] This provided the basis for the work of Schleyer and co-workers who employed the method as a probe for testing levels of aromaticity, which has become a rather popular method.[24–26]

Wolinski provided the next major development in off-nucleus shielding calculations by examining the changes in the shielding tensor described in equation 1.1 along the molecular axis in a number of molecules.[27] He was able to state that variations in isotropic shielding were correlated with those seen in electron density.

Kleinpeter *et al* were the first to propose grids of probes in the molecular plane of benzene and use those grids to provide insight into anti-aromaticity and aromaticity and substituent effects.[28–30] Kleinpeter's early work involved nodes spaced at 0.5 Å, which when one considers the typical length of a chemical bond being 1-3 Å, is rather a large interval, and as a consequence, the finer details of the surface generated will likely be missing.

The more recent work of Karadakov and Horner features more finely spaced grids of ghost atoms (0.05 Å), and has revealed the more subtle features of these types of surfaces and provides extremely clear visual representations of aromaticity and anti-aromaticity.[31] This has been extended to include heterocycles and provide insight into the effect of aromaticity on bond strength.[32,33] This approach was also taken in a studies of a number of other carbon compounds, including some longer conjugated systems, as well as ethane, ethene and ethyne.[34] Their success in doing so is to such an extent that shielding patterns around the nucleus are used to distinguish between the extent of s and p orbital hybridisation at different carbon centres, and the shielding along and around chemical bonds gives a clear indication of relative bond strengths and orders.

In this thesis, attempts are made to extend this method of investigation to a number of organometallic compounds involved in GRF. An additional study has also been performed on the bonding in dicarbon using these techniques and promises to give a unique perspective on the much-debated quadruple bond.

2 Elements of Theory

This section provides the theoretical backdrop of the methods used throughout quantum chemistry. It is not a thorough discussion, but is enough to give a brief overview of how investigations like the ones in this thesis are performed computationally, and how the ideas were first formulated. A more in-depth view of quantum chemistry can be gained from a variety of books included in the bibliography.[35–37]

We begin with a brief discussion the Schrödinger equation before moving on to exclusion and antisymmetric wave functions. A summary of Hartree-Fock (HF) theory is included, along with a summary of basis sets and how they are constructed and a stepwise self consistent field procedure. A variety of extensions to the HF method are also discussed, including Møller-Plesset perturbation (MP) theory, configuration interaction, complete active space wave functions and, though not an extension of HF, density functional theory (DFT).

2.1 The Schrödinger Equation

The problem we wish to solve is non-specific. The technique must be applicable to all chemical systems, or indeed, all systems containing quantum particles. The many-electron system is one consisting of N electrons moving in an electrostatic field. Say we have an electron, x, at $\vec{x}$ then the potential energy of x while in the electrostatic field is $V(\vec{x})$. Now the first approximation is made, which is the omission of magnetic interactions and to focus on electron-electron interactions and the effect of the external field, with the external field being generated by the nuclei. Were the electrons not to interact at all, the Hamiltonian operator for the system would be

$$\hat{H}_0 = \sum_{i=1}^{N} \left[-\frac{\hbar^2}{2m} \nabla_i^2 + V(\vec{x}_i) \right] \tag{2.1}$$

but clearly, the electrons do interact. And so a correction term is appended to equation 2.1 which takes this into account. We shall denote this correction as $\hat{H}'$, and state that it is the potential energy due to the Coulombic interactions of the electrons.

$$\hat{H}' = \frac{1}{2} \sum_{i \neq j}^{N} \sum_{i \neq j}^{N} \frac{e^2}{4\pi\epsilon_0 |\vec{x}_i - \vec{x}_j|} \tag{2.2}$$

If we make the transition to atomic units and re-write the Hamiltonian operator taking into account, explicitly, all interactions present in a molecule we get

$$\hat{H} = -\sum_{i=1}^{N} \frac{1}{2} \nabla_i^2 - \sum_{I=1}^{M} \frac{1}{2M_I} \nabla_I^2 - \sum_{i=1}^{N} \sum_{I=1}^{M} \frac{Z_I}{r_{iI}} + \sum_{i=1}^{N} \sum_{j>i}^{N} \frac{1}{r_{ij}} + \sum_{I=1}^{M} \sum_{J>I}^{M} \frac{Z_I Z_J}{R_{IJ}} \tag{2.3}$$

where from left to right, the terms are the kinetic energy of the electrons, kinetic energy of the nuclei, nucleus-electron attraction, electron-electron repulsion and nucleus-nucleus repulsion. ∇^2 is the Laplacian operator, M is the number of nuclei, I and J are labels for nuclei, i and j are labels for electrons, Z_I is the nuclear charge of nucleus I, r_{ij} is the distance between electron i and electron j and finally, R_{IJ} is the distance between nuclei I and J.

The famous form of the Schrödinger equation and the way it is most commonly written is in the general form of an eigenvalue-eigenfunction equation,

$$\hat{H}\Psi = E\Psi \tag{2.4}$$

which is to say that when the operator acts upon the eigenfunction, in this case a many-particle wave function, the product of the operation is a constant, the eigenvalue, multiplied by the same eigenfunction, which in this case is the energy for our system in its current state. An illustrative example of an eigenvalue-eigenfunction equation is to set the operator as the differential operator d/dx and the wave function as e^x, then

$$\frac{d}{dx}e^x = 1 \times e^x \tag{2.5}$$

where the eigenvalue in the equation is 1. It is impossible to solve equation 2.4 for all systems other than those which are extremely small, and not of much use to a chemist. So, further approximations are made. The mass of an electron in comparison even to the mass of a single proton, is tiny. As a result of this difference in mass between atomic nuclei and electrons, the nuclei may be considered as fixed - their motion is negligibly slow. The system is now reduced to a set of electrons moving in a field of fixed nuclei. So we may remove the terms in equation 2.3 which are concerned with nuclear motion to produce the electronic Hamiltonian,

$$\hat{H}_{elec} = -\sum_{i=1}^{N}\frac{1}{2}\nabla_i^2 - \sum_{i=1}^{N}\sum_{I=1}^{M}\frac{Z_I}{r_{iI}} + \sum_{i=1}^{N}\sum_{j>i}^{N}\frac{1}{r_{ij}} \tag{2.6}$$

from which the subscript is dropped as it assumes the mantle of $\hat{H}$ in equation 2.4. This is the Born-Oppenheimer approximation. Now we have specified the operator we will be concerned with and briefly seen the relationship between eigenfunctions and eigenvalues, all that remains to be seen is a way to construct the wave function, Ψ.

2.2 Pauli Exclusion and Antisymmetric wave functions

So far, we have neglected an important part of quantum mechanics - spin. Spin up and spin down functions, α and β are the mathematical way of including spin in our formulation of the many-electron problem. Together with these functions we define a spin co-ordinate, ω, which is arbitrary and takes a value depending on which spin function it is paired with. Before including the spin functions and coordinates in the model, we insist that they are complete and orthonormal.

$$\begin{aligned} \int d\omega\ \alpha(\omega)^*\alpha(\omega) &= \int d\omega\ \beta(\omega)^*\beta(\omega) = 1 \\ \int d\omega\ \alpha(\omega)^*\beta(\omega) &= \int d\omega\ \beta(\omega)^*\alpha(\omega) = 0 \end{aligned} \tag{2.7}$$

which may be re-written in bra-ket notation as

$$\begin{aligned} \langle\alpha|\alpha\rangle &= \langle\beta|\beta\rangle = 1 \\ \langle\alpha|\beta\rangle &= \langle\beta|\alpha\rangle = 0 \end{aligned} \tag{2.8}$$

which will be the standard notation hereafter.

The wave function of a system of particles must be either symmetric or anti-symmetric in the coordinates of the particles. Particles whose wave functions are symmetric are called bosons. Photons, for instance, are bosons and so are described in a system of N photons by a symmetric wave function. Electrons, on the other hand are fermions and so a system of N electrons must be described by an antisymmetric wave function. An antisymmetric wave function is one which, upon the interchange electronic co-ordinates changes its sign.

$$\Psi(\vec{x}_1, \vec{x}_2, ..., \vec{x}_5, ..., \vec{x}_N) = -\Psi(\vec{x}_1, \vec{x}_5, ..., \vec{x}_2, ..., \vec{x}_N) \tag{2.9}$$

Equation 2.9 is an example of an antisymmetric wave function, but as we have already seen, we must take spin into account, and so we define spin orbitals as being the product of a spatial orbital, one which is formed using electronic coordinates, and

a spin function α or β. We set the spin orbital, $\chi(x)$, equal to $\psi(\vec{x})\alpha(\omega)$ or $\psi(\vec{x})\beta(\omega)$. Note that the orthonormality of the spin functions is imposed on the spin orbitals. Hereafter, the arrow atop x in the equations is dropped as we say x is the set of coordinates $x = \{r, \omega\}$ not limited to position but also including the spin coordinate,

$$\langle \chi(x_i) | \chi(x_j) \rangle = \delta_{ij} \tag{2.10}$$

where δ_{ij} is the Kronecker delta symbol where if $i = j$, $\delta_{ij} = 1$ and if $i \neq j$, $\delta_{ij} = 0$.

Were it not for the antisymmetry requirement, we could construct a wave function in the form of a Hartree product, which is simply the product of the spin orbitals and would yield an energy equivalent to the sum of the energies of the spin orbitals. Unfortunately, this wave function is not antisymmetric and so it cannot be used.

The solution to the problem comes in the form of determinantal wave functions. To illustrate, let us write the Hartree product for a two electron system,

$$\Psi_{12}^{\text{HP}}(x_1, x_2) = \chi_1(x_1)\chi_2(x_2) \tag{2.11}$$

and by interchanging their co-ordinates,

$$\Psi_{21}^{\text{HP}}(x_2, x_1) = \chi_1(x_2)\chi_2(x_1) \tag{2.12}$$

we see no change in sign. If we subtract these two functions from one another and normalise we get

$$\Psi(x_1, x_2) = \frac{1}{\sqrt{2}} \left[\chi_1(x_1)\chi_2(x_2) - \chi_1(x_2)\chi_2(x_1) \right] \tag{2.13}$$

which may be written as a Slater determinant.

$$\Psi(x_1, x_2) = \frac{1}{\sqrt{2}} \begin{vmatrix} \chi_1(x_1) & \chi_2(x_1) \\ \chi_1(x_2) & \chi_2(x_2) \end{vmatrix} \tag{2.14}$$

In this way, we have a wave function which does not distinguish between electrons, and in fact, considers all electrons in all orbitals for any size of system. We also see by inspection that setting the $x_1 = x_2$ causes the wave function to vanish, which is the mathematical way of saying "two electrons with the same spin cannot occupy the same spatial orbital", or more formally, "two electrons cannot have identical sets of quantum numbers". Generalising the result in equation 2.14 for an N electron system involves writing an $N \times N$ determinant and varying x_i by row number, χ_i by column number and the normalisation term being set to $\left(\sqrt{N!}\right)^{-1}$.

2.3 The Variation Principle

Given that the Schrödinger equation is an eigenvalue-eigenfunction equation, we are able to manipulate it to express E_0 as a functional of the set of spin orbitals we generated according to section 2.2, $\{\chi(x_i)\}$ for a single determinant. Let us write the Schrödinger equation in bra-ket notation to make this procedure clear.

$$\begin{aligned} \hat{H}\left|\Psi_0\right\rangle &= E_0\left|\Psi_0\right\rangle \\ \text{multiplying on the left by } \left\langle\Psi_0\right|\text{...} \quad \left\langle\Psi_0\right|\hat{H}\left|\Psi_0\right\rangle &= E_0\left\langle\Psi_0|\Psi_0\right\rangle \\ \text{we know } \left\langle\Psi_0|\Psi_0\right\rangle = 1\text{, so} \quad E_0 &= \left\langle\Psi_0\right|\hat{H}\left|\Psi_0\right\rangle \end{aligned} \tag{2.15}$$

Where the denominator is not equal to one by the orthonormality of the spin functions, we are tasked with minimising the energy with respect to the spin orbitals. The exact energy is given by

$$E_{\text{Exact}} = \frac{\left\langle\Psi_{\text{Exact}}\right|\hat{H}\left|\Psi_{\text{Exact}}\right\rangle}{\left\langle\Psi_{\text{Exact}}|\Psi_{\text{Exact}}\right\rangle} \tag{2.16}$$

So, if we had a trial wave function, we could calculate an approximate energy, $E[\Psi]$. According to the variation principle, $E[\Psi] \geq E_{\text{Exact}}$. One method of building a trial wave function is to construct a function which intrinsically obeys Pauli exclusion, by insisting the spin functions be antisymmetric and the spatial parts be symmetric. The most commonly practised method of wave function ansatz is to linearly combine a number of basis functions.

$$\begin{aligned} \Psi &= \sum_a C_a\Psi_a \quad \text{where} \quad \Psi_a = |\Psi_{a1}\Psi_{a2}\cdots\Psi_{aN}| \\ \text{then} \quad E[\Psi] &= \frac{\left\langle\sum_a C_a\Psi_a\right|\hat{H}\left|\sum_b C_b\Psi_b\right\rangle}{\left\langle\sum_a C_a\Psi_a\right|\sum_b C_b\Psi_b\right\rangle} = \frac{\sum_a\sum_b C_aC_b\left\langle\Psi_a\right|\hat{H}\left|\Psi_b\right\rangle}{\sum_a\sum_b C_aC_b\left\langle\Psi_a\,|\,\Psi_b\right\rangle} \end{aligned} \tag{2.17}$$

We cannot make much progress from here without a method by which to evaluate Hamiltonian matrix elements. We are operating under the criterion that the Slater

determinants are orthonormal. This is not absolutely necessary, but makes things much simpler.

Slater-Condon Rules

By evaluating Hamiltonian operators between Slater determinants and considering the definitions of the Coulomb and exchange integrals we arrive at the Slater-Condon rules. If we consider three different Slater determinants,

$$\begin{aligned} \Psi &= |\psi_1\psi_2...\psi_i...\psi_j...\psi_N| \\ \Psi_i^p &= |\psi_1\psi_2...\psi_p...\psi_j...\psi_N| \\ \Psi_{ij}^{pq} &= |\psi_1\psi_2...\psi_p...\psi_q...\psi_N| \\ \text{for which} \quad \{\psi(x)|i &= 1,2,...,N,N+1,...\}, \quad \langle\psi_i \,|\, \psi_j\rangle = \delta_{ij} \end{aligned} \tag{2.18}$$

where each differs from the last by a single orbital, stopping at two substitutions (Hamiltonian matrix elements between Slater determinants differing by three or more orbitals are zero and so are not worth considering), we are able to construct rather a large set of determinants from which to construct a trial wave function.

Now we define three operators which are convenient for the evaluation of Hamiltonian matrix elements.

$$\langle\Psi|\,\hat{H}\,|\Psi\rangle = \sum_{i=1}^{N}\langle\psi_i|\,\hat{h}\,|\psi_i\rangle + \frac{1}{2}\sum_{i=1}^{N}\sum_{j=1}^{N}\left(\langle\psi_i\psi_j|\,\frac{1}{r_{ij}}\,|\psi_i\psi_j\rangle - \langle\psi_i\psi_j|\,\frac{1}{r_{ij}}\,|\psi_j\psi_i\rangle\right) \tag{2.19}$$

where

$$\begin{aligned} \langle\psi_i|\,\hat{h}\,|\psi_j\rangle &= \int \chi_i^*(x)\hat{h}\chi_i(x) \quad dx \\ &= h_i \end{aligned} \tag{2.20}$$

and

$$\langle \psi_i \psi_j | \frac{1}{r_{ij}} | \psi_i \psi_j \rangle = \iint \chi_i^*(x_1)\chi_j^*(x_2)\frac{1}{r_{12}}\chi_i(x_1)\chi_j(x_2) \quad dx_1 dx_2 \\ = J_{ij} \quad \text{(The Coulomb Integral)} \tag{2.21}$$

and

$$\langle \psi_i \psi_j | \frac{1}{r_{ij}} | \psi_j \psi_i \rangle = \iint \chi_i^*(x_1)\chi_j^*(x_2)\frac{1}{r_{12}}\chi_j(x_1)\chi_i(x_2) \quad dx_1 dx_2 \\ = K_{ij} \quad \text{(The Exchange Integral)} \tag{2.22}$$

From these integrals the Coulomb and Exchange operators are defined.

$$\hat{J}_j(x_1)\chi_i(x_1) = \left[\int \chi_j^*(x_2)\chi_j(x_2)\frac{1}{r_{12}} \quad dx_2 \right] \chi_i(x_1) \\ \text{(The Coulomb Operator)} \tag{2.23}$$

and

$$\hat{K}_j(x_1)\chi_i(x_1) = \left[\int \chi_j^*((x_2)\chi_i(x_2)\frac{1}{r_{12}} \quad dx_2 \right] \chi_j(x_1) \\ \text{(The Exchange Operator)} \tag{2.24}$$

The classical equivalent of the Coulomb operator is the repulsion experienced by electron i in orbital χ_i due to the $N-1$ electrons in the surrounding $N-1$ occupied orbitals. The exchange integral has no classical interpretation and is unique to quantum mechanics - it is a physical manifestation of the antisymmetry requirement.

2.4 Hartree-Fock Theory

The preceding sections have encroached on this section's territory for the treatment of HF theory. The groundwork has been laid for a succinct treatment of the main points of HF theory, but ideas from previous sections will be drawn on repeatedly and may make this section feel more disjointed than those which came before.

We are at a stage where we have constructed a trial wave function which takes the form of a Slater determinant. The energy expectation value, so long as we operate under the assumption that the occupied orbitals are orthonormal, is given by

$$\frac{\langle\psi|\,\hat{H}\,|\psi\rangle}{\langle\psi\,|\,\psi\rangle} = \sum_{i=1}^{N} h_i + \sum_{i=1}^{N}\sum_{j>i}^{N} (J_{ij} - K_{ij}) \tag{2.25}$$

From the minimisation of this expression comes the eigenvalue-eigenfunction equation

$$\left[\hat{h}(x_1) + \sum_{j\neq i} \hat{J}_i(x_1) - \sum_{j\neq i} \hat{K}_i(x_1)\right] \chi_i(x_1) = \epsilon_i \chi_i(x_1) \tag{2.26}$$

Note that from the orthonormality of the spin orbitals we are able to remove the restriction over the sum in equation 2.25 and present the Fock operator and the Fock equation.

$$\hat{f}(x_1) = \hat{h}(x_1) + \sum_{i=1}^{N/2} \hat{J}_i(x_1) - \hat{K}_i(x_1) \tag{2.27}$$

and

$$\hat{f}\,|\chi_i\rangle = \epsilon_i\,|\chi_i\rangle \tag{2.28}$$

The solutions to the Fock equation are the orbital energies corresponding to each spin orbital, which are the equation's eigenfunctions. Much like the Schrödinger

equation, the exact solutions to this are elusive and only attainable for atoms. For larger systems, basis sets are used and a number of matrix equations are generated which need to be solved. The Fock equation has a functional dependence on the set of orbitals and so solving it requires an iterative procedure.

The Hartree-Fock Roothaan Equations

Now we are aware of which problem we wish to solve. Roothaan suggested the introduction a set of known basis functions which would reduce the problem to a number of algebraic equations soluble with matrix methods. The basis functions take the form

$$\psi_i = \sum_{p=1}^{K} c_{pi}\phi_p \tag{2.29}$$

c_{pi} is the expansion coefficient for basis function ϕ_p in the construction of orbital ψ_i. Clearly one may never use, in practise, an infinite basis set as would be needed were this method to provide an exact wave function, or as would be the case in HF theory, the wave function which corresponds to the energy at the HF limit (which will be discussed later on). We may re-write the Fock equation as

$$\hat{f}(x_1)\sum_{p=1}^{K} c_{pi}\phi_p(x_1) = \epsilon_i \sum_{p=1}^{K} c_{pi}\phi_p(x_1) \tag{2.30}$$

from which, we obtain

$$\sum_{p=1}^{K} c_{pi}\left\langle \phi_q(x_1)\right| \hat{f}\left|\phi_p(x_1)\right\rangle = \epsilon_i \sum_{p=1}^{K} c_{pi}\left\langle \phi_q(x_1)\,\middle|\,\phi_p(x_1)\right\rangle \tag{2.31}$$

and thus define the overlap and Fock Hermitian matrices, $\mathbb{S}$ and $\mathbb{F}$, respectively, as containing the elements

$$\begin{aligned} S_{qp} &= \langle \phi_q(x_1) \,|\, \phi_p(x_1) \rangle \\ \text{and} \quad F_{qp} &= \langle \phi_q(x_1) | \, \hat{f} \, | \phi_p(x_1) \rangle \end{aligned} \tag{2.32}$$

Having defined these, we are able to write the Hartree-Fock Roothaan equation which provides us with yet another unsolvable problem

$$\mathbb{FC} = \mathbb{SC}\epsilon \tag{2.33}$$

The density matrix, $\mathbb{D}$, is included as, without it, the coefficients of expansion disappear if we note the form of the elements in the Fock matrix. The elements of $\mathbb{D}$ are given by

$$D_{rs} = 2 \sum_{j=1}^{n} c_{rj}^{*} c_{sj} \tag{2.34}$$

recalling the original form of the energy expression in equation 2.25 and the multiple operators we have defined since, it is possible to re-write it as

$$E = \frac{1}{2} \sum_{pq} D_{pq} \left(h_{pq} + F_{pq} \right) \tag{2.35}$$

2.5 Self-Consistent Field Method

For any HF procedure, there are a number of steps to follow which are to be outlined in this section. The logic behind SCF is simply to guess at a wave function, calculate the charge density, calculate the potential energy and solve the Schrödinger equation, calculate the charge density for a second time and check it against the first value we calculated. If the charge density is the same (or more realistically, within some predefined parameter) as the original charge density then the procedure is finished, if not, go back and modify the wave function and try again. Rinse and repeat.

The procedure is, of course more complex than that, and is outlined roughly here but it is worth mentioning that some quantities not defined before now are mentioned and will be briefly explained ad-hoc.

1. We choose a set of nuclear coordinates $\{\mathbf{R}_A\}$, a number of electrons N and the atomic numbers of the various atoms $\{Z_A\}$ in the molecule. We also choose a basis set $\{\phi_i\}$.

2. Now we calculate all required integrals, those of the overlap matrix, S_{ij}, the single electron integrals h_{ij} and the two electron integrals $\langle ij \,|\, kl \rangle$

3. Diagonalise $\mathbb{S}$ and calculate $\mathbb{X}$ (the transformation matrix) by taking the inverse square root of $\mathbb{S}$.

4. Take a guess at the density matrix $\mathbb{D}$, or equivalently, the matrix containing the expansion coefficients from the previous section.

5. Calculate the full two electron contribution, and add this to the one electron contribution to obtain the Fock matrix.

6. Transform the Fock matrix using $\mathbb{X}$ (i.e $\mathbb{F}' = \mathbb{X}^\dagger \mathbb{F} \mathbb{X}$)

7. Diagonalise $\mathbb{F}'$ and use this to form a new density matrix, $\mathbb{D}$.

8. Check for convergence by comparing the new and initial density matrices. If they are the same, use the matrices to calculate any quantities of interest, if they are not, return to step 5 with the new density matrix and try again.

To obtain the energy front he procedure above is to calculate the electronic energy of a set of N electrons moving in a field of point charges, as per the Born-Oppenheimer

approximation, and finally append the nuclear energy. The HF limit was mentioned in passing, and now seems like the appropriate time to elaborate on its real meaning. To calculate the energy of a system using the HF procedure is to use a single determinantal wave function. Within HF theory, the motion of electrons with opposite spins is uncorrelated, this is obviously a problem. Were we to have available to us, a complete and infinite basis set, the energy we calculate would still be incorrect and is labelled the "HF limit". The difference between the HF limit and the exact solution to the Schrödinger equation is called the correlation energy.

$$E_{corr} = E_{\text{Exact}} - E_{HF} \tag{2.36}$$

There have been a number of advances which seek to take this energy into account. The basic deficiency of the basis set remains, but by extending the wave function to including multiple Slater determinants, a better solution is made available. Alternatively, it is possible to modify the Hamiltonian to include a correctional term.

2.6 Many-Body Perturbation Theory (MBPT)

Møller-Plesset Perturbation (MP) theory is an extension of many body perturbation theory. The general idea is to divide the Hamiltonian into two parts in such a manner such that the first part is soluble exactly and the second is the perturbation which is assumed to be small in comparison to the first term, and improves the calculated energy. Here is the general formulation of MBPT, which is used very frequently throughout quantum chemistry.

$$\hat{H} = \hat{H}_0 + \lambda \hat{V} \tag{2.37}$$

It is implied by the assumption that $\hat{V}$ is small, that the perturbed wave function and energy may be written as a power series in $\hat{V}$ using the as-yet undefined parameter λ.

$$\begin{aligned} \Psi &= \psi^{(0)} + \lambda\psi^{(1)} + \lambda^2\psi^{(2)} + ... \\ E &= E^{(0)} + \lambda E^{(1)} + \lambda^2 E^{(2)} + ... \end{aligned} \tag{2.38}$$

Substituting this into the Schrödinger equation yields

$$\left(\hat{H}_0 + \lambda\hat{V}\right)\left(\psi^{(0)} + \lambda\psi^{(1)} + ...\right) = \left(E^{(0)} + \lambda E^{(1)} + ...\right)\left(\psi^{(0)} + \lambda\psi^{(1)} + ...\right) \tag{2.39}$$

which, when the products have been expanded out, allows us to set coefficients on each side equal to one another for all λ^x. So for every order of perturbation we generate an equation, the first three are presented here.

$$\begin{aligned} \left(\hat{H}_0 - E^{(0)}\right)\psi^{(0)} &= 0 \\ \left(\hat{H}_0 - E^{(0)}\right)\psi^{(1)} &= \left(E^{(1)} - \hat{V}\right)\psi^{(0)} \\ \left(\hat{H}_0 - E^{(0)}\right)\psi^{(2)} &= \left(E^{(1)} - \hat{V}\right)\psi^{(1)} + E^{(2)}\psi^{(0)} \end{aligned} \tag{2.40}$$

In MP theory, $\hat{H}_0$ is the sum of one electron Fock operators. Let us now consider the case where this is so. We set

$$\hat{H}_0 = \sum_i \hat{F}(x_i) \tag{2.41}$$

So, The first line of equation 2.40 multiplied by $\langle\psi^{(0)}|$ gives us

$$\begin{aligned} \langle\psi^{(0)}| \hat{H}_0 - E^{(0)} |\psi^{(0)}\rangle &= 0 \\ \langle\psi^{(0)}| \hat{H}_0 |\psi^{(0)}\rangle = E^{(0)} \langle\psi^{(0)} | \psi^{(0)}\rangle &= E^{(0)} \end{aligned} \tag{2.42}$$

So, the first energy term in equation 2.38 is simply the sum of the orbital energies

$$E^{(0)} = \sum_i \epsilon_i \tag{2.43}$$

Moving swiftly along to the second line of equation 2.40 and taking the same inner product as we did in deriving the expression for $E^{(0)}$...

$$\begin{aligned} \langle\psi^{(0)}| \hat{H}_0 - E^{(0)} |\psi^{(1)}\rangle &= \langle\psi^{(0)}| \left(E^{(1)} - \hat{V}\right) |\psi^{(0)}\rangle \\ \langle\psi^{(0)}| \hat{H}_0 |\psi^{(1)}\rangle - E^{(0)} \langle\psi^{(0)} | \psi^{(1)}\rangle &= E^{(1)} \langle\psi^{(0)} | \psi^{(0)}\rangle - \langle\psi^{(0)}| \hat{V} |\psi^{(0)}\rangle \end{aligned} \tag{2.44}$$

By the Hermitian nature of $\hat{H}_0$ it is possible to interchange the position of the operator and the ket in the first term of the second line in equation 2.44 and obtain the expression for the second energy term, $E^{(1)}$.

$$E^{(1)} = \langle\psi^{(0)}| \hat{V} |\psi^{(0)}\rangle \quad \left[= E_{HF} - E^{(0)}\right] \tag{2.45}$$

So far, we've calculated the same energy as HF theory produces as we've only reconstructed the full Hamiltonian from the fragments to which we broke it down. For

the third and final correction covered here, we take the same approach as for the previous two

$$\begin{aligned}\left\langle \Psi^{(0)} \right| \left(\hat{H}_0 - E^{(0)} \right) \left| \psi^{(2)} \right\rangle = \left\langle \Psi^{(0)} \right| \left(E^{(1)} - \hat{V} \right) \left| \psi^{(1)} \right\rangle + E^{(2)} \left\langle \psi^{(0)} \,\middle|\, \psi^{(0)} \right\rangle \\ E^{(2)} = \left\langle \psi^{(0)} \right| \left(\hat{V} - E \right) \left| \psi^{(1)} \right\rangle = \left\langle \psi^{(0)} \right| \hat{V} \left| \psi^{(1)} \right\rangle\end{aligned} \tag{2.46}$$

but it his case, the energy term is dependent on $\psi^{(1)}$, which we do not have. So, we form it from a linear combination of substituted wave functions (or, equivalently, excited determinants) and then solve for the coefficients of those wave functions. First we take the inner product of the general expression with a random wave function ψ_r, solve for the coefficient of expansion c_r by invoking the orthonormality relation once more.

$$\begin{aligned}\sum_{sub} c_{sub} \left\langle \Psi_r \right| \left(\hat{H}_0 - E^{(0)} \right) \left| \psi_{sub} \right\rangle = E^{(1)} \left\langle \psi_r \,\middle|\, \psi^{(0)} \right\rangle - \left\langle \psi_r \right| \hat{V} \left| \psi^{(0)} \right\rangle \\ \sum_{sub} c_{sub} \left(\left\langle \Psi_r \right| \hat{H}_0 \left| \psi_{sub} \right\rangle - \left\langle \psi_r \right| E^{(0)} \left| \psi_{sub} \right\rangle \right) = E^{(1)} \left\langle \psi_r \,\middle|\, \psi^{(0)} \right\rangle - \left\langle \psi_r \right| \hat{V} \left| \psi^{(0)} \right\rangle\end{aligned} \tag{2.47}$$

From the orthonormality of the functions used, we are able to obtain

$$c_r = \frac{\left\langle \psi_r \right| \hat{V} \left| \psi^{(0)} \right\rangle}{E^{(0)} - E_r} \tag{2.48}$$

$$\text{and} \quad \psi^{(1)} = \sum_r \left(\frac{\left\langle \psi_r \right| \hat{V} \left| \psi^{(0)} \right\rangle}{E^{(0)} - E_r} \right) \psi_r \tag{2.49}$$

from which we are able to deduce that the closer the substituted wave function is to the ground state wave function, the greater the contribution it makes to the perturbation. Thus the expression for $E^{(2)}$ is given by

$$E^{(2)} = \sum_r \frac{\left\langle \psi^{(0)} \right| \hat{V} \left| \psi_r \right\rangle \left\langle \psi_r \right| \hat{V} \left| \psi^{(0)} \right\rangle}{E^{(0)} - E_r} \tag{2.50}$$

Note that by Brillouin's Theorem of non-interacting singly substituted wave functions, the numerator of the above expression is only non-zero for doubly excited determinants. Triply excited determinants yield a numerator of zero as has been discussed previously. Note that this is a way of actively correcting for the correlation energy mentioned at the close of the previous section. Excited determinants are used as a perturbed wave function with the correctional operator as a means of closing the gap to some extent.

Further correctional terms may be calculated, but the procedure involved is much more complicated and for that reason is not presented in this thesis.

2.7 Density Functional Theory (DFT)

A functional is, in plain terms, a function of a function. Modern DFT is based on the Hohenberg-Kohn theorem which states that there exists a unique functional which determines the ground state energy and electronic density exactly. Electronic density is given by

$$\begin{aligned} N &= \int \rho(r) \quad dr \\ \text{where} \quad \rho(r_1) &= \int \cdots \int |\Psi(x_1, x_2, ..., x_N)|^2 \, d\omega_1 dx_2 ... dx_N. \end{aligned} \tag{2.51}$$

The wave function is represented as single Slater determinant in DFT. The total energy expression is

$$\begin{aligned} E_{DFT}[\rho] &= T_s[\rho] + E_{en}[\rho] + J[\rho] + E_{XC}[\rho] \\ \text{where} \quad T_s[\rho] &= \sum_{i=1}^{N} \langle \psi_i | -\frac{1}{2}\nabla^2 | \psi_i \rangle \\ \text{and} \quad E_{en}[\rho] &= -\sum_{I=1}^{M} \int \frac{Z_I \rho(r)}{|R_I - r|} \quad dr \\ \text{and} \quad J[\rho] &= \frac{1}{2} \iint \frac{\rho(r_1)\rho(r_2)}{|r_1 - r_2|} \quad dr_1 dr_2 \\ \text{and} \quad E_{XC}[\rho] &= (T[\rho] - T_s[\rho]) + (E_{ee}[\rho] - J[\rho]) \end{aligned} \tag{2.52}$$

where the second line is the kinetic energy calculated from a Slater determinant, the third line is the potential energy of attraction between electrons and nuclei, the fourth line is the potential energy of repulsion between electrons and the final line is the exchange correlation term. The assumptions made in the derivation of the term for electron correlation prevents DFT from being classed as a truly *ab initio* technique. It is from this weakness that DFT draws its unique strength and earns its place among the most used quantum chemical methods. The functionals are largely empirical and as a result are inferior to the other methods discussed, however, they occupy the perfect position in terms of computational cost and accuracy of the results. However, structures optimised using DFT should be justified through the use of *ab initio* methods. If, for example, a transition state exists for a DFT but not for an MP2

calculation it is extremely likely that it is not a true transition state and it exists as a result of this deficiency. New DFT functionals are being developed constantly. A very popular functional is the Becke 3-parameter Lee-Yang-Parr functional, which has been used extensively across chemistry with success.

2.8 Configuration Interaction (CI)

Perhaps the best way to describe CI is by example, and so this section is presented as a brief discussion of the full CI (FCI) expansion of the wave function for minimal basis H_2. If a complete basis set were available, the FCI wave function would be perfect and provide an exact solution to the Schrödinger equation. It is the most accurate method available at present. The general form of the FCI wave function is a linear combination of excited Slater determinants.

$$|\Psi\rangle = c_0 |\psi_0\rangle + \sum_{ra} c_a^r |\psi_a^r\rangle + \sum_{a<b} \sum_{r<s} c_{ab}^{rs} |\psi_{ab}^{rs}\rangle + \sum_{a<b<c} \sum_{r<s<t} c_{abc}^{rst} |\psi_{abc}^{rst}\rangle + \cdots \tag{2.53}$$

The FCI wave function for minimal basis H_2 is deduced by simply picturing the ground state, considering all singly excited electron configurations and spin configurations and writing the appropriate expression, before writing the doubly excited wave function down. There are only 6 unique determinants in this case, and only the ground and doubly excited states are of the appropriate symmetry to appear in the expansion of the wave function.

$$|\Psi_0\rangle = c_0 |\psi_0\rangle + c_{12}^{34} |\psi_{12}^{34}\rangle \tag{2.54}$$

While in this case the number of determinants is reasonably small, it is clear to see how, for larger systems, this number will become too much to consider even with the most powerful computers available. To provide a way around this issue, coupled cluster methods have been developed. While the coupled cluster approximation (CCA) has issues of its own, it is the latest amongst modern quantum chemical techniques and is a very promising field. CCA is not discussed in this thesis. The actual number of determinants it is possible to form from N electrons and M spin orbitals is given by the binomial coefficient

$$\binom{M}{N} = \frac{M!}{N!\,(M-N)!}. \tag{2.55}$$

2.9 Complete Active Space (CAS) Theory

Having already touched on the difficulties involved in constructing FCI expansions, it seems a good time to give the briefest of introductions for CAS theory. CAS is essentially a toned-down version of FCI with an impressive ability to model systems whose most interesting characteristics are governed by a small fraction of the total electronic population. For instance, in benzene the chemical bonding and electronic transitions are heavily reliant on the delocalised rings of electrons above and below the molecular plane. Using CAS theory, we choose the orbitals we are interested in, which for benzene are the 6 π orbitals, and treat them as if we are doing a FCI calculation. This limited CI approach is excellent for calculating the properties of molecules of similar ilk to benzene, such as cyclobutadiene or even the ever-popular cyclopentadienyl anion.

Perhaps the area where CAS truly excels in computational chemistry is in the modelling of bonds which are breaking. HF and MP2 calculations predict incorrect products, for instance, of dissociating the O-H bond in a water molecule. Where HF and MP2 predict OH^- and H^+, CAS theory, assuming the appropriate orbitals are selected as being the so-called “active space”, correctly predicts the radical species, $^\bullet OH$ and $H^\bullet$.

2.10 Basis Sets

Basis sets are essentially the elements of a function space or inner product space as defined in linear algebra. There are two main classes of functions in use. These are Slater and Gaussian type orbitals. The 1s Slater orbital for the hydrogen atom is given by

$$\chi_{SO,1s} = \sqrt{\left(\frac{\zeta^3}{\pi}\right)} e^{\zeta r} \tag{2.56}$$

and predicts exactly the real ground state energy, -0.5 au. The hydrogen 1s Gaussian-type orbital is given by

$$\chi_{GO,1s} = \left(\frac{2\alpha}{\pi}\right)^{\frac{3}{4}} e^{-\alpha r^2} \tag{2.57}$$

and predicts $E = -0.4224$ au. This is corrected by taking a linear combination of Gaussian-type orbitals with modified exponential factors

$$\phi_{1s}(r) = \sum_{p=1}^{n} c_p \chi_{GO,1s}\left(r, \alpha_p\right) \tag{2.58}$$

as n is increased, the energy becomes closer and closer to -0.5 au, reaching -0.499999 au at $n = 10$. At first glance it may seem that Gaussian orbitals are the weaker candidate, but their flexibility and unique traits make them more manageable. That is, the product of two Slater orbitals is some other function, and the product of two Gaussian orbitals is another Gaussian orbital. As a result, their ineffectiveness as single function approximations is unimportant and they are employed in the vast majority of quantum chemical packages today.

Correlation-Consistent Basis Sets

Dunning and co-workers developed prior to the turn of the millennium some of the most widely used basis sets.[38] They are denoted by "cc-pVNZ" (where N=D, T, Q, 5,

6, ...) and bring with them a both a flexibility in terms of accuracy and computational cost, and a standard by which to compare results. Not dissimilar to Pople basis sets, which are not discussed here as they are not used at any point in this thesis, the name of each basis set may be broken down to describe their characteristics. 'cc' stands for 'correlation consistent', 'p' for 'polarised', 'V' for 'valence' and 'Z' for the Greek letter 'zeta' (ζ).

The flexibility in terms of accuracy arises from the choice of N. cc-pVDZ is a double-zeta basis set, and includes twice as many functions as the minimal basis, cc-pVTZ three times as many and so on. For heavier atoms, such as bromine and iodine, a special basis set may be formed to which '-PP' is appended to any of the previous names and stands for 'pseudopotential'. A pseudopotential is a way of replacing the motion of the core electrons of an atom with an effective potential to cheapen the computational cost of calculating the properties of molecules containing heavy elements.

3 Computational Details

All calculations contained within this document were performed with the Gaussian 09 quantum chemical package.[39] Optimisations of both ground and transition states are performed under the "Opt(VeryTight)" criteria. In most cases it is necessary to include the keyword "CalcAll", but in a small minority of cases, "CalcFC" or "CalcHFFC" will suffice. Ground states are confirmed as minima on the PES by an absence of imaginary frequencies in the Hessian matrix, generated using the "Freq" keyword. Transition states are also confirmed by frequency analysis, that is, a single imaginary frequency in the Hessian matrix. All optimisations to ground and transition states were attempted using three methods; B3LYP, B3LYP-D3 and MP2. B3LYP-D3 is requested using the keyword "EmpiricalDispersion=GD3BJ". In conjunction with density functionals, the "Int(Grid=Ultrafine)" keyword was used. Two basis sets were used; LANL2DZ and cc-pVDZ(-PP). In the case that the calculation involve chlorine, cc-pVDZ was used, where bromine or iodine were involved, cc-pVDZ-PP is chosen using the "Gen" basis and "Pseudo=Read" keyword. CASSCF is elected as the appropriate method for the calculations included in section 5 and is used with the cc-pVQZ basis.

For the magnetic shielding calculations, HF (GRF section) and MP2 (dicarbon section) are used with the same basis set arrangement as used for the optimisations in the GRF section, and the cc-pVQZ basis set is used in the dicarbon section. The keywords "SCF(Tight)" and "NMR" are employed. Spacing between ghost atoms will be made clear in each case throughout this document. Input files for the magnetic shielding calculations are generated using a number of in-house codes. An example code is included in appendix 7.1.

The counterpoise method of eliminating BSSE is requested using the "Counterpoise= X" keyword. "MaxCyc= X" is used frequently throughout, with $X > 200$ often necessary in both ground and transition state optimisations. All transition state calculations needed the "NoEigenTest" and "TS" keywords. "Scan" is used in the C_2 section for examining the PES as bonds are lengthened. Further difficulties in calculations involving magnesium clusters and internal co-ordinates warranted the use of the "Opt(Cartesian)" keyword.

Optimisations involving diethyl ether coordinated systems are particularly prob-

lematic and often take several times the number of cycles as dimethyl ether complexes, often having the first eigenvalue of the Hessian matrix less than 5 cm^{-1}. Convergence of these complexes from a good starting geometry takes a very large number cycles, even with the “CalcAll” keyword.

Images of molecules were created using Molekel, and images of molecular orbitals were created using the “gmolden” executable from the Molden software package.

4 Results Concerning Grignard Reagent Formation

Given that the presence of very specific solvent molecules is well known to be essential to the action of a Grignard reagent, it makes good sense to begin with a study of the effects these solvents have on the bonding in RMgX. After solvent effects, one more than likely associates Grignard's reaction with various halides and so this will be the next port of call. Once these two factors have been reviewed, we turn to an analysis of the changes in bonding along the reaction surface through a number of transition states. In the study of these PES, it quickly became apparent that they are extremely flat, indicated by very low vibrational frequencies in the Hessian matrix, making optimisations difficult and costly computationally. The presence of solvent interactions produces a dilemma of sorts, in that to get the correct energy one must take into account BSSE, but to do this the cost of the calculation becomes untenable in some cases. Where possible, the counterpoise method of removing BSSE has been implemented. Were there more time available, every structure would have been subjected to this.

4.1 Solvent Effects

This section inludes a very rudimentary study of solvent effects in GRF. In fact, the word “solvated” is used rather loosely. Two solvent molecules at any one time are considered and no further shells of solvation have been studied, however, these are potentially important in a number of steps in GRF and are thus in need of some attention in the literature. Such a study was unfortunately beyong the scope of the project with which this thesis is concerned. All chosen solvents are optimised together with their complexed form.

The solvation of the Mg centre of a Grignard reagent alters the geometry of the R-Mg-X spine significantly. The decrease in bond angle along the spine is the most notable difference. This section includes a comprehensive study of the effect of ether co-ordination using magnetic shielding calculations.

Currently, the role of the solvent in GRF is thought to be solely to remove the Grignard’s reagent from the magnesium surface and carry it into the reaction media. And once there, it is free to react. This sequence of events is witnessed when one simulates the reaction in ether. The most commonly used solvents are tetrahydrofuran (THF) and diethyl ether (DEE). DEE is used in this study, along with dimethyl ether (DME). DME is selected as a solvent in many cases primarily because it is more manageable computationally as it seemingly generates less-flat PES.

Five solvents are considered; DEE, DME and analogues of the latter with Hydrogen atoms being sequentially replaced with Fluorine atoms.

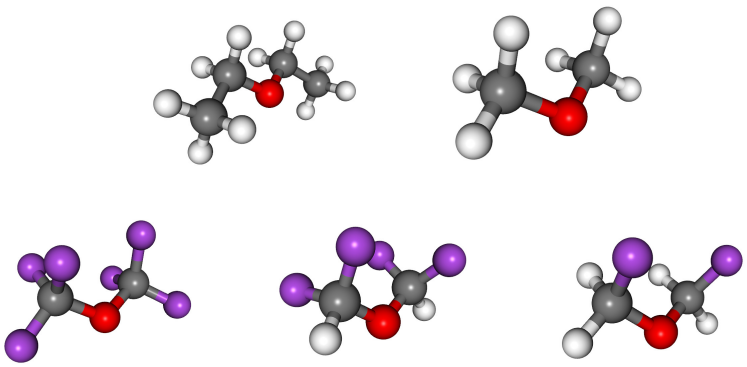

Figure 4.1: Solvents used to study electron withdrawing effects in Grignard reagents. Top (left to right); DEE and DME. Bottom (left to right); $(CF_3)_2O$, $(CHF_2)_2O$ and $(CH_2F)_2O$. All optimised at the MP2/cc-pVDZ level. Grey atoms are carbons, white are hydrogen atoms, purple are fluorine atoms and red are oxygen atoms.

These are chosen as they represent a simple, stepwise increase in the electron donating character of the solvent.

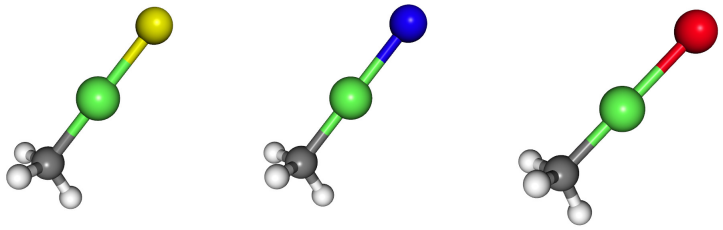

Figure 4.2: Unsolvated Grignard species RMgX where R=CH_3 and, from left to right X=Cl, Br and I.

Upon solvation with DME, the C-Mg-X bond angle decreases from 180^o to approximately 138^o, in the order $\delta(\angle\text{(C-Mg-Cl)}) > \delta(\angle\text{(C-Mg-Br)}) > \delta(\angle\text{(C-Mg-I)})$. This sequential decrease in the change bond angle is likely a result of the increasing atomic radii of the halogens, and their increasingly long range influence on the structure of species binding to the magnesium centre. As one may expect, when beginning a study involving halogens, trends emerge and often follow the pattern seen here where changes are larger in the species where X=I than those earlier in the series.

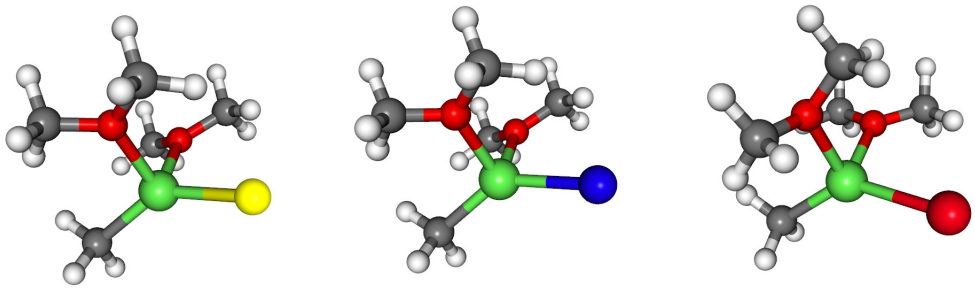

Figure 4.3: Solvated Grignard species corresponding to their unsolvated counter parts in Fig 4.2, where from right to left, X=Cl, Br and I

For brevity, trends in the bond length data collected are summarised here and tables are provided for the reader in appendix 7.2 as evidence. The acquisition of B3LYP-D3 data for complexes containing bromine is particularly difficult, with most attempts yielding multiple imaginary frequencies in the Hessian matrix thus indicating these so-called ground state geometries were not at local minima on the PES and so were discarded as bad results. It is seen in Fig 4.3 that there is an absence of a plane of symmetry in optimised geometries. In the series of B3LYP/LANL2DZ calculations, both Mg-O bond lengths are equivalent in the individual complexes, most

likely owing to the lack of diffuse functions and dispersion effects on the heavier halogens. Contrasting these with the C-Mg bond lengths, one observes that in the unsolvated compounds bond lengths decrease in the order, C-Mg(X=I) $>$ C-Mg(X=Br) $>$ C-Mg(X=Cl), whereas in the solvated compounds they increase in the order C-Mg(X=I) $<$ C-Mg(X=Br) $<$ C-Mg(X=Cl). It is from this observation that the interest in the Mg-O interaction stems.

One may put together a case in which these observations are explained in their entirety using arguments of formal oxidation states, the periodic table and elementary organic chemistry. That is, in the unsolvated case, the ability of the halogen to stabilise the δ-positive magnesium atom decreases in the order I $>$ Br $>$ Cl, simply because iodine has the greatest number of electrons in diffuse, heavily shielded orbitals. As a result, it is expected that the electrons between the carbon and magnesium nuclei experience a lower effective nuclear charge from the magnesium and thus the bond lengthens. In the solvated case, the sheer size of an iodine atom in combination with the coordinated ether molecules more than likely leads to significant steric effects. This halo-solvent interaction is manifested in the increase in Mg-O and Mg-I internuclear separation and subsequent increase in magnesium's demand for electron density from the carbon atom, hence the shorter C-Mg bond length, with electron donating effects taking precedence over steric effects for chlorine, and vice versa for the iodine (with bromine falling somewhere between the two). The increase in differences between bond lengths as basis set size is increased along with the trends in bond lengths as steric bulk is increased (DME to DEE) lends support to this argument. That said, it is not a particularly satisfying explanation, it should also be noted that the descriptor "bond length" is used with no intended implication that bond strength is in any way correlated to it.

Before exploring the effect an electron-withdrawing solvent has on Grignard reagent structure, it is necessary to build a picture of the impact of simple ether co-ordination. To do this, magnetic shielding calculations are performed with ghost atoms placed along the C-Mg bond in a small selection of molecules. Six systems are studied, RMgX where R=CH_3 and X=Cl, Br and I and R=C_6H_5 and X=Cl, Br and I. The study forms the ground work for a real solvent study by considering the minimum possible number of solvent molecules.

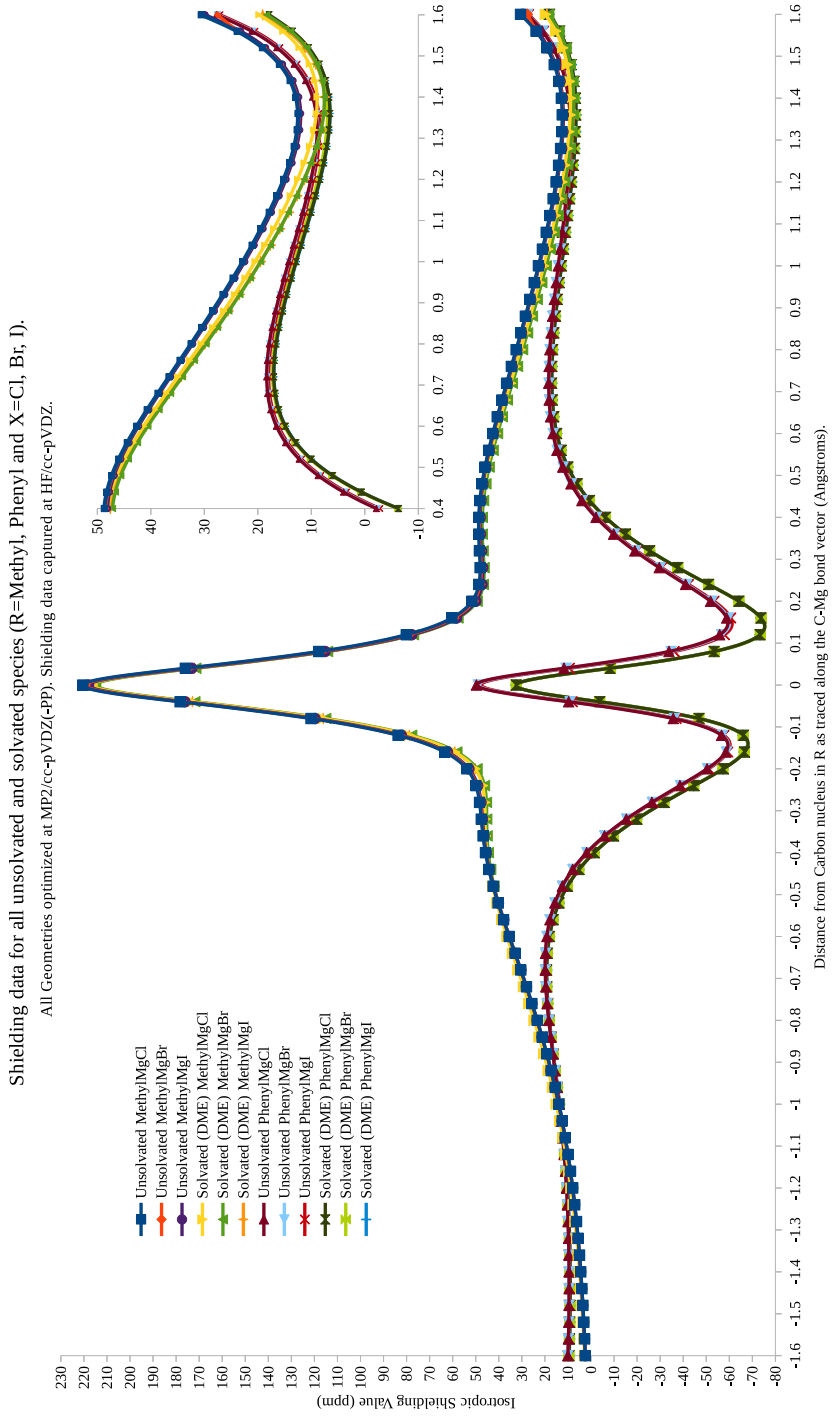

Figure 4.4: Shielding data taken along the C-Mg bond showing the differences in bond strength between R groups, halogens and solvent environment. In the top right hand corner is an increased resolution image of the 0.4-1.6 Ansgtrom region.

The raw data taken from these calculations shows more detail about the electronic behaviour between the carbon and magnesium atoms in each compound, in terms of isotropic shielding, for comparison. With minimal manipulation, it is possible to generate relative plots which offer a greater resolution. This is done by choosing a

data set and subtracting the others from it.

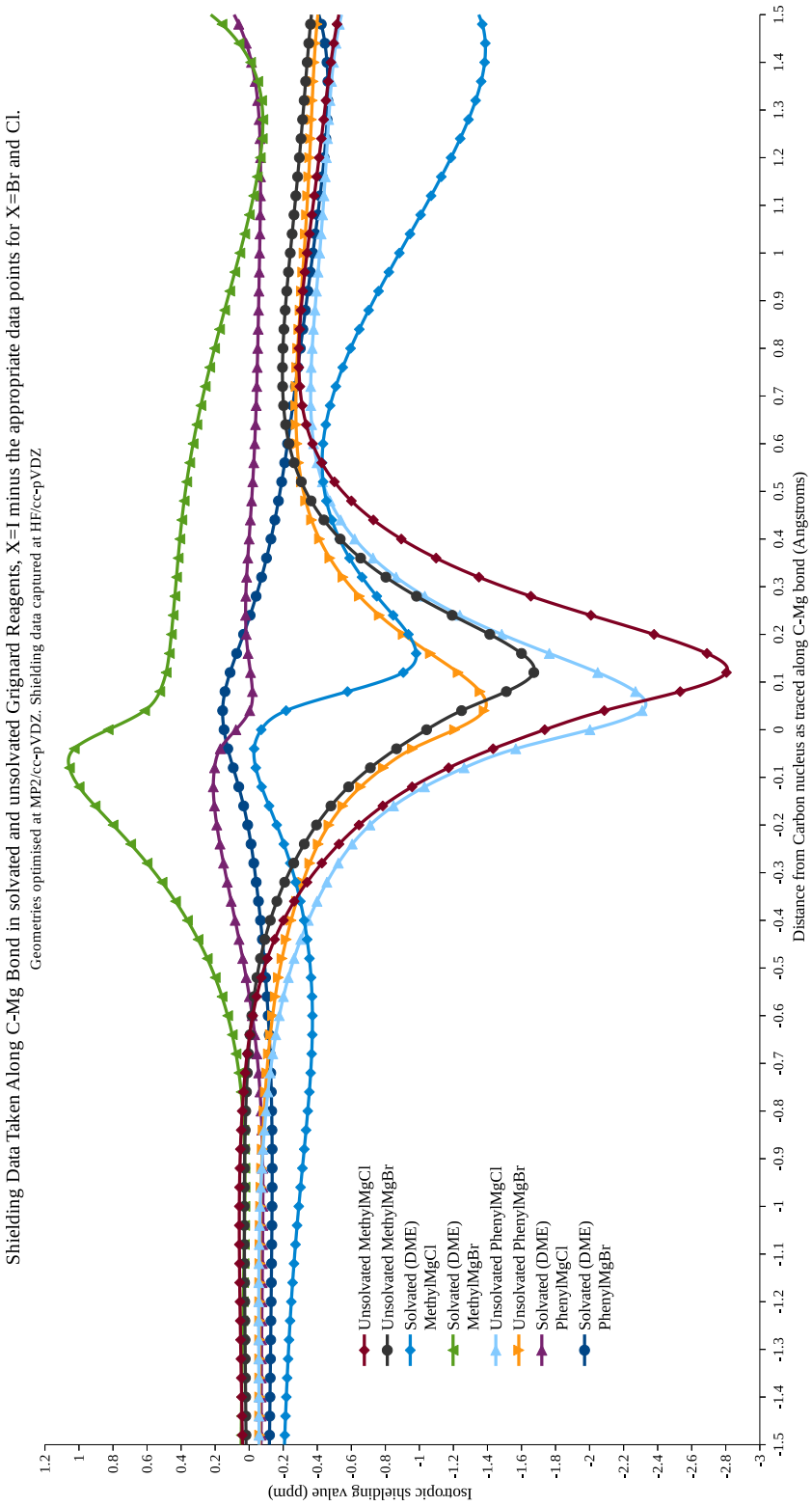

Figure 4.5: Shielding data taken along the C-Mg bond showing the differences in bond strength between R groups, halogens and solvent environments. The data points for X=Cl and Br have been subtracted from the X=I data point to increase resolution and give a picture of relative bond strengths.

It is seen immediately that the C-Mg bond strength when R=CH_3 is greater than when R=C_6H_5. Also noticeable is that the impact of solvation on the C-Mg bond is much greater in the R=CH_3 case, with shielding decreasing significantly on formation. The change observed for R=C_6H_5 is much less dramatic. The most obvious explanation for this is that the delocalised π electron density has the ability to shift around the ring in a bid to neutralise external effects. That is, as the Mg-bound carbon draws electron density from the magnesium, electrostatic effects with electrons in neighbouring bonds lead to a distortion of the hexagonal ring through a lengthening of the bonds closest to the C-Mg region. Justification of this effect is seen clearly by isotropic shielding calculations on finely space ghost atoms in the molecular plane of the phenyl ring, as alluded to in section 1.3.

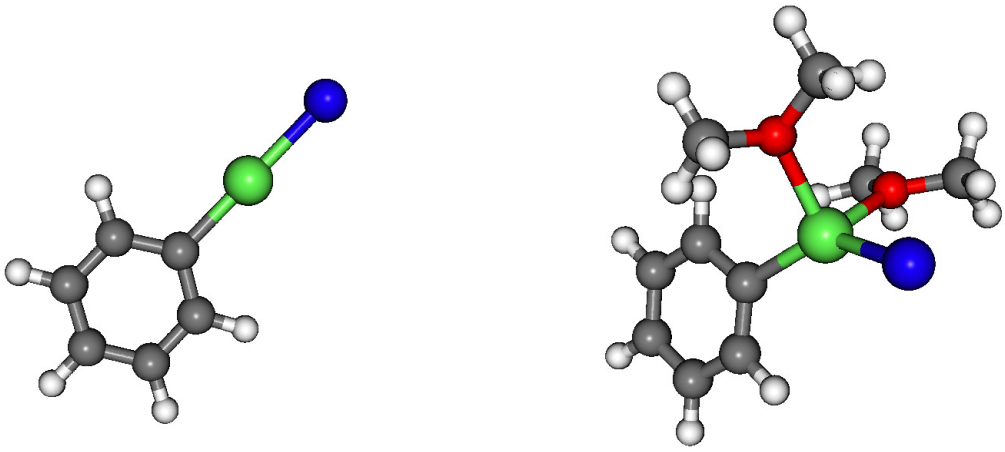

Figure 4.6: Aromatic Grignard reagent geometries (optimised at the MP2/cc-pVDZ-PP level); unsolvated (left) and solvated with DME (right), X=Br.

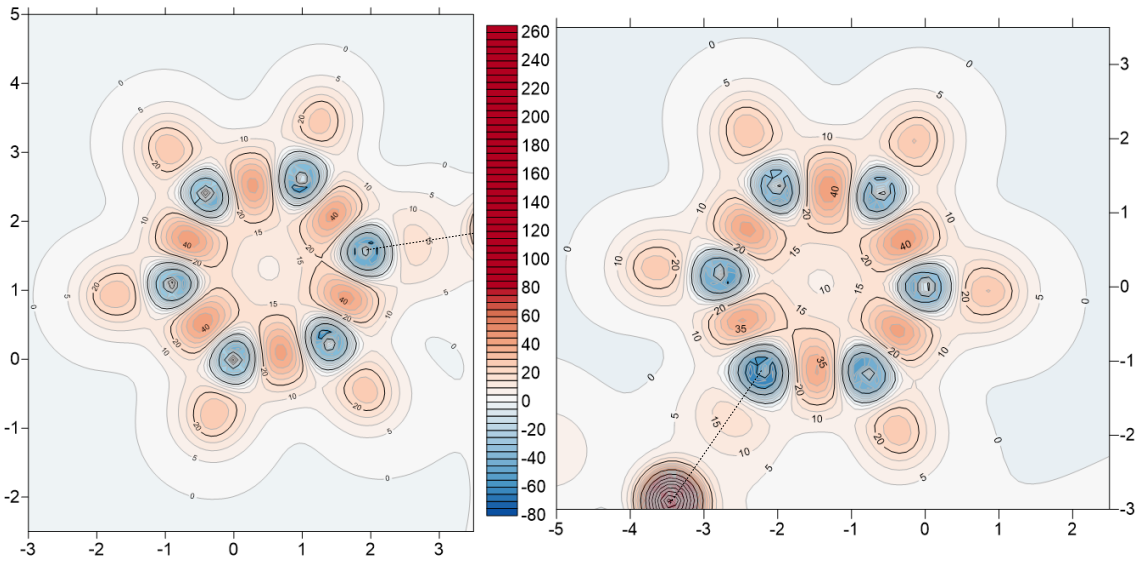

Figure 4.7: Isotropic shielding (ppm) data captured at HF/cc-pVDZ-PP. The image was generated using a plane of ghost atoms in the molecular plane of the phenyl group with a resolution of 0.1 Å. Contour lines are every 5 ppm. The geometries used here are for unsolvated R-Mg-Br (left) and R-Mg-Br solvated with DME (right). Both were optimised at the MP2/cc-pVDZ-PP level. A dotted line has been added along the C-Mg bond to help determine the orientation of the ring in conjunction with figure 4.6.

As postulated, there is a shift in isotropic shielding, and thus a suggested shift in electron density, with larger values appearing towards the section of of the ring furthest from the C-Mg bond upon solvation, and the region between the carbon and magnesium nuclei remains largely unchanged. This alteration in electron localisation is manifested in the contour lines at 10, 30 and 40 ppm. There is an increased area at the back of the aromatic ring at 10 ppm. Between the carbon and hydrogen nuclei furthest from the Mg atom and solvent, we observe the beginnings of a 30ppm contour line not present in the unsolvated picture. Finally, we see a greater isotropic shielding in the carbon-carbon bonds furthest from the Mg atom in the solvated case than the unsolvated case, indicated by the increase in area at 40 ppm. These effects could be shown more clearly by including more contour lines, but in the interest of resolution and giving a better quality picture of the full system, a contour interval of 5ppm is selected as a happy medium. This ability to counteract solvation effects on C-Mg bond length renders R-Mg-X where R = C_6H_5 a less sensitive complex to solvent type.

By varying the electron density available to the oxygen atoms coordinated to the magnesium center, it is possible to get a picture of the solvent's impact on the C-Mg-X

spine. The chosen method of investigation is, again, isotropic shielding calculations involving ghost atoms along the vector of the C-Mg bond. Bond length analysis offers further insight, in that there is a strong correlation between increasing electron density available to the oxygen atom, and an increasing C-Mg bond length for all halogens. Data are provided in the appendix to support this claim. Geometries are taken from the highest level of theory available (MP2/cc-pVDZ-PP) in the current data set, and examined analogous to the previous complexes in this section.

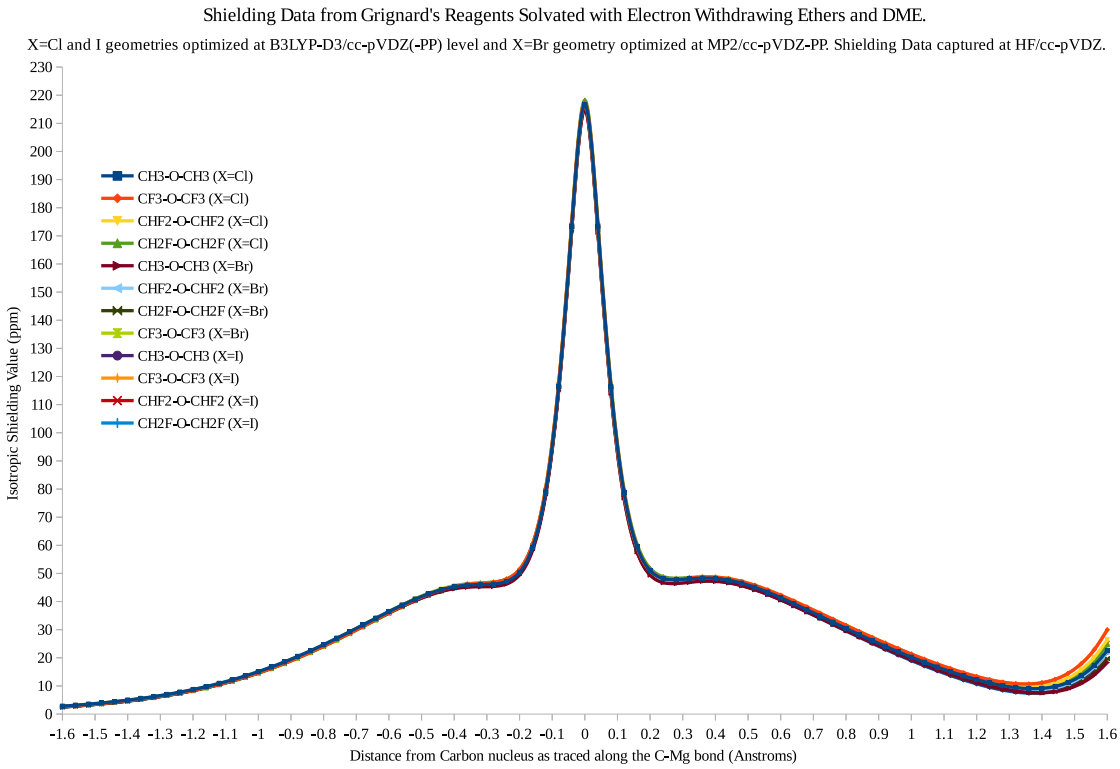

Figure 4.8: Shielding data along the vector beginning 1.6 Å before the Carbon nucleus in the R group, and continuing along the C-Mg bond in R-Mg-X (X=Cl, Br and I) for 1.6 Å (one every 0.04 Å) for all solvent types excluding DEE.

In Fig 4.8 it is evident that the most significant difference between electronic environments is located between the carbon and magnesium centres, not far from the beginning of a peak for the magnesium atom. Not coincidentally, were one to attribute strengths not just to bonds but to sections of bonds, one might say that the weakest point of the bond, the minimum on an isotropic shielding plot, in this case is the point at which the plots diverge the most. This provides a reasonable basis on which to order the relative C-Mg bond strengths of the products of GRF.

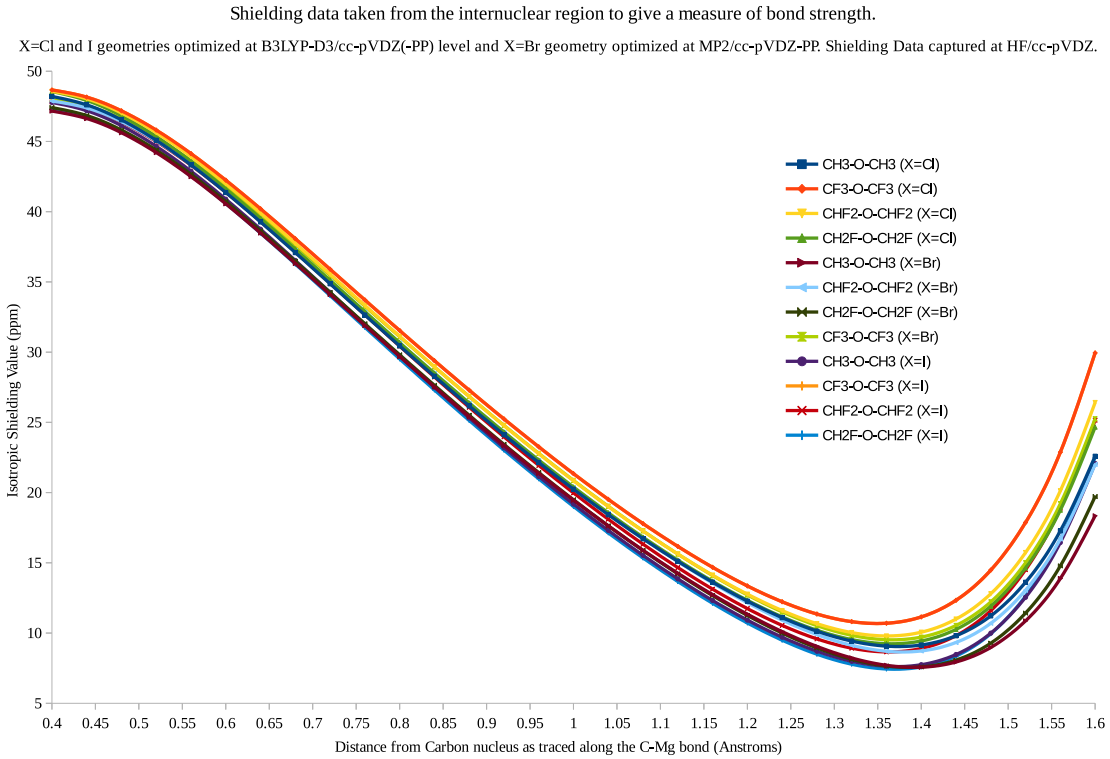

Figure 4.9: Shielding data along the vector beginning 0.4 Å after the Carbon nucleus in the R group, and continuing along the C-Mg bond in R-Mg-X (X=Cl, Br and I) for 1.2 Å (one point every 0.04 Å). This figure provides a superior resolution between nuclei compared with Fig 4.8.

By looking carefully at Fig 4.9 and examining the trend for each halogen individually, the expected pattern emerges; E(C-Mg:$(CH_3)_2O$) < E(C-Mg:$(CH_2F)_2O$) < E(C-Mg:$(CHF_2)_2O$) < E(C-Mg:$(CF_3)_2O$). Also to be taken from this image is the relationship between bond strength and halogen. It is obvious that chlorine has the least electron density to offer the magnesium atom and this is reflected in the change in C-Mg bond strength as the solvent is varied. Interestingly, when considering the C-Mg bond strengths in the complexes containing bromine and iodine, extremely similar quantities are measured, especially on the occasion that $(CH_3)_2O$ is the chosen solvent.

The data suggest that there is some measure of balance between solvent interaction and halogen used. For instance, to weaken the bond as much as possible, one may expect to need iodine and DME present. It is seen here that a very similar electronic environment may be achieved using bromine and $(CH_2F)_2O$. The case changes completely when one has chlorine present in the complex, and even the most electron-donating of solvents cannot weaken the C-Mg bond to the same extent as

chlorine's heavier counterparts. The almost continuous set of bond strengths allows, the fine-tuning of bond length and bond energy.

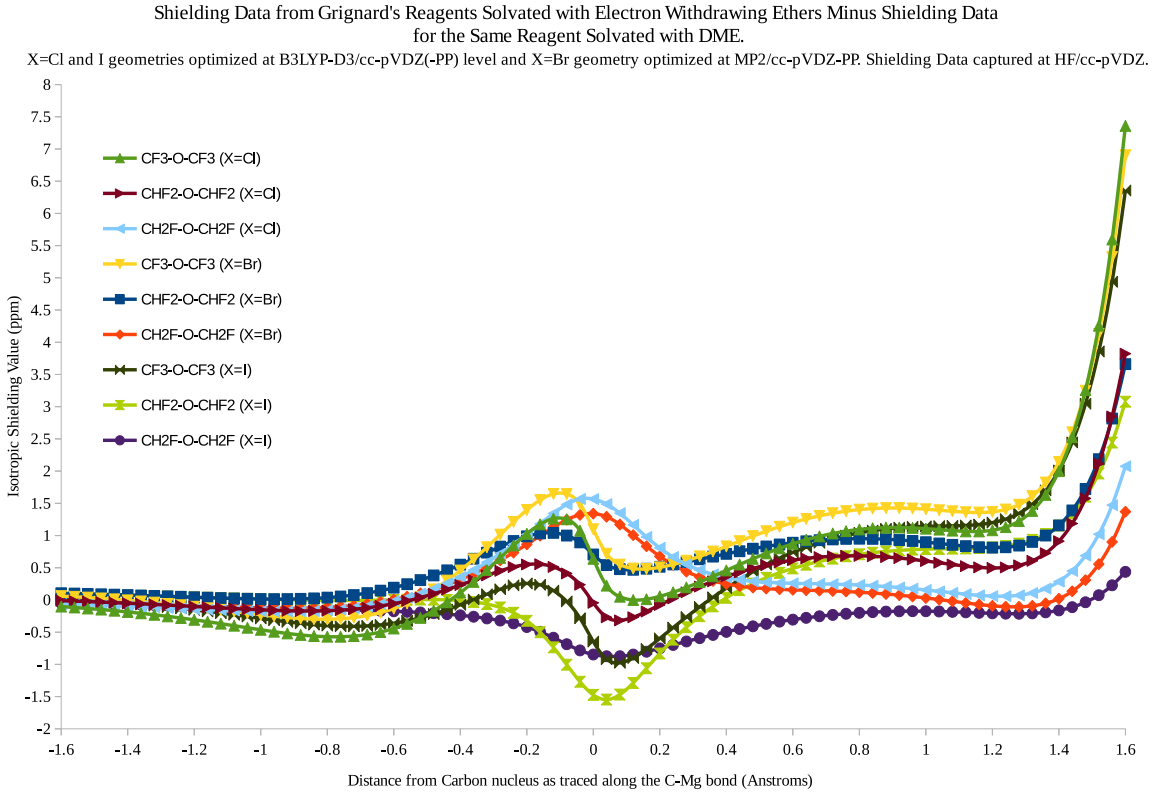

Figure 4.10: Shielding data along the vector beginning 1.6 Å before the Carbon nucleus in the R group, and continuing along the C-Mg bond in R-Mg-X (X=Cl, Br and I) for 1.6 Å (one every 0.04 Å). All data points have been subtracted from their DME solvated counterparts.

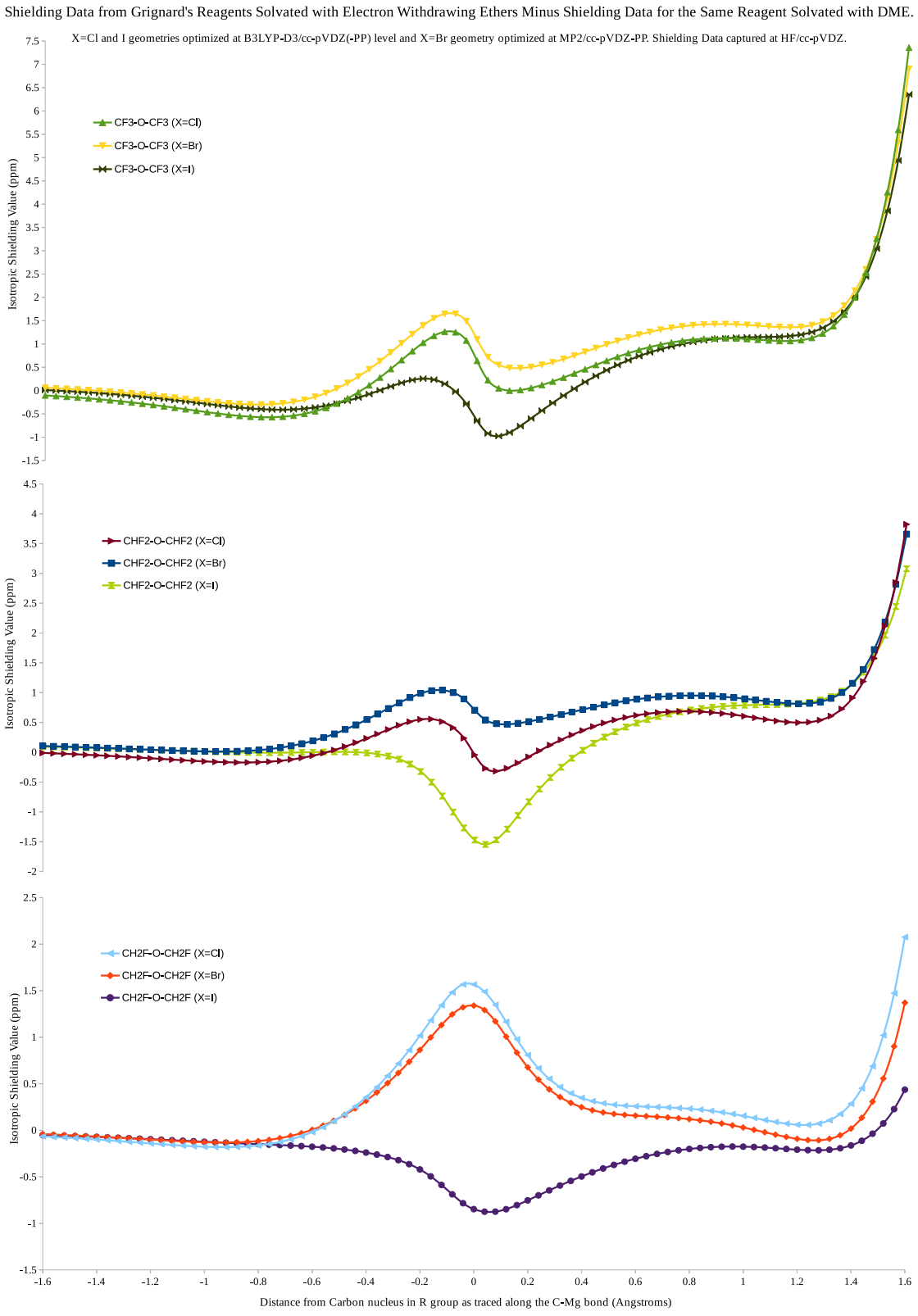

Figure 4.11: The same data presented in Fig. 4.10 and plotted according to solvent type.

A clear trend is visible, where a greater shielding value between nuclei corresponds to a stronger bond, showing that the strength of the C-Mg bond not only

varies with X but also with solvent. X=Br is seen to be the set of complexes most sensitive to solvent type.

Binding energies are calculated for the interaction of the ether molecule with the magnesium centre. These are generated from,

$$E_{(O-Mg)} = E_{(solv.\ R-Mg-X)} - (2 \times E_{(solvent)} + E_{(R-Mg-X)}) \tag{4.1}$$

by freezing the geometry of the segments of the molecule being considered and calculating their energy independently, one gains a more accurate value (there is no correction for basis set superposition error). The reported quantities are as expected. The strongest O-Mg bonds are present in the complexes with the least electron withdrawing character. As each hydrogen atom is replaced with a fluorine atom, the calculated vibrational frequencies increase - a feature which shows solvent type has a major effect on the potential energy surface. Local minima for the solvents containing fluorine atoms were significantly easier to locate when compared with the ever-so flat surface we are tasked with navigating for the rest of the study. The changes in the frequencies calculated correspond to the replacement of the original PES with a more heavily featured one, that is, one whose gradient to the saddle point of interest is steeper and more easily followed). Without performing any additional calculations, it suggests that barrier heights increase as the electron-withdrawing nature of the solvent is increased and subsequently, so is the energy required to induce change in the system.

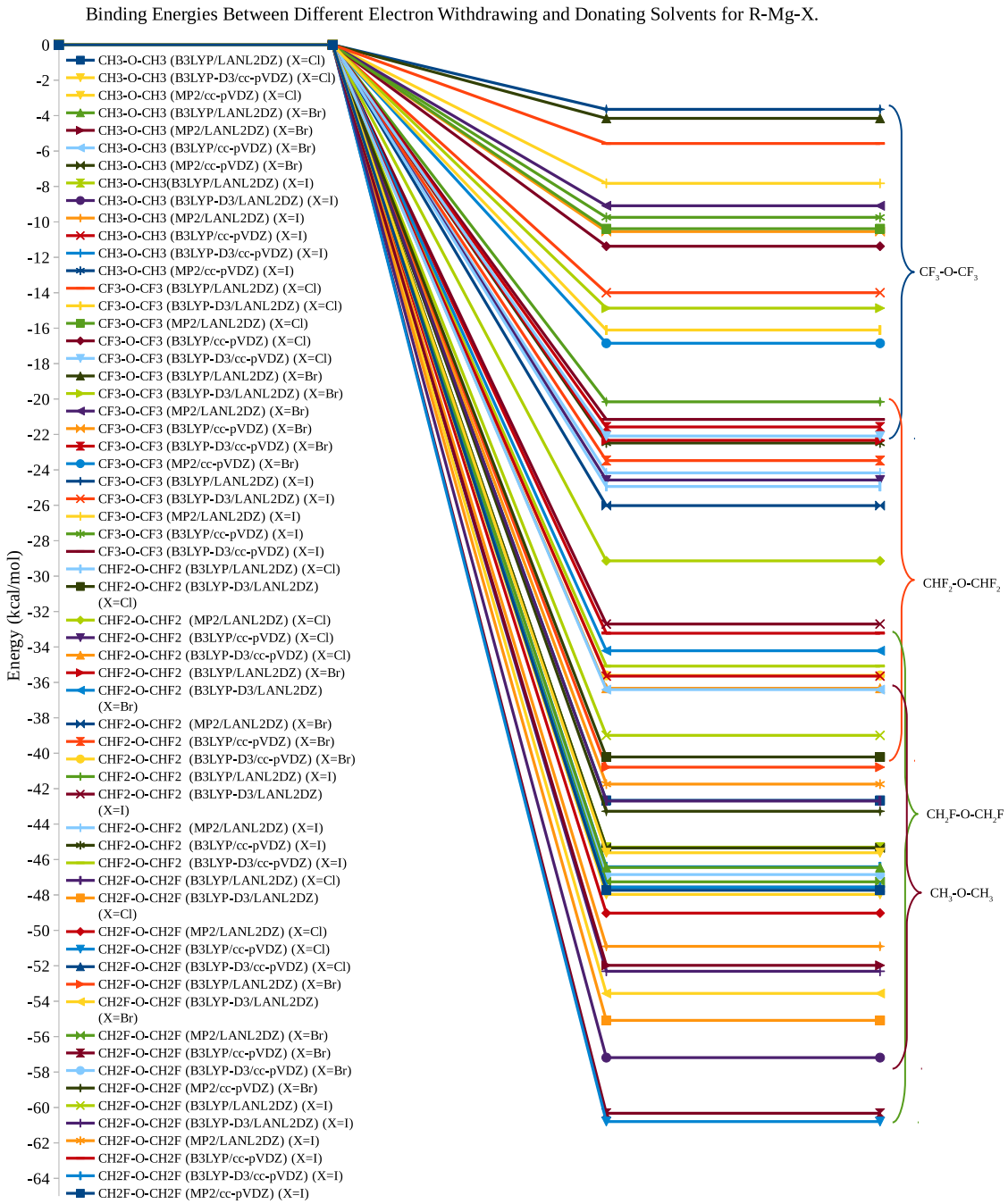

Figure 4.12: Binding energies for various solvents with R-Mg-X (C=Cl, Br and I, R=CH_3) over a selection of method/basis set combinations.

It is evident between the shielding and binding energy data that there is a strong correlation between C-Mg bond strength and Mg-O binding energies; the more electron-withrawing the solvent is, the less negative the binding energy and the stronger the C-Mg bond in the corresponding complex. In a manner not dissimilar to observations in Jahn-Teller active complexes, where equatorial ligands experience a

decrease in bond length as axial ligands experience an increase and vice versa, as the solvent molecules draw increasing amounts of electron density away from the magnesium (and in turn shorten the Mg-O bond lengths), the C-Mg bond is lengthened.

Here we observe the general trend that as electron density is pulled away from the oxygen in the ether, which is bound to the magnesium atom, the binding energy becomes less negative, which coincides with less impact on the bond length in the Grignard reagent. As electron density becomes increasingly available to the oxygen, the impact on bond length in the Grignard reagent increases, we know from chemical kinetics that a lengthening of the "bond-to-break" renders it more likely to react. As the binding energy of the solvent decreases, the longer the carbon-magnesium bond becomes.

4.2 New Solvent Interactions in GRF

At the risk of becoming monotonous and for a clearer meaning in this section, the term “electron donating character” is replaced with “Lewis basicity’, a well-defined concept. It is also known from general chemistry, that the halogens have the ability to act as both Lewis acids and bases, and that ether solvents are Lewis bases. Halogen bonding is a weak interaction experienced by halogen-containing molecules in Lewis basic solvents. Where most organic chemistry textbooks explain that ether solvents are chosen for GRF as they are aprotic and for little else, here it is suggested that the assumption that the solvent’s only role in GRF is to be unreactive and to remove the reagent from the magnesium surface is misplaced and does not survive a consideration of solvent-halogen interactions. Halogen bonds are weaker than hydrogen bonds, increasing in strength in the order F $<$ Cl $<$ Br $<$ I and are challenging computationally. As such, the molecule chosen for the initial study should be one with a simple structure and no atoms present with the potential to mask the interaction. To this end, methyl iodide, and DME are chosen. DME for computational convenience, and iodine as the halogen to simplify the search for a minimum by providing the strongest interaction possible.

The importance of long range interactions places additional strain on the role of the basis set, and to avoid error arising from an insufficient number of basis functions, the LANL2DZ basis is not considered, along with B3LYP and B3LYP-D3. The MP2 method is used in combination with the cc-pVDZ-PP basis set. Early attempts included attempting to calculate the interaction between methyl iodide and a single DME molecule. No local minima were found. Interestingly, upon the introduction of a second solvent molecule and at great computational expense, a minimum is detected corresponding to a complex with a lengthened C-I bond. A likely explanation for the unsuccessful attempt with a single DME molecule is that the absence of the stabilising hydrogen bonding effect from the second DME molecule resulted in a flattened PES. Though there is little doubt that a local minimum exists to which the single DME-I interaction corresponds, it was not located in this study.

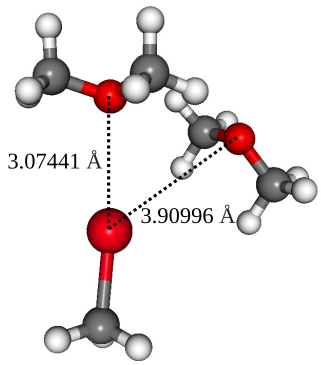

Figure 4.13: Geometry of the $I(CH_3)((CH_3)_2O)$ complex, optimised at the MP2/cc-pVDZ-PP level, with labelled halo-solvent distances.

The introduction of the second solvent molecule, which we shall call DME(2), is thought to be purely to stabilise the first solvent molecule, which we shall call DME(1). That is, the I-DME(1) internuclear distance is 3.0 Å, and the I-DME(2) internuclear distance is 3.9 Å. So, the I-DME(2) interaction is non-existent, or at least negligible. Further evidence of the I-O interaction in DME(1) is the disparity between the hydrogen bonds. Where there is little or no interaction with the halogen, the hydrogen bond length is 2.5 Å, that is, the distance between the oxygen atom in DME(2) and a hydrogen atom in DME(1). For DME(1), where an effect from the iodine is felt more keenly, the hydrogen bond length is 2.7 Å. As expected, the ether molecule forming a Lewis adduct with the iodine (which is less electron dense) forms a weaker bond with a nearby hydrogen.

With no DME present the carbon-magnesium internuclear distance is 2.15060 Å, when the two solvent molecules are introduced, the bond length is extended to 2.15345 Å. So, with a lengthened bond, and a geometry which excludes the possibility of magnesium-halogen primary interactions in the transition states, for solvent effects to be important for the mechanism there must also exist at least one transition state for which the primary interaction is between the carbon atom in the R group and the magnesium surface. Further credibility is given to this possibility upon the consideration of the calculated Mulliken charges, which indicate that in the $I(CH_3)(DME)_2$ complex there is a significantly more negative charge on the carbon atom in the R group than the iodine. The barrier to solvation was found to be 8 kcal/mol. While these solvent effects are less impressive than those observed when

the R-Mg-X spine is solvated, they may yet prove to be important.

4.3 Reaction Pathways

Having reviewed the role solvent type plays in the structure of the reacting species in a typical Grignard reagent's transformation, a number of transition states are studied. Most are already known and operate under the "iodine-magnesium primary interactions are the only reasonable options" assumption, along with a new transition state where iodine is complexed with two DME molecules and the geometry of the methyl group is inverted upon approach to the magnesium surface. The latter has been completely unstudied in the literature and is an entirely new approach to the GRF mechanism.

In section 4.1, the effect of solvent type and the general structure of the Grignard reagent has been discussed at some length. For the Grignard reagent to be removed from the surface and carried into the reaction media, the Grignard reagent must also form at the surface. The almost axiomatic observation that while still bound to the metal, the sequence R-Mg-X must exist, provides us with a choke point for transition states and reaction paths. If the radical intermediates are, in fact, free at some point in the reaction then they must return to the surface to complete the R-Mg-X sequence and be removed by the solvent to form the reagent we are interested in. Were the radical not to be free at any point, then the whole picture is slightly less complex. By building transition states with the propensity for forming the geometry corresponding to a local minimum as the reaction proceeds, it is more likely that the study is moving in the right direction.

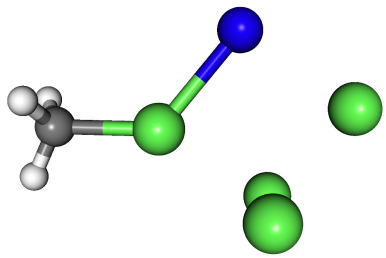

Figure 4.14: A cluster-based approximation to a stationary point which must be a feature in the majority of GRF reaction pathways, and all pathways passing through a tetrahedral or pseudo-tetrahedral anomaly on the solid surface.

The structure shown in Fig 4.14 is expected to be an essential intermediate in the

Mg_4 cluster approximation and so must be a feature of all potential energy surfaces, supporting both diffusion based mechanisms and oxidative insertion mechanisms. As mentioned in section 1.1 (see references therein) Tulub *et al* showed that there is no barrier to the solvation of this species.[8]

4.4 Transition States With Halogen-Magnesium Primary Interactions

As mentioned previously, the assumption made in all approaches to the study of GRF is that the only possible reaction channel is one in which the halogen interacts with the magnesium first, possibly liberating a carbon radical, possibly embarking down an ionic reaction pathway. In this section, this assumption is not questioned and known transition states are explored using new methods. Transition states here are presented in order of increasing energy according to the best common method and basis set combination. That is, the combination for which the full data set is available (MP2/LANL2DZ, X=Br).

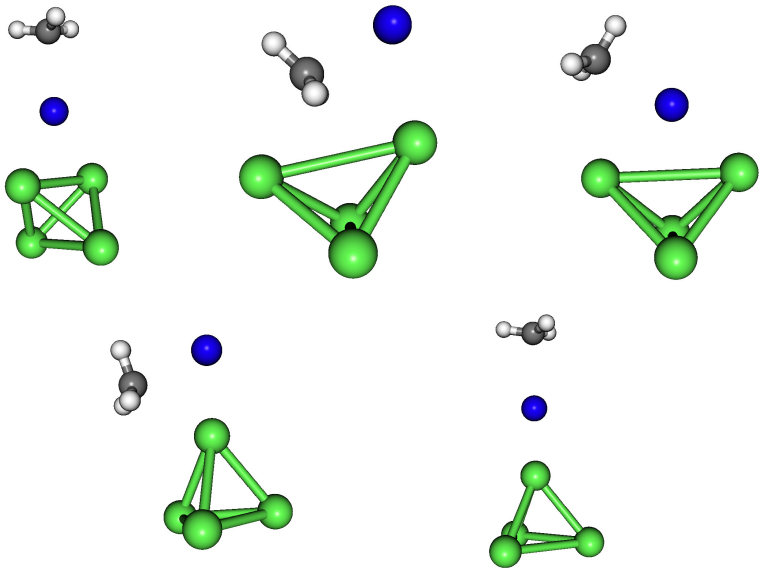

Figure 4.15: The transition states from the top left to the bottom right are (where R is a methyl group) inspected in sections 4.4.2, 4.4.3, 4.4.4, 4.4.1 and 4.4.5 respectively.

4.4.1 A Transition State Derived from General Oxidative Addition (TSI)

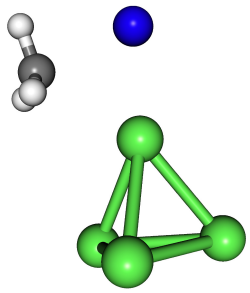

Figure 4.16: The geometry of the transition state derived from general oxidative addition (TSI hereafter).

A general oxidative addition mechanism is more than likely to be the first considered by any chemist upon inspection of the reactants and products of GRF. According to Occam's razor, this is the most feasible mechanism of all (as it resembles very closely the mechanism of reaction for a single Mg atom with a methyl halide), with a reasonably obvious transition state structure (referred to as TSI-X where X is a halogen present hereafter as homage to the insertion mechanism it reflects which was first investigated by Davis[40]). And it is the lowest in energy across the series of calculations involving TSI-Br and the MP2/LANL2DZ method/basis set combination is used. Each transition state in this section is featured as point along a reaction pathway, frontier orbitals are considered and the region surrounding the R group is investigated using magnetic shielding calculations.

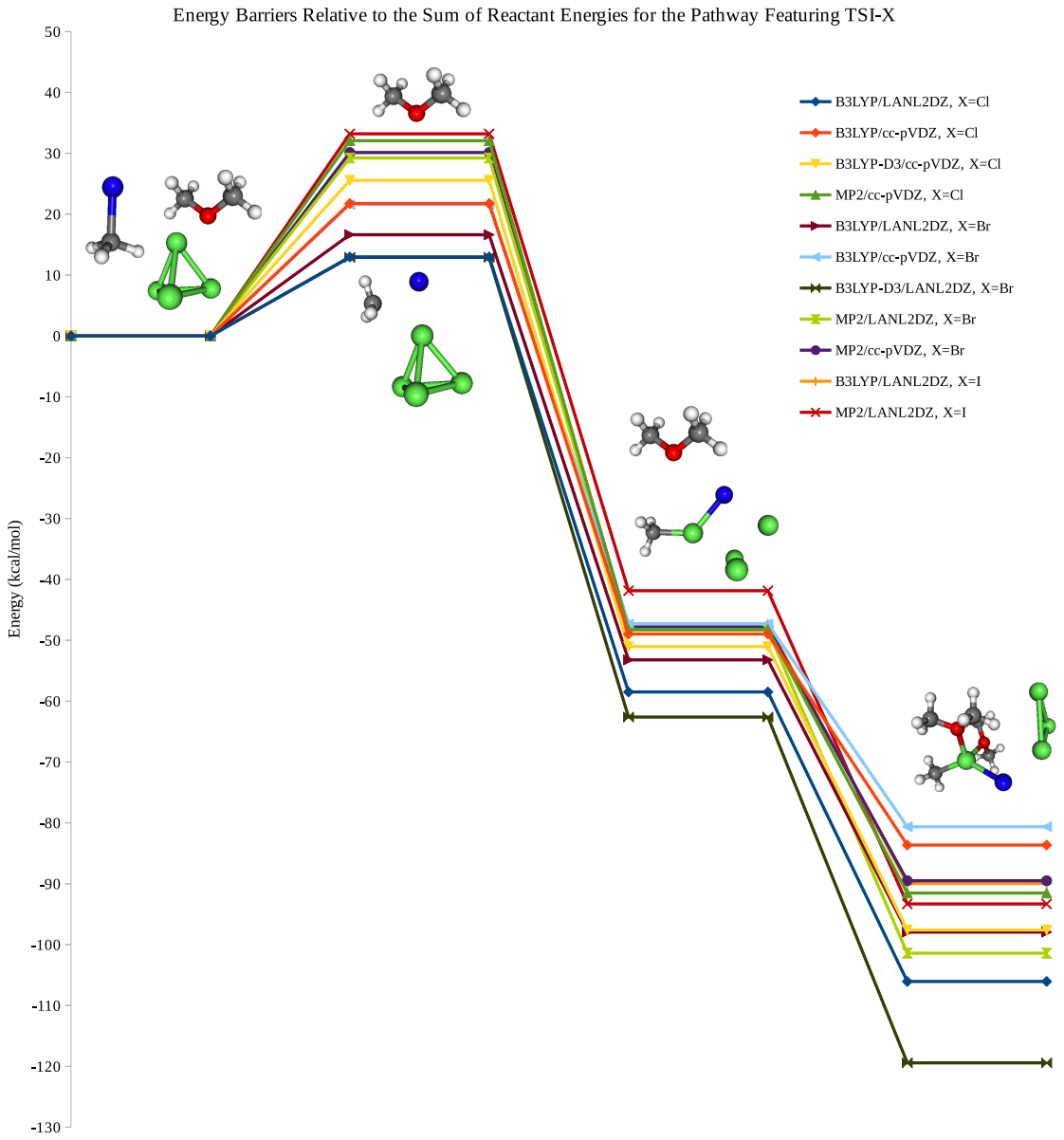

Figure 4.17: A graphical representation of the energy barriers encountered along the pathway passing through TSI en route to forming the liberated Grignard reagent, with images indicating the geometry corresponding to each platform.

The manner in which this pathway is presented is not intended to place any doubt upon the work of Garst *et al*, for there is little doubt that it is entirely feasible for the CH_3 pseudo-radical species to move into the reaction media and become a free radical, in fact, there is some evidence to support this, as is described shortly.[3,6,41,42] The possibility is not studied directly as it offers little to the overall mechanism for the removal of the Grignard reagent from the metal surface, and minima on the potential energy surface for Mg_4X are so plentiful it would not be a prudent use of time to

identify the one with the lowest overall energy, especially when one considers that the cluster itself is used to approximate a full solid lattice. The intermediate complex between transition state and product is generated by simply forming a bond between the carbon atom and node of the magnesium solid lattice and increasing the C-Mg-X bond angle.

Entropy and Gibbs free energy are calculated as relative values by subtracting the sum of each quantity taken from the frequency calculation performed on the reactants. This is performed at each step of the reaction, each time subtracting the same value to keep the reported quantities presentable on in the same graphic for comparison. For example, the transition state in the pathway concerning halogen X investigated with method/basis set combination M/B the thermodynamic value for the reactants containing X at M/B (together with solvent and magnesium cluster at M/B) was subtracted from the value calculated for the transition state.

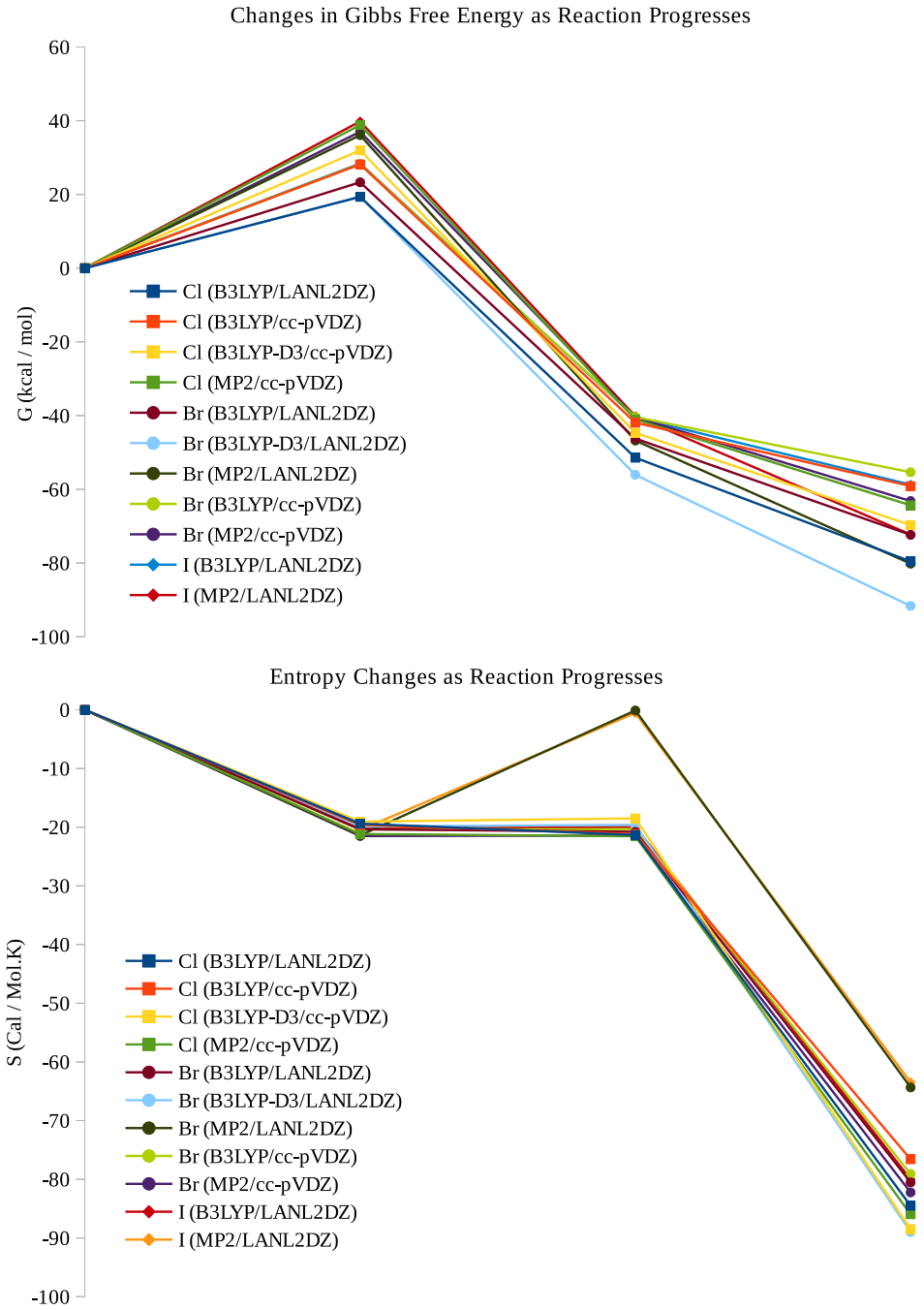

Figure 4.18: Gibbs free energy and entropy profiles for the reaction pathway passing through TSI. Along the x-axis the points are (relative to the sum of the thermodynamic values of the reactants); reactants, TSI-X, the local minimum, and the solvated, liberated Grignard reagent.

Inspection of figure 4.18 reveals that at 298.15 K, all transformations are spontaneous except, as was always to be the case, the formation of the transition state from the reactants, with the step involving the solvation of the local minimum perhaps less favourable than one may have expected, but favourable nonetheless. The spon-

taneous removal of the Grignard reagent from the magnesium surface is shown here to not be an entropy driven process, with ΔS being a negative quantity for all points along the reaction surface (within most method/basis set combinations). That is, within the approximation neglecting all solvent effects along the pathway and only including solvent contributions retrospectively as constant values to be added at all points other than the last including the liberation of the R-Mg-X fragment, there are no entropically favourable steps, but also none which are not spontaneous at room temperature if the outlying MP2/LANL2DZ results are ignored. The exothermic nature of the reaction is implied by the results seen here.

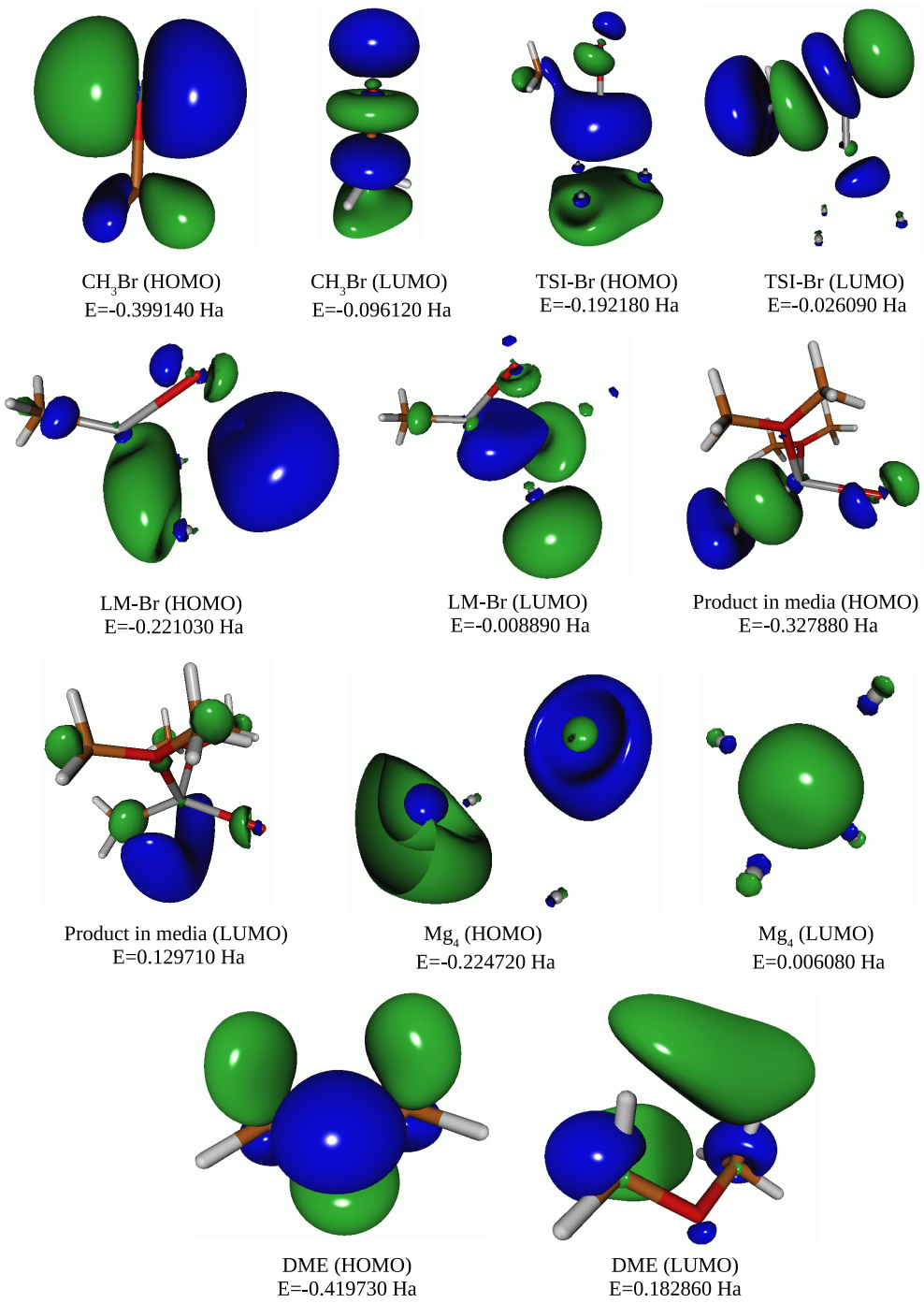

Figure 4.19: Frontier orbitals for all species included in the reaction pathway, together with orbital energies (Ha)

Figure 4.19 showcases the frontier molecular orbitals for all species involved in the reaction pathway. These go part of the way towards explaining the observed trends. The HOMO in the transition state could not be any clearer in indicating a bond forming between the R group and the magnesium and the subsequent formation of the geometry corresponding the local minimum. It is common practise in

inorganic chemistry to use the HOMO-LUMO gap pas a parameter by which to measure the relative stability of complexes. In this case, the order is exactly that which one may expect, TSI-Br $<$ product in media $<$ LM $<$ CH_3Br.

All notable interactions experienced by the R-group at the first stage of the reaction are now investigated using magnetic shielding calculations equivalent to those in section 4.1. The chosen bonds are as follows: for CH_3X; C-X; for TSI-X, C-X and C-Mg.

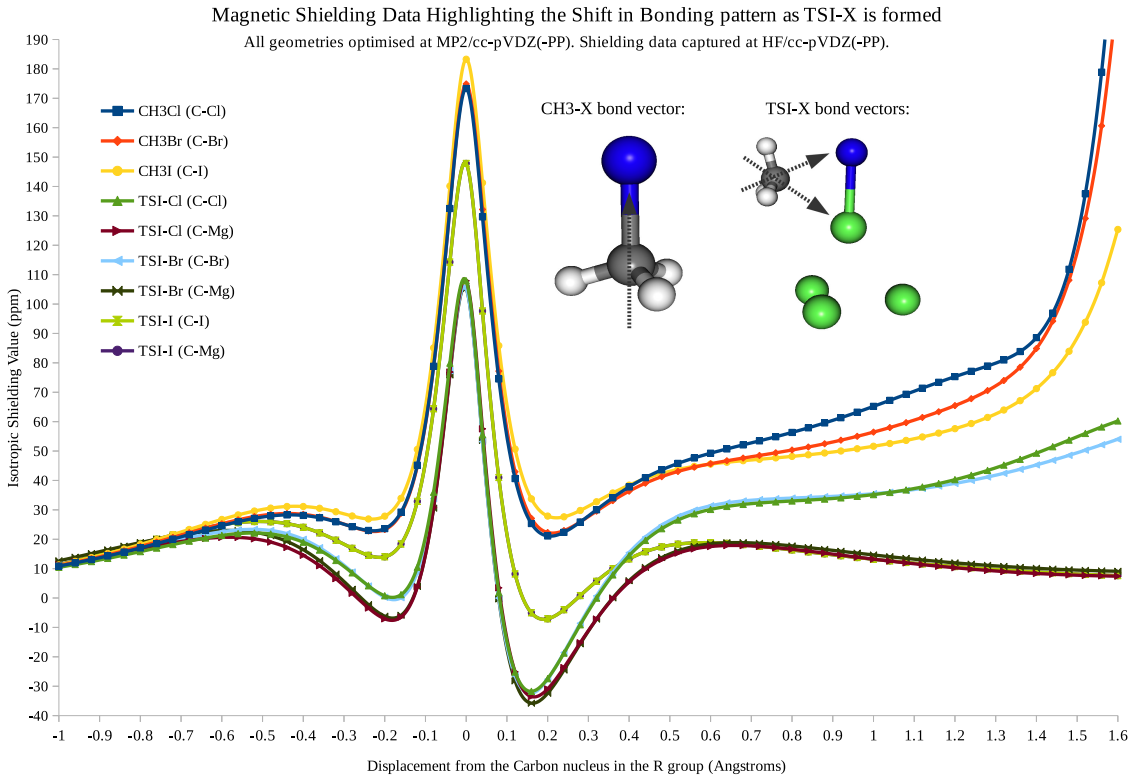

Figure 4.20: Shielding data along the vector beginning 1.0 Å before the Carbon nucleus in the R group and continuing along the C-I and C-Mg bonds for 1.6 Å (one point every 0.04 Å), for the methyl halides and TSI.

Figure 4.20 shows very clearly the variation in bonding as the transition state is formed from CH_3X. A significant decrease in shielding is observed between the carbon and halogen as Mg_4 is introduced and the transition state is formed, compared with the shielding seen along the unperturbed C-X bond. The interaction between the carbon and the magnesium cluster is measured as being extremely weak. Discrepancies between the pre-nucleus shielding is explained by the presence of H atoms on the R group. The program used to generate the co-ordinates of the ghost atoms is included in the appendix.

Garst states that the loss of the majority of the optical activity of an organic halide is evidence of free radical intermediates.[6] Walborsky also provides data wherein the optical character of a Grignard reagent manufactured from pure enantiomeric organyl halides becomes increasingly racemic along the sequence X=Cl, Br, I.[4] The plots seen in figure 4.20 provide some insight into this as there is a dramatically reduced interaction between the R group and the iodine atom, to the point that the line is almost lost amongst the C-Mg data. The shielding pattern at the carbon nucleus also varies significantly from the others, with increased isotropic shielding seen close to the centre of the carbon atom.

4.4.2 A Transition State Derived from a Vertical Approach to a Lattice Edge

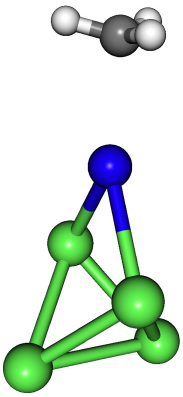

Figure 4.21: The geometry of the transition state derived a vertical approach to lattice edge (TSVE hereafter).

Figure 4.21 shows the first of the transition states taken from general geometric arguments of a cluster, or surface, being in solution with a free and mobile methyl halide. Operating under the assumption that the halogen is the first point of contact with the surface one must decide between the two available sites; edge or node. An edge-on approach is considered here, where first contact has been made while the C-X-Mg bond angle is 90°. The co-ordination of the halogen to two nodes on the solid surface induces a lengthening response in the C-X bond, with little doubt that this ends in the dissociation of the C-X bond and the liberation of a free radical. This is exactly the type of mechanism which vindicates much of Garst's work in radical trapping and by-product analysis. It is not difficult to see how this structure could very quickly become the local minimum described in the preceding section, and indeed, how it is

linked to a second transition state, the one discussed in section 4.4.4. This transition state has been studied extensively by Tulub *et al* al for a number of R groups but, again, for no halogen heavier than chlorine.[7,9] Further studies on this transition state have been performed by Xu *et al* more recently. Though limited in both R group and halogen, considering only a small number of bromine-containing structures, it includes a wide study of local minima and ground state geometries optimised using a single DFT functional. The clusters considered range in size from a single magnesium atom up to Mg_{10}, they report a good balance between computational expense and calculated energies using the Mg_4 cluster.[10]

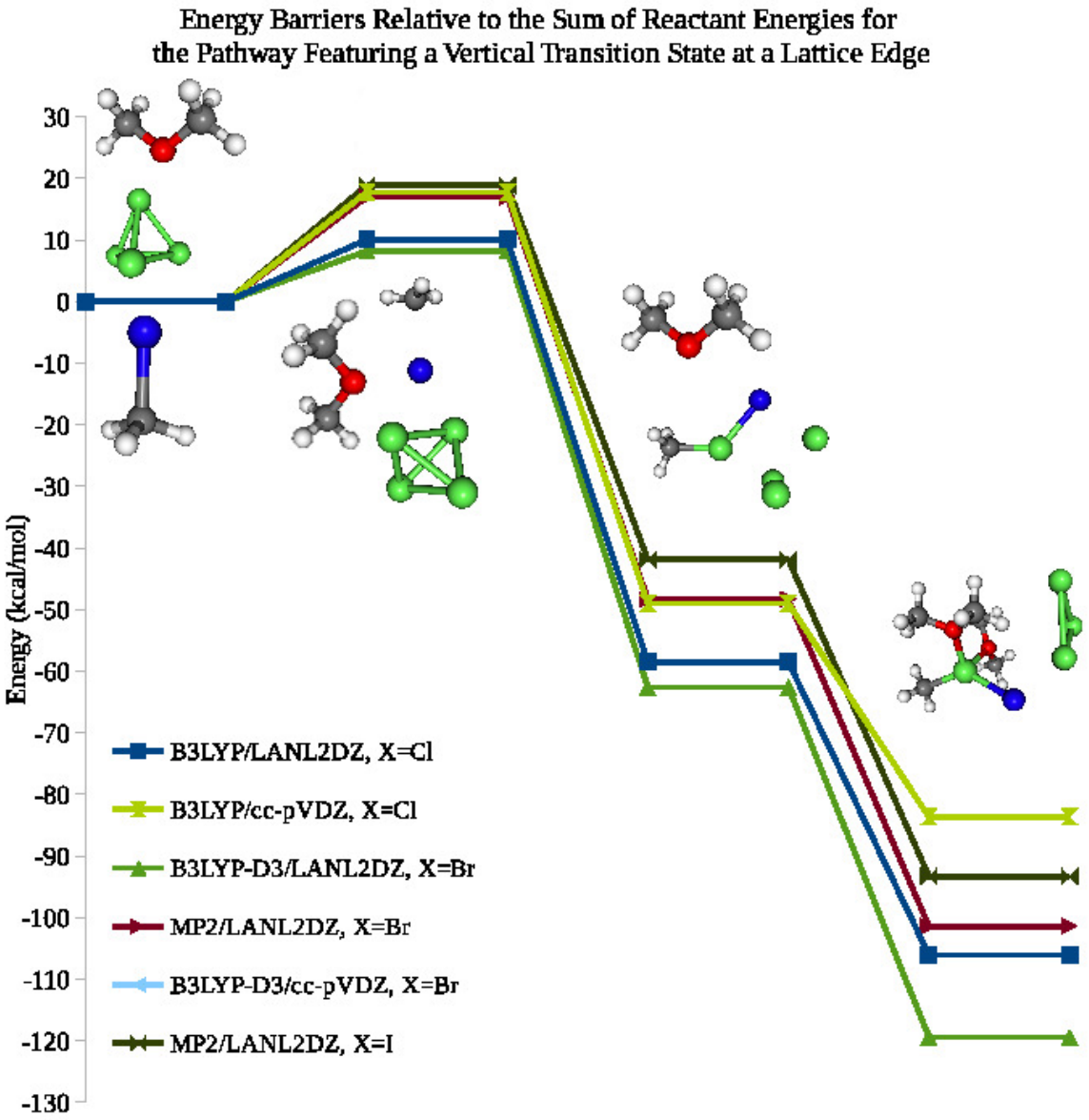

Figure 4.22: A graphical representation of the energy barriers encountered along the pathway passing through TSVE en route to forming the liberated Grignard reagent, with images indicating the geometry corresponding to each platform.

Upon the formation of the transition state in figure 4.22, one may look ahead to the geometry corresponding to a local minimum between it and the liberated Grignard reagent. For this to form, which in this case it must, the methyl group must move into the reaction media and return to an identical site on the solid surface, or, at the very least remain weakly bound to the halogen and move in the general direction of either of the two magnesium nodes bound to the halogen. While, the latter is certainly a possibility, the chance of it being a reasonable proposition diminishes as the radius of the halogen atom decreases from iodine down to chlorine.

Assuming this weak interaction is enough to retain the methyl group within reasonable distance of the halogen and prevent any inversion and rotation, and as such remove its “free-radical” status and render it being some pseudo-radical species, this supports Walborsky’s work involving optically biased products using heavy halogens, and racemic mixtures of products using chlorine.[4]

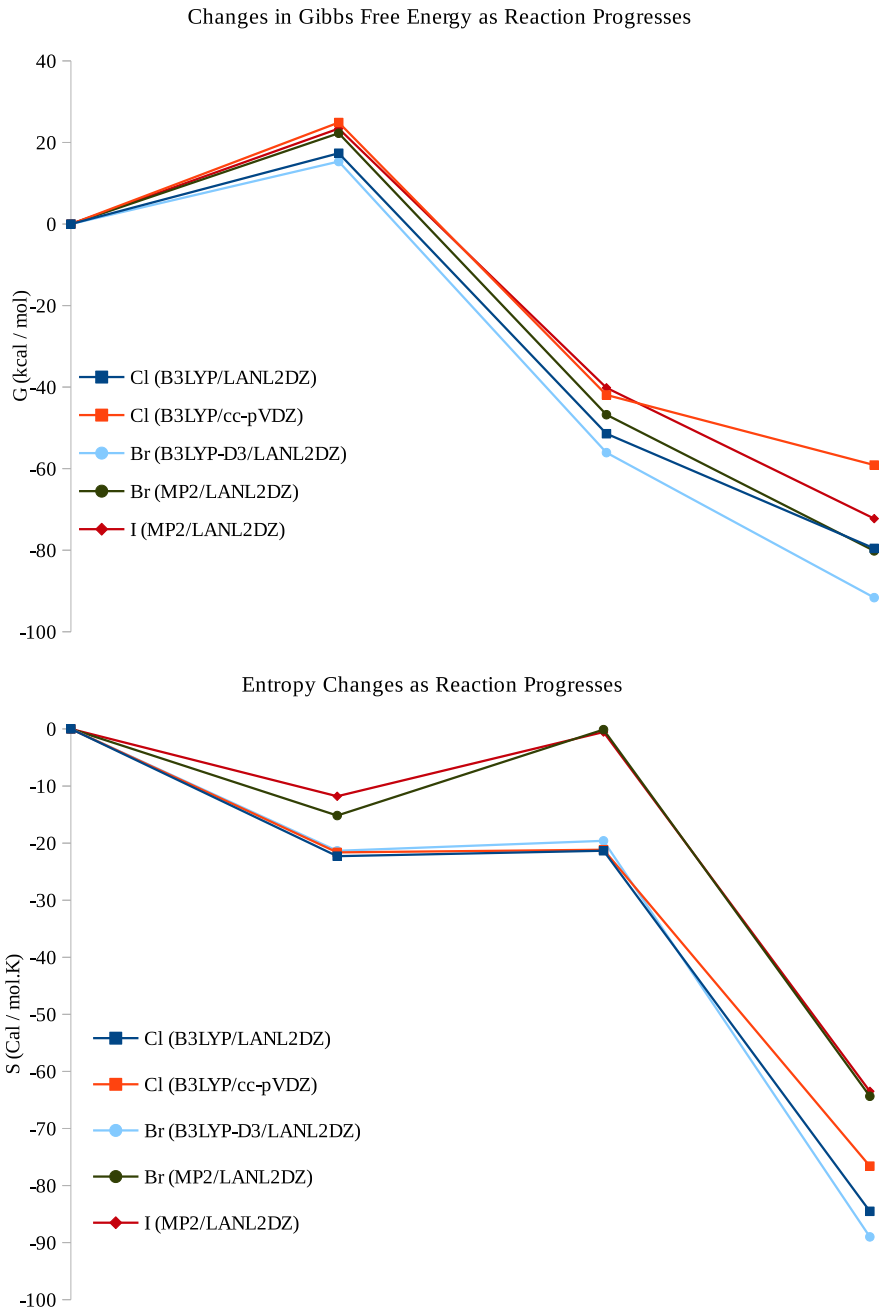

Figure 4.23: Gibbs free energy and entropy profiles for the reaction pathway passing through TSVE.

In figure 4.23, it is seen that in all cases, the transformation of the transition

state into the structure corresponding to the local minimum is an entropy driven process, which is in contrast to that seen in the preceding section. It should be noted, though, that the influence of the entropy change on the Gibbs free energy is extremely small given the similar S values for the transition state and local minimum. All transformations post-transition state are spontaneous.

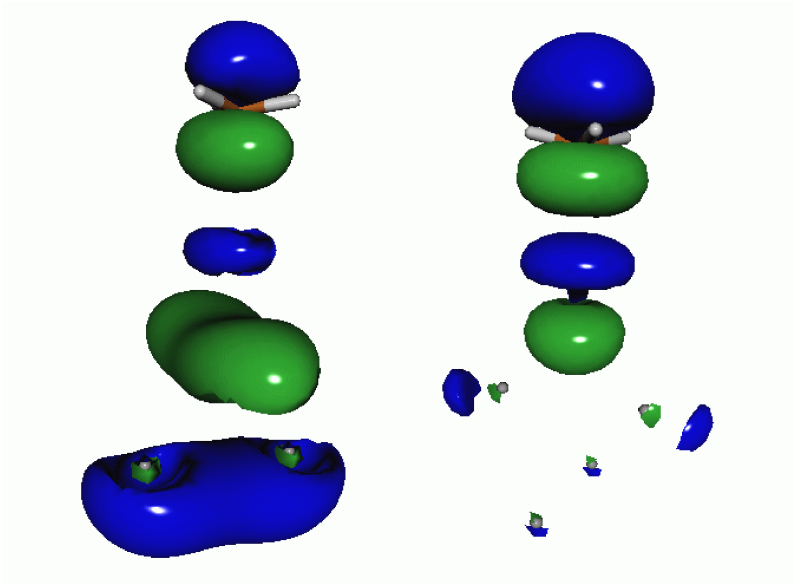

TSVE-Br (HOMO): -0.175930 Ha TSVE-Br (LUMO): -0.021920 Ha

Figure 4.24: Frontier orbitals for TSVE together with orbital energies, calculated for X=Br and a geometry optimised at the MP2/LANL2DZ level.

The frontier orbitals shown in 4.24 show powerful antibonding interactions between the halogen and methyl group, corresponding to a breaking bond. The phase match between the carbon and magnesium in the HOMO is suggestive of the expected motion of the methyl radical, in the case of heavier halogens which may or may not lend a binding and somewhat stabilising effect to the radical in the form of large, diffuse orbitals. The data presented for this transision state, along with its easily accessible geometry suggests it may play a significant part in GRF. As we see throughout these studies, the likelihood of there being one dominant transition state for GRF is slim. So far we have two similar transition states with similar energies.

All notable interactions are now studied using NMR shielding calculations with ghost atoms printed along vectors between atoms. In this case, the only one of interest is the interaction between the carbon and halogen and how that varies along the series; chlorine, bromine and iodine.

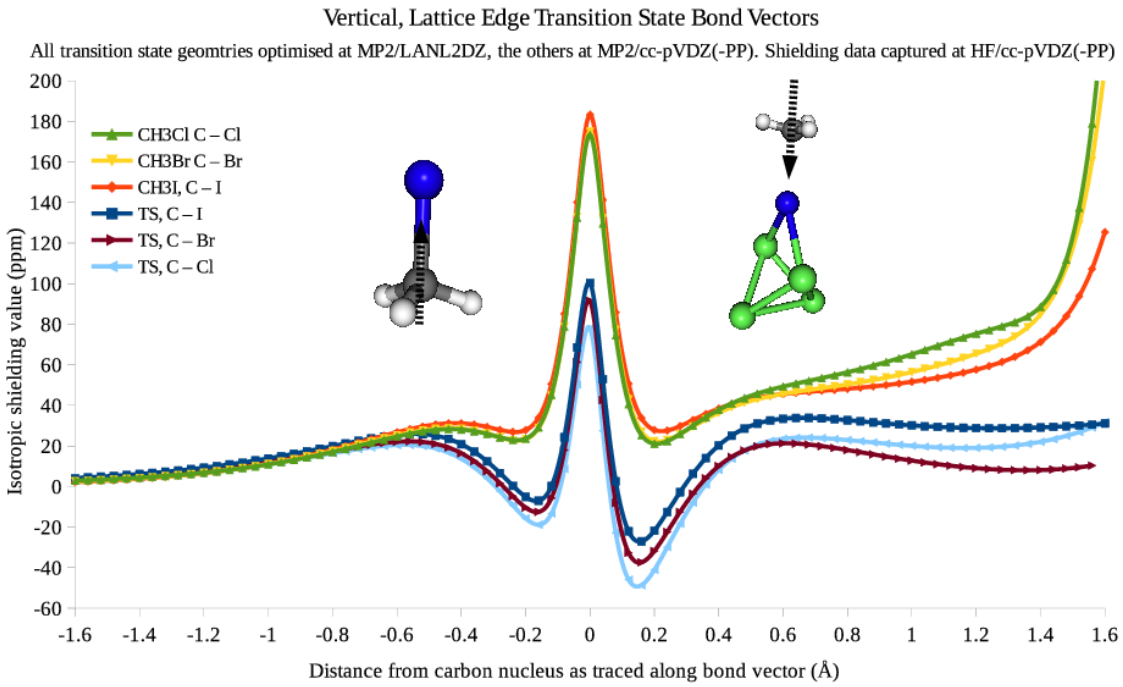

Figure 4.25: Shielding data along the vector beginning 1.6 Å before the Carbon nucleus in the R group and continuing along the C-I bond for 1.6 Å (one point every 0.04 Å), for the methyl halides and TSVE.

It is known from basic NMR theory that if one places a nucleus of a non-electron withdrawing atom in the vicinity of an electronegative atom or group, it will be "deshielded". To deshield an atom or group is to increase its chemical shift by the removal of electron density, magnetic induction or perhaps by some other effect. So, it should be noted that in some cases where the shielding calculations are carried out on ghost atoms in close proximity to chlorine atoms, the values may be distorted and not give a representation of bond strength but rather of the electron withdrawing power of a lighter halogen. Looking at figure 4.25, We see that this is likely to be the case. Interestingly, shielding between carbon and iodine in the transition state is far higher than both chlorine and bromine at all points, indicating a higher density of electrons between the two. In fact, the shielding in the transition state is not at all far from the shielding in methyl iodide. This lends some valuable support to the idea of an ongoing carbon iodine interaction as the local minimum corresponds to an unsolvated and as yet bound-to-the-surface Grignard reagent.

4.4.3 A Four Center Transition State

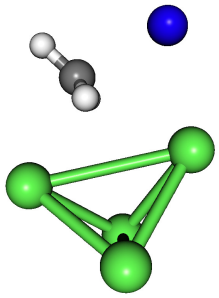

Figure 4.26: The geometry of the transition state dependent on four centres (TS4C hereafter).

While this is included in the section for transition states formed by the halogen first coming into contact with the magnesium cluster, perhaps followed by the carbon, there is little about the structure itself which gives a clue as to whether it is the carbon or iodine which partakes in the earliest stages of co-ordination. This transition state has been studied by both Tulub and Xu as a result of accepting the proposition that because the halogen is bigger, and more electron dense with a lower co-ordination number, it must be the first point of contact. As a result, it is presented with the others generated using that approach. Much like the vertical transition state seen in section 4.4.2, this geometry is attainable through simple rotation of the methyl halide at the lattice edge. However, unlike its vertical counterpart, this transition state does not seem as though it is likely to lead to the formation of the Grignard reagent at a surface we have become accustomed to. That is, where we see in the preceding transition states a very clear picture of how the carbon-halogen bond may break and how, in the long term, the product is formed, here the only obvious course for the reaction to take does not lead to the products we are interested in, i.e, the opening of the cluster to form a flat diamond with the methyl and halogen at opposite ends. This is the case for all halogens.

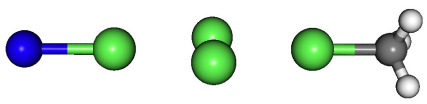

Figure 4.27: Flat product with kite shaped magnesium cluster separating the halogen and R group.

Figure 4.27 shows the product a pathway traced through the transition state seen in figure 4.26. Clearly, there is no possible way to liberate the R-Mg-X sequence from this structure without forcing the proverbial square peg through the round hole. The solvation of the magnesium atom bound to the halogen restores something approaching tetrahedral geometry to the cluster as presented in Tulub's work, and as such, potentially provides a route back to the Grignard reagent at the surface.[7] The computational expense involved in scanning the surface as the halogen rotates around the magnesium and sits back into the geometry we expect to be present before the product can be formed is simply unjustifiable for this study.

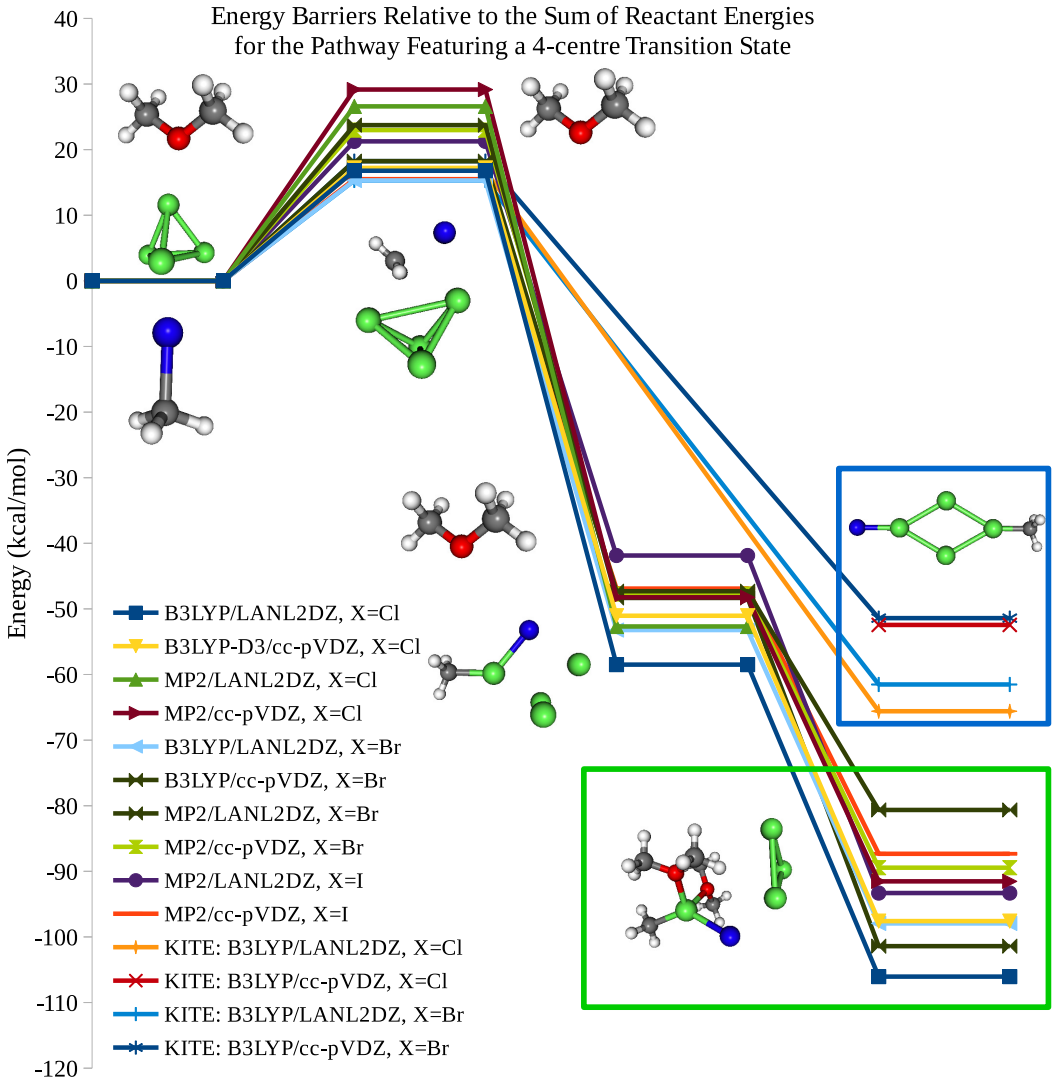

Figure 4.28: A graphical representation of the energy barriers encountered along the pathway passing through TS4C en route to forming the liberated Grignard reagent or the planar molecule, with images indicating the geometry corresponding to each platform.

The presentation of the pathway of which the flat product is a feature is not intended to mislead. It is simply placed in the same column as the solvated product for clarity; were it placed with the local minimum, the resolution would suffer. As can be seen in figure 4.28, the kite shaped, flat product is of a similar energy to the Grignard reagent at the surface, so it is obvious how this complicates the mechanism. To solvate the appropriate magnesium atom in the flat product and form the necessary complex to remove the Grignard reagent, one would certainly have to scale an energy barrier of some sort, more than likely rather a large one given the steric effects of the solvent molecules.

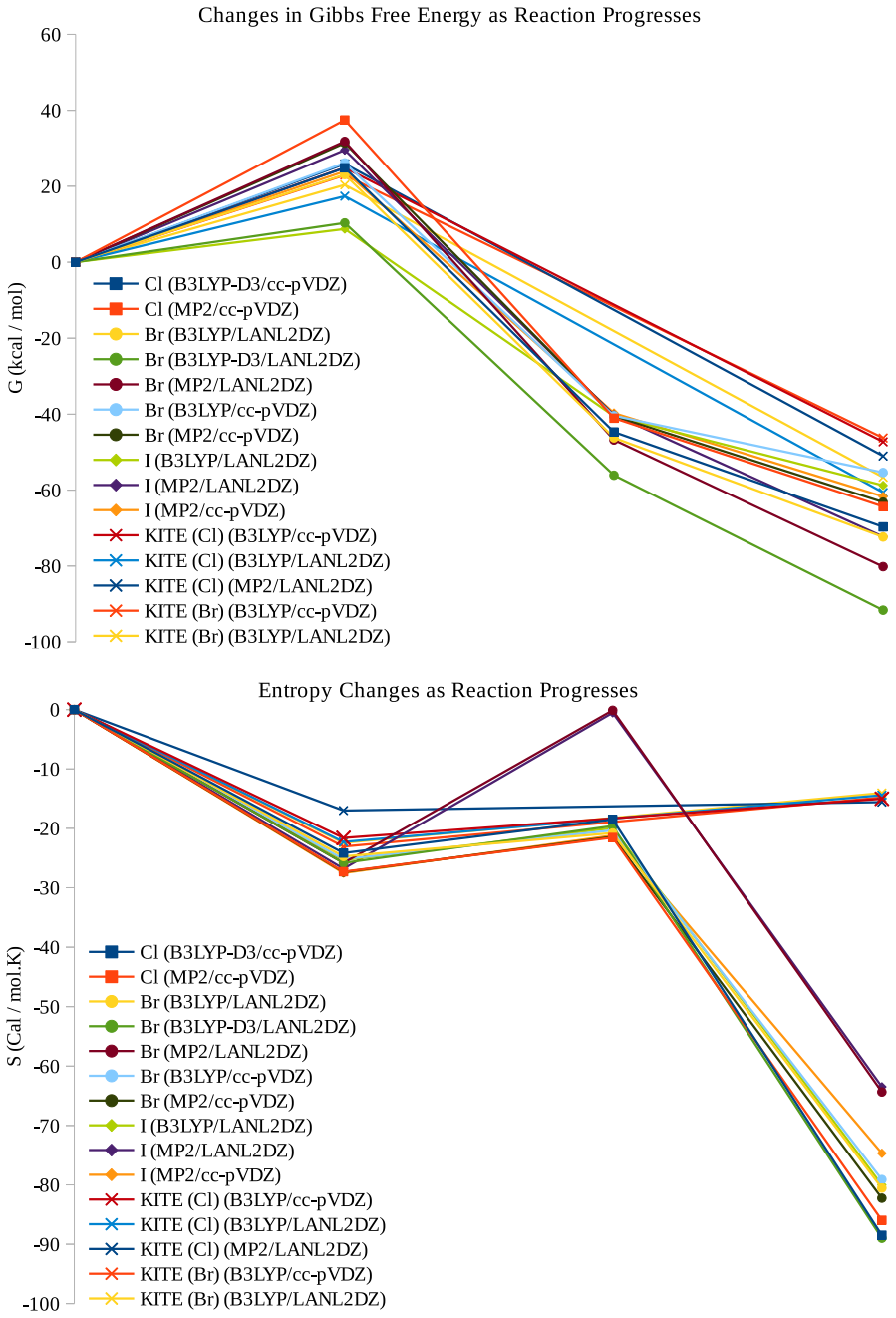

Figure 4.29: Gibbs free energy and entropy profiles for the reaction pathway passing through TS4C, including the flat product indicated by KITE in the legend.

Figure 4.29 indicates that all species are spontaneously formed along the pathway including the four-centre transition state at room temperature, with the formation of the final product from the stable intermediate, the Grignard reagent still coordinated to the magnesium surface, seemingly less spontaneous than the preceding step. The Gibbs free energy profile of the reaction is very similar to the one seen previously, the Entropy profile is more interesting. Unlike the previous transition state, here

it is seen that the conversion from transition state to local minimum is entropically favourable. The conversion of the transition state to the flat cluster from which we have difficulty forming the desired R-Mg-X sequence, is more entropically favourable than the local minimum, and the reaction is thus forced in that direction.

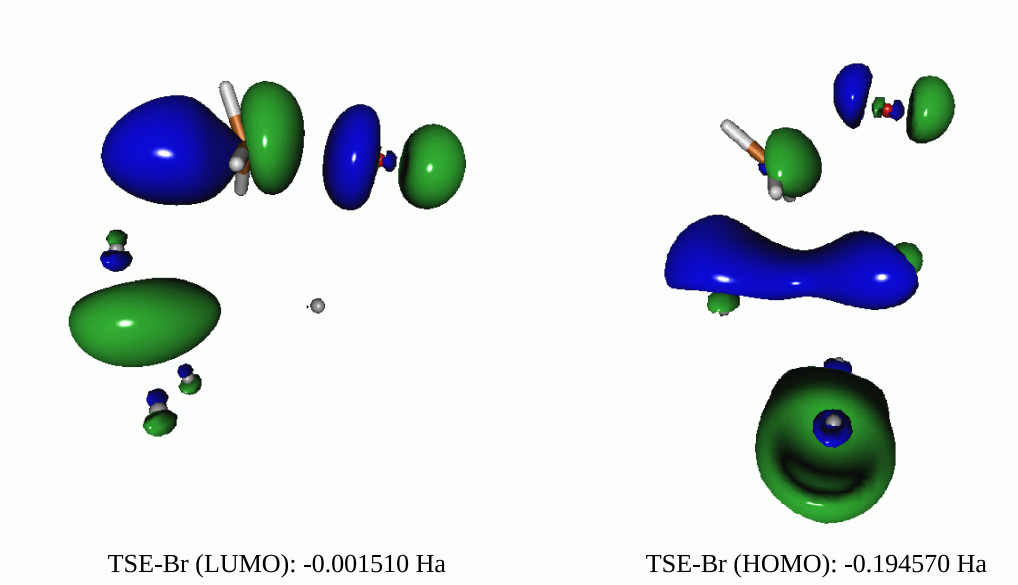

TSE-Br (LUMO): -0.001510 Ha TSE-Br (HOMO): -0.194570 Ha

Figure 4.30: Frontier orbitals for TS4C together with orbital energies, calculated for X=Br and a geometry optimised at the MP2/LANL2DZ level.

Figure 4.30 shows a weak bonding interaction in the HOMO between the carbon and magnesium cluster. The MO picture suggests an inversion of the methyl group, which is not to be unexpected. If we assume (as is most likely) that after the opening of the cluster the methyl group is retained at the surface, the non-pure optical character of the product mixture observed in experimental studies is unexpected, and suggests this is a very minor pathway in the overall reaction scheme.

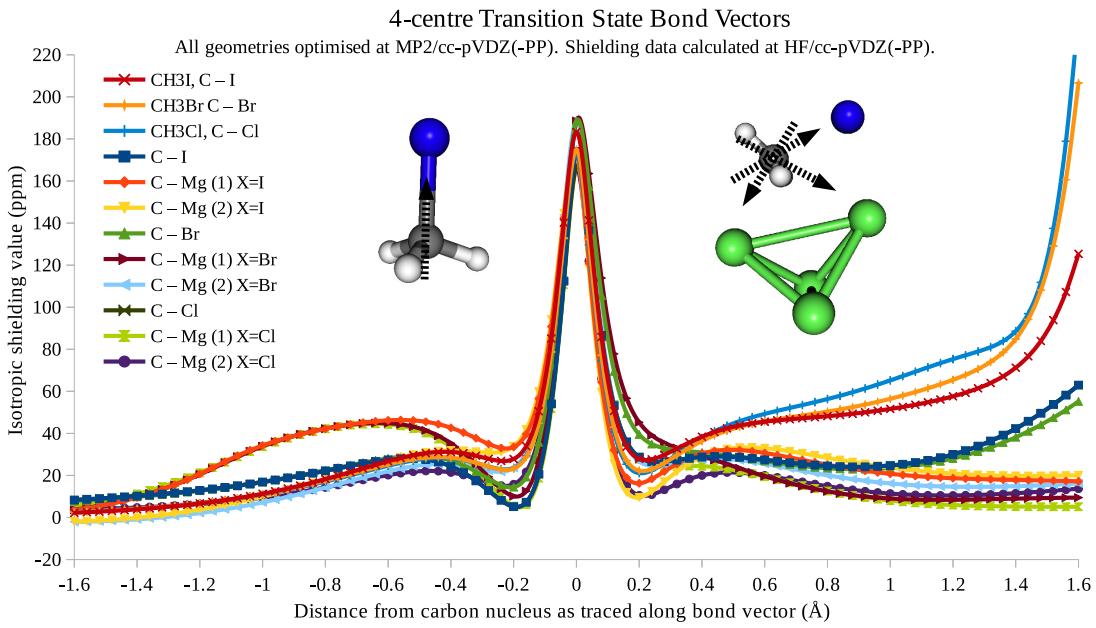

Figure 4.31: Shielding data along the vector beginning 1.6 Å before the Carbon nucleus in the R group and continuing along both C-Mg bonds, and the C-I bond for 1.6 Å (one point every 0.04 Å), for the methyl halides and TS4C. Labels (1) and (2) for C-Mg interactions are assigned clockwise beginning at the C-I bond vector.

When used in conjunction with figure 4.30, figure 4.31 indicates that the interactions between the carbon and the magnesium atom closest to itself and the one closest to the halogen atom are quite similar despite distortion effects from the electronegative halogen atoms on the calculated shielding values. This breathes a small amount of life into the idea that, perhaps upon the sufficient lengthening of the carbon-halogen bond, and some rotation of the halogen atom, one may form something resembling the transition state in section 4.4.1 and consequently form the stable intermediate containing the R-Mg-X sequence.

4.4.4 A Transition State Derived from an Angled Approach to a Lattice Edge

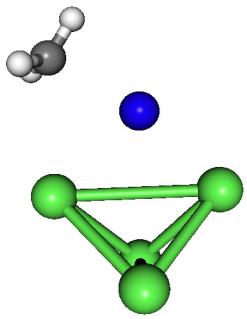

Figure 4.32: The geometry of the transition state derived from an angled approach to a lattice edge (TS4C hereafter).

This transition state is extremely similar to the one discussed in section 4.4.2. So similar, it is entirely possible that it is a feature of the same reaction pathway. But it has been considered as a transition state in its own right. As for the vertical transition state, there is the possibility that there is an ongoing interaction between the adsorbed halogen atom and the methyl group which is liberated as either a radical species, or as some weakly bound pseudo-radical. If the latter, it stands to reason that the two may well be features of the same reaction channel. If the former, the possibility still exists though diminished as the methyl radical would have to approach the cluster from an unfavourable direction (right by the halogen). Furthermore, for this to be a second saddle point along a potential energy surface, a local minimum would have to be found between the two, otherwise there is no justification for two structures, both with single imaginary frequencies in the Hessian matrix within the same reaction profile.

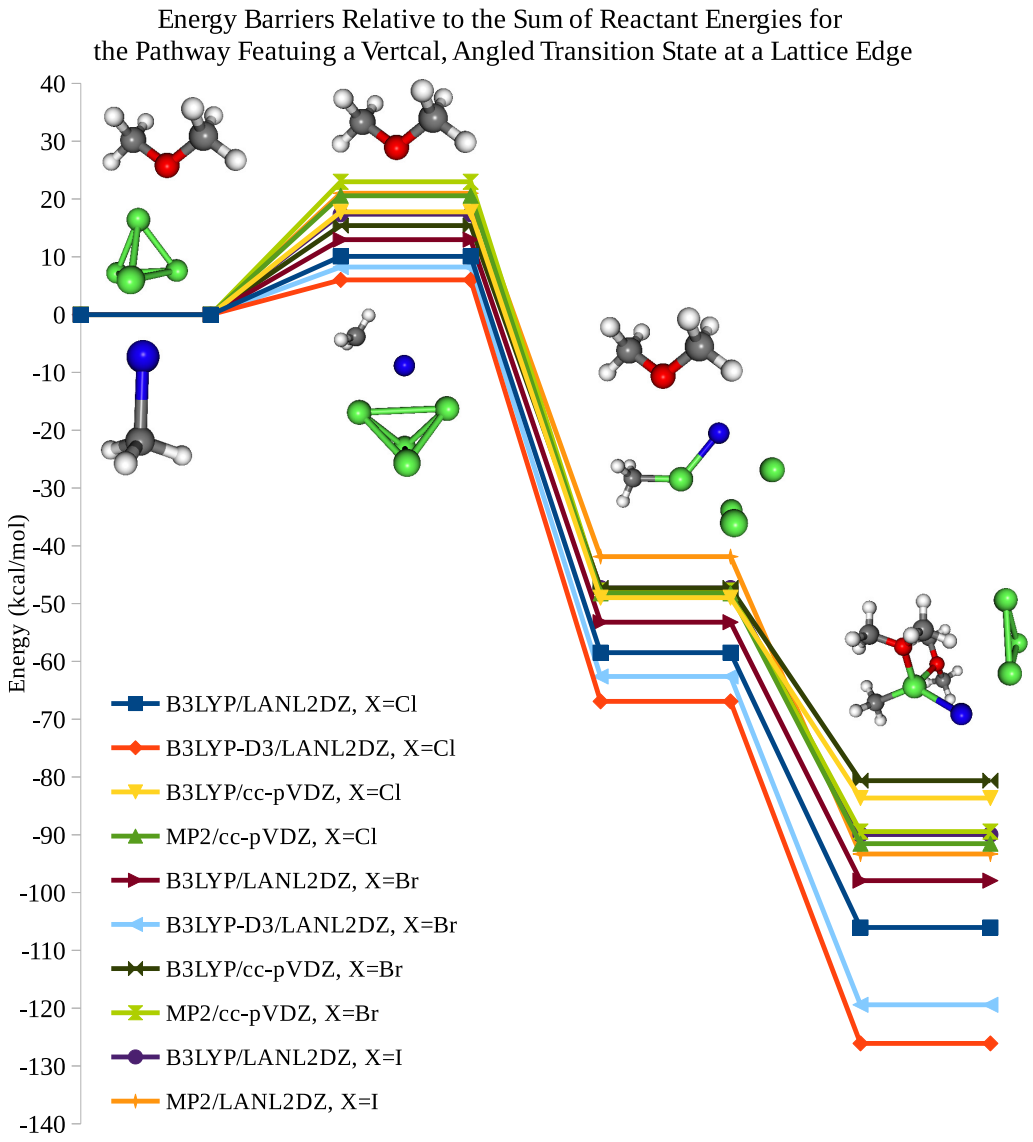

Figure 4.33: A graphical representation of the energy barriers encountered along the pathway passing through TSAE en route to forming the liberated Grignard reagent, with images indicating the geometry corresponding to each platform.

The initial barrier to the reaction is greatest where iodine is the halogen present, then bromine, and finally, chlorine. This is in line with what is expected given the trend in atomic radii moving through chlorine, bromine and iodine, and the location of the methyl group.

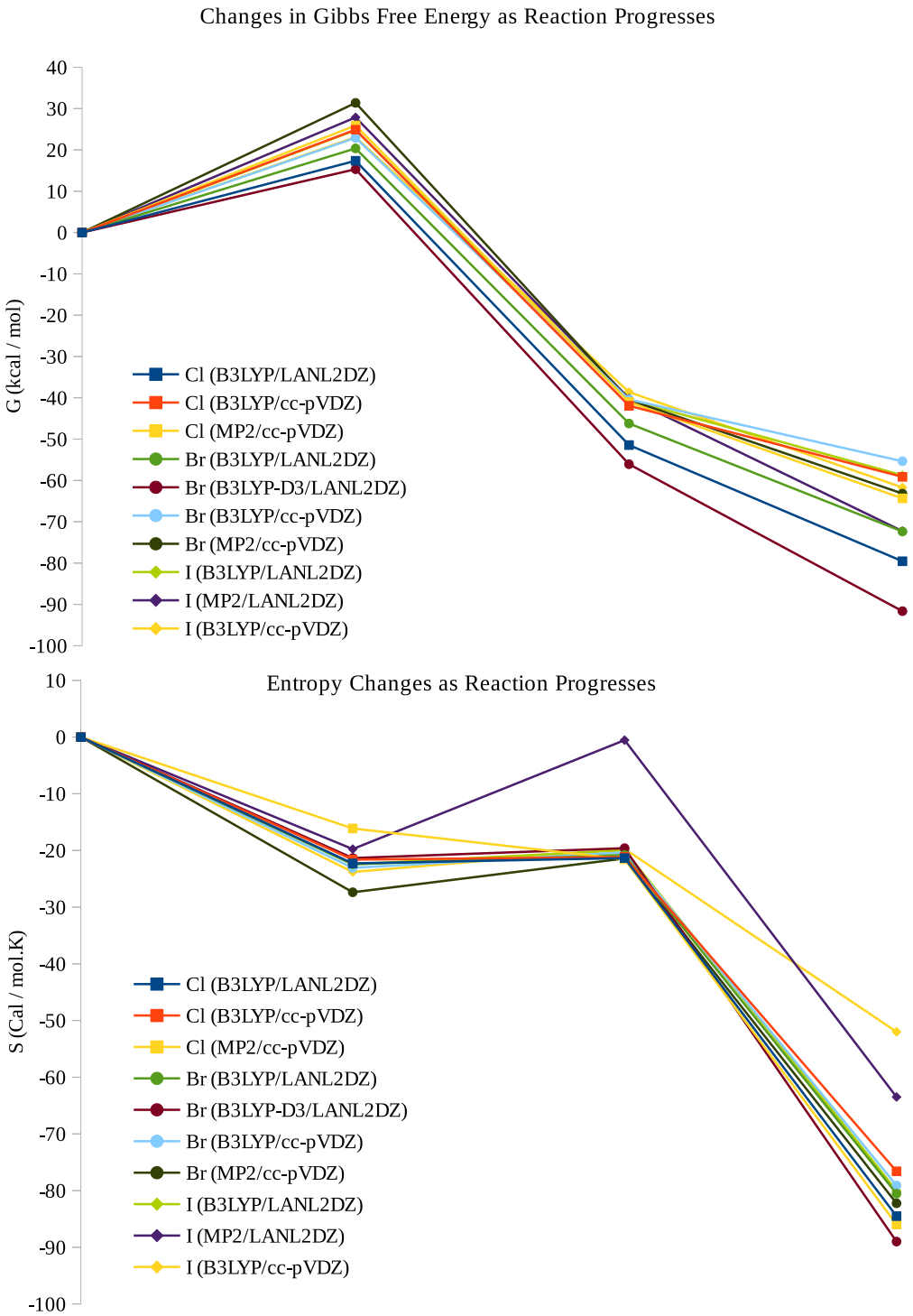

Figure 4.34: Gibbs free energy and entropy profiles for the reaction pathway passing through TSAE.

As has been the case in all reaction pathways, all transformations other than the initial formation of the transition state are spontaneous. Figure 4.34 also indicates that the change occurring in the system as we trace from transition state to local

minimum is one which is entropy driven (in most calculations this is shown to be true, with X=Cl, MP2/cc-pVDZ being the exception). Just as previously, the entropy contribution to the driving of the reaction is likely to be small with the change from transition state to local minimum shown to lie within the region of 0-20 J $mol^{-1}K^{-1}$.

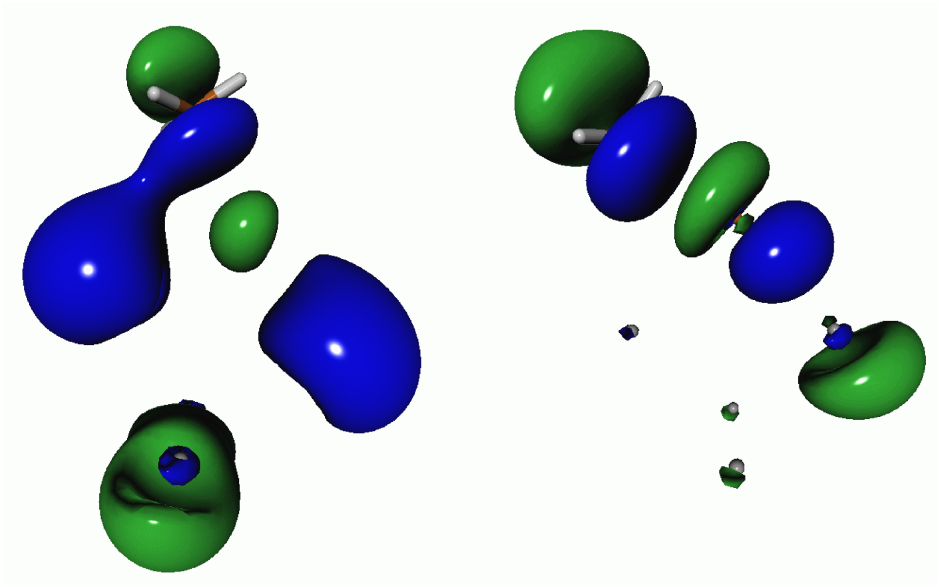

TSVA-Br(HOMO): -0.176790 Ha TSVA-Br(LUMO): -0.014510 Ha

Figure 4.35: Frontier orbitals for TSAE together with orbital energies, calculated for X=Br and a geometry optimised at the MP2/LANL2DZ level.

The frontier orbitals in figure 4.35 could not be more clear, and remove any need for shielding plots to be included. It is beyond all reasonable doubt that this structure and the local minimum between the transition state and product are connected, and thus, it is beyond all reasonable doubt that the transition state is also connected to the products. While this reaction pathway is not the lowest energy in the series considered, it is an excellent example of how a transition state leads to the products in GRF.

4.4.5 A Transition State Derived from a Vertical Approach to a Lattice Node

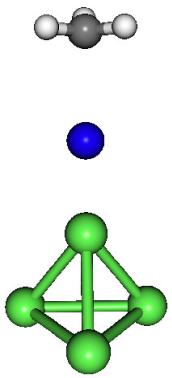

Figure 4.36: The geometry of the transition state derived from a vertical approach to a lattice node (TSVN hereafter).

The transition state shown in figure 4.36 is the node-based version of the transition state discussed in section 4.4.2. The geometry for this transition state is generated again by simple rotation of R-X at the magnesium surface, but in this case, the molecule at the surface is of a different orientation. This transition state represents the most basic of all possible transfers of the halogen atom to the surface and subsequent liberation of the methyl radical. It is as if a wire connects the carbon and magnesium atom and the halogen simply runs down the wire, away from the carbon and begins to form a bond with the magnesium cluster. For this structure to be a transition state along the pathway we are interested in, under the assumption that the methyl radical is entirely free, it must return to the surface at the appropriate location, or alternatively, hijack another site nearby which has been generated by either this pathway, or the one featured in section 4.4.2. Of course, the halogen in this structure is not in the appropriate position for the formation of the minimum and complicates the pathway in a minor way - rotation around the cluster and binding with a second magnesium atom are necessary. It is not unreasonable to expect this to have very little effect on the overall energy of the system.

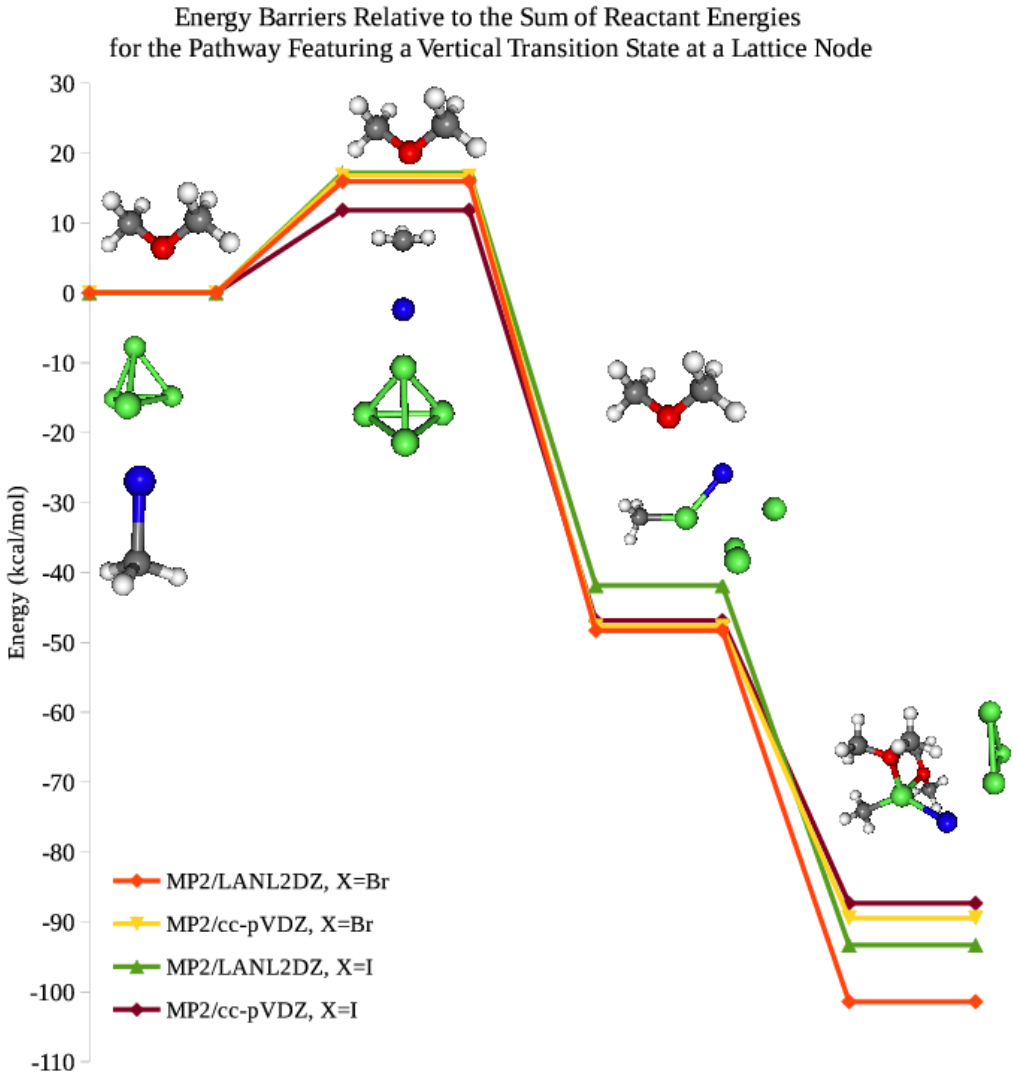

Figure 4.37: A graphical representation of the energy barriers encountered along the pathway passing through TSVN en route to forming the liberated Grignard reagent, with images indicating the geometry corresponding to each platform.

The intrinsic flexibility of this transition state to counteract features of each halogen which may have given some preference to one over the others and find the lowest possible energy renders it rather an uninteresting pathway. Substituting lighter halogens for heavier ones simply lengthens the C-X bond and vice versa, couple this with the halogens all being members of the same group of the periodic table and their consequently inevitable similarities, and similar energy barriers for the formation of the transition states is the expected, and observed, result.

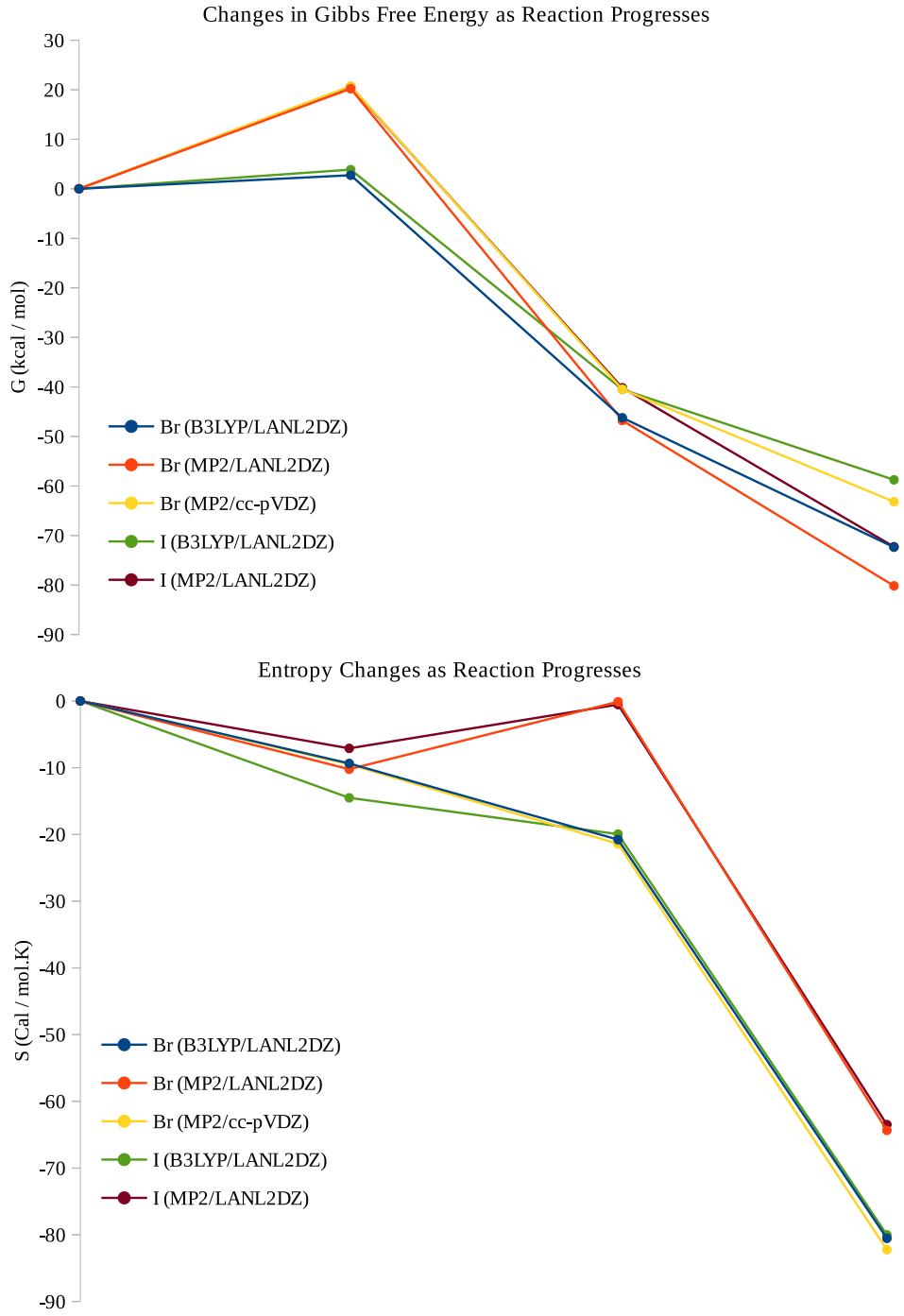

Figure 4.38: Gibbs free energy and entropy profiles for the reaction pathway passing through TSVN.

Ignoring the anomalous MP2/LANL2DZ results in the entropy profile in figure 4.38, the conversion of the transition state to the local minimum is entropically unfavourable. Given their similarities, it makes sense to compare these results with those in figure 4.23, where the entropy values for the local minimum and transition state are extremely similar. It is clear that this is a less unfavourable pathway

in terms of entropy changes, but unfavourable nonetheless. Rather surprisingly, the results gathered using the B3LYP functional indicate a Gibbs energy change from reactant to transition state of only a few kcal / mol, with MP2 calculations indicating larger Gibbs energy changes.

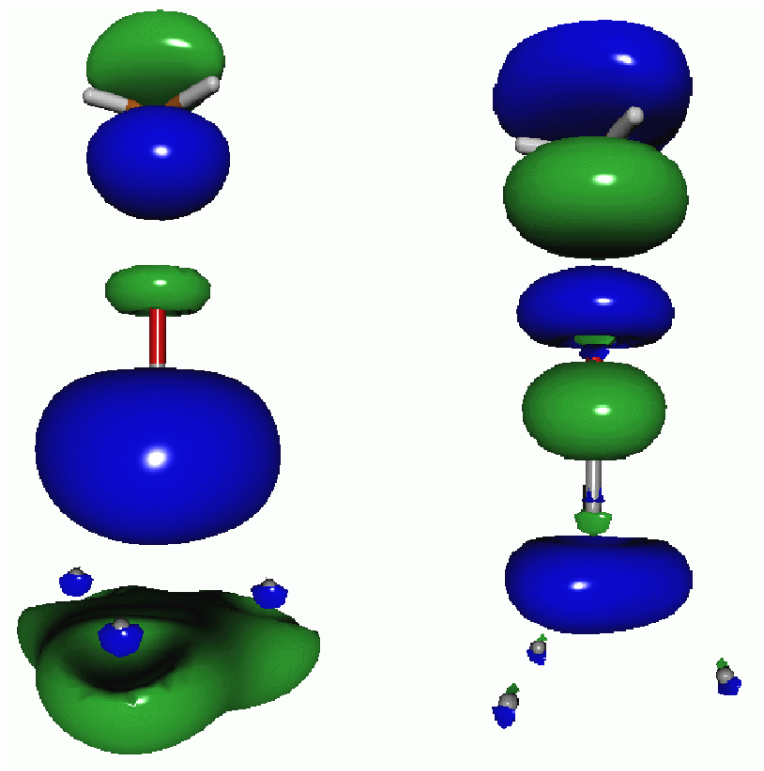

Figure 4.39: Frontier orbitals for TSVN together with orbital energies, calculated for X=Br and a geometry optimised at the MP2/LANL2DZ level.

The molecular orbital picture in shown in figure 4.39 could hardly be clearer in the indication of a breaking C-X bond. Both the HOMO and LUMO display powerfully antibonding interactions between the carbon and halogen along with anti-bonding, but much less anti-bonding, interactions between the magnesium and halogen. By lack of magnesium atoms and other points of transfer for the methyl group, this transition state truly isolates free-radical generation as the only viable way to proceed.

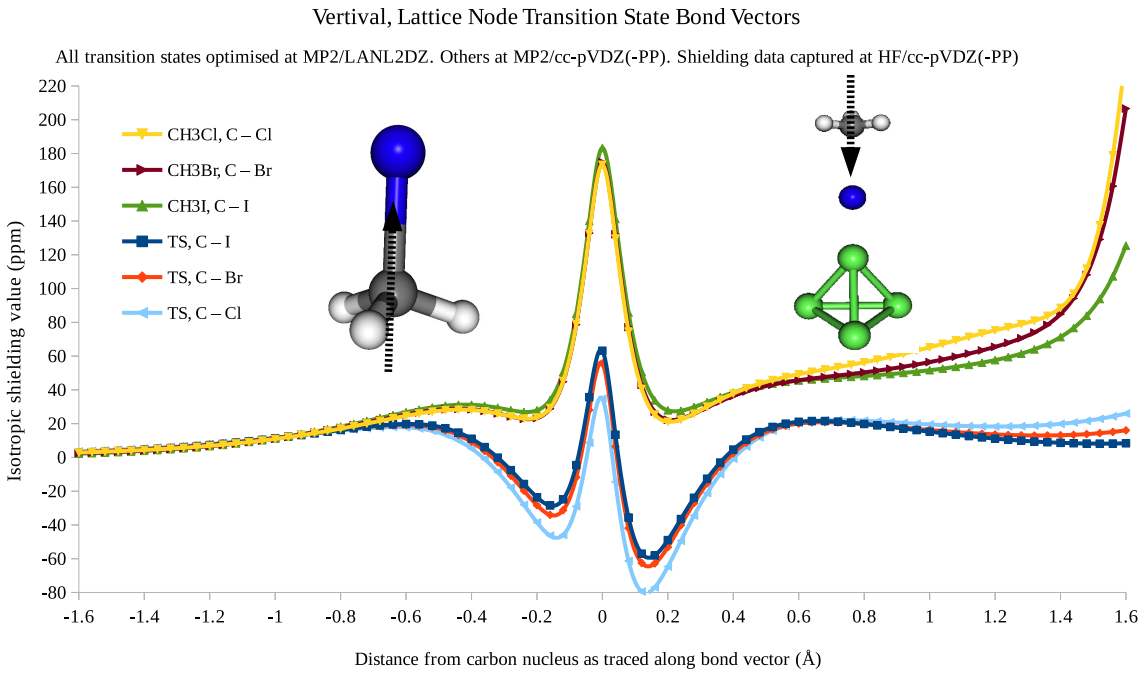

Figure 4.40: Shielding data along the vector beginning 1.6 Å before the Carbon nucleus in the R group and continuing along the C-I bond for 1.6 Å (one point every 0.04 Å), for the methyl halides and TSVN.

The similarities in the shielding patterns of the methyl halide and transition state are exactly as expected upon the lengthening of the bond, and follow almost exactly the same pattern. The lack of electron density and deshielding effects close to the carbon nucleus, and between the nuclei is a sign of the breakdown of orbital overlaps and thus the breaking of the bond. The shielding at the carbon nucleus in the case where the nearby halogen is iodine is significantly lower than the other two, yet has the highest shielding value between nuclei is suggestive of a species resembling a free-radical. The dip in shielding before the nucleus is also more severe than for chlorine and bromine, again indicative of a free radical species.

4.5 Transition States With Carbon-Magnesium Primary Interactions

Much has already been made of the importance of solvent effects in GRF. Likewise, the existence of halogen bonds has been discussed a number of times, so rather than cover this again a transition state is provided as proof of the solvent's importance in steps other than the one involving the removal of the reagent from the surface. Here, presented for the first time, is a transition state which was only locatable with the halogen-solvent interaction present. The idea behind this was generated, in part, by the rejection of the the-halogen-must-touchdown-first assumption. A vast amount of time spent attempting to locate a transition state with primary carbon-magnesium interactions without solvent molecules present was fruitless. In addition, attempting to locate a transition state using only one solvent molecule to increase time efficiency was of no use. Introducing the second solvent molecule had the desired effect, and a genuine transition state corresponding to the breaking of the C-X bond was located.

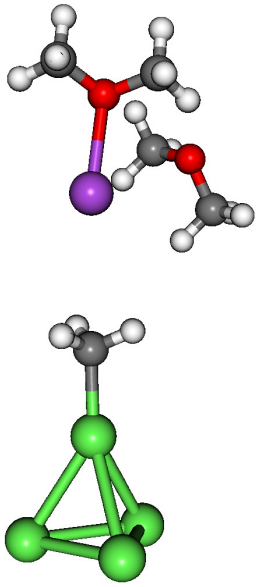

Figure 4.41: Geometry of the transition state dependent on halogen-bonding interactions with two solvent molecules (TSHB).

This transition state is a direct derivative of the complex discussed in section 4.2. Where, in order to form the geometry seen above, the DME coordinated methyl iodide was taken and the C-I bond extended by 50%, the H-C-I bond angle reduced and placed above a node in the magnesium cluster. The location of this complex

was extremely costly computationally and required the repeated revision of input files which failed to locate a minimum on an extraordinarily flat PES. The geometry shown in figure 4.41 is a completely genuine transition state with a single imaginary frequency in the Hessian matrix and is optimised under the most stringent criteria available using the Gaussian 09 quantum chemical package.

It is known from general chemistry that the strength of the halogen bonding interaction invariably increases as one moves down group seven of the periodic table, i.e, the bonding interaction between the Lewis acid and base increases according to the series Cl $<$ Br $<$ I. As such, this initial study has been carried out only for X=I. But it is expected that such complexes exist also for the lighter halogens.

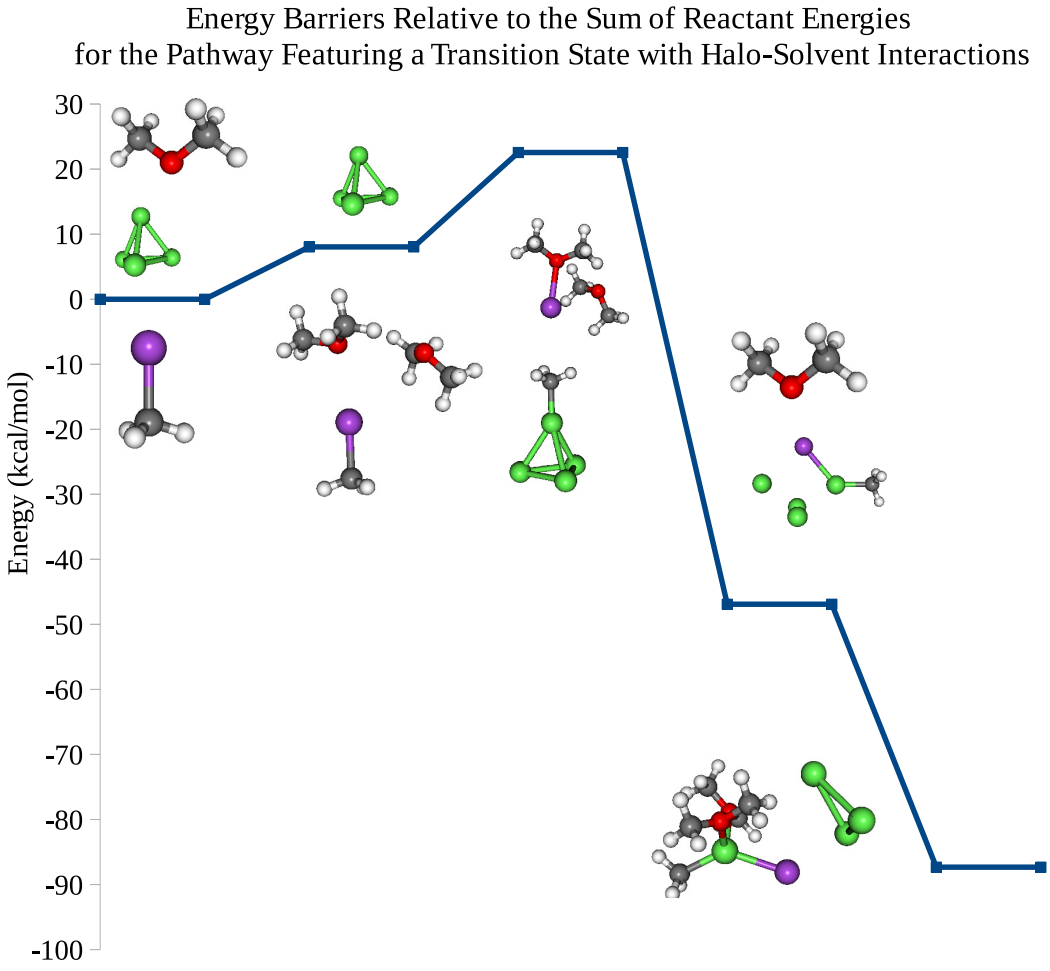

Figure 4.42: Energy barriers corresponding to each step of the reaction which passes through TSHB, with images depicting the structures which correspond to each stationary point.

It is seen in 4.42 that the barrier to forming the transition state from the reac-

tants, if the step including the coordination of the solvent molecules to the halogen is ignored, is very similar to the other transition states discussed in the preceding sections. It has been well-documented that the barrier to reaction decreases with the size of the magnesium cluster.[43] It is suggested in the same work that the calculated barriers of reaction in these pathways sits at around 10 kcal/mol^{-1} is in "reasonable agreement" with experimental values of 8 kcal/mol^{-1}.[10,44] Any experimental values calculated are done so with the reagents dissolved in the reaction mixture, and as such, will be not with respect to the sum of the reactants as is the first platform on the energy profile above, but will be with respect to the second platform. As such, future work should be performed in the same manner.

It is an unfortunate truth that through a shortage of time, or more truthfully, as a consequence of the time spent isolating the geometries of the halogen bonded complexes, that no minimum was found corresponding to the deposition of the iodine on the edge of the cluster. One should expect there to be a minimum after the transition state corresponding to the cluster bonded to the methyl group, with the dissociated and complexed iodine nearby, and a further first-order saddle point corresponding to the dropping off of the iodine atom at the edge of the cluster and subsequent breaking of the I-O halogen bonds.

Upon inspection of the various bond lengths at different stages along the reaction pathway we see that solvating methyl iodide gives us a complex in which the C-I bond is extended by more than 0.003 Å, clearly a constructive change in the bid to form the transition state. It is also observed in the transition state geometry that the I-O bond lengths have shortened significantly. The shorter I-O bond has contracted from 3.074 Å to 2.42596 Å, and the longer I-O bond from 3.909 Å to 3.464 Å. These changes are the characteristics of an interaction not present in attempts to locate this transition state without solvent molecules present, and are indicative of a stabilising interaction as the C-I bond is broken. A shortening of the hydrogen bonds between solvent molecules is also observed with the two values being 2.220 Å and 2.829 Å as opposed to those previously seen (see section 4.2) of 3.074Å and 3.909 Å. In addition to their impact on the transition state, the solvent interactions indicate that any reaction pathway involving transition states with halogen-magnesium primary interactions must involve the reactants becoming undissolved.

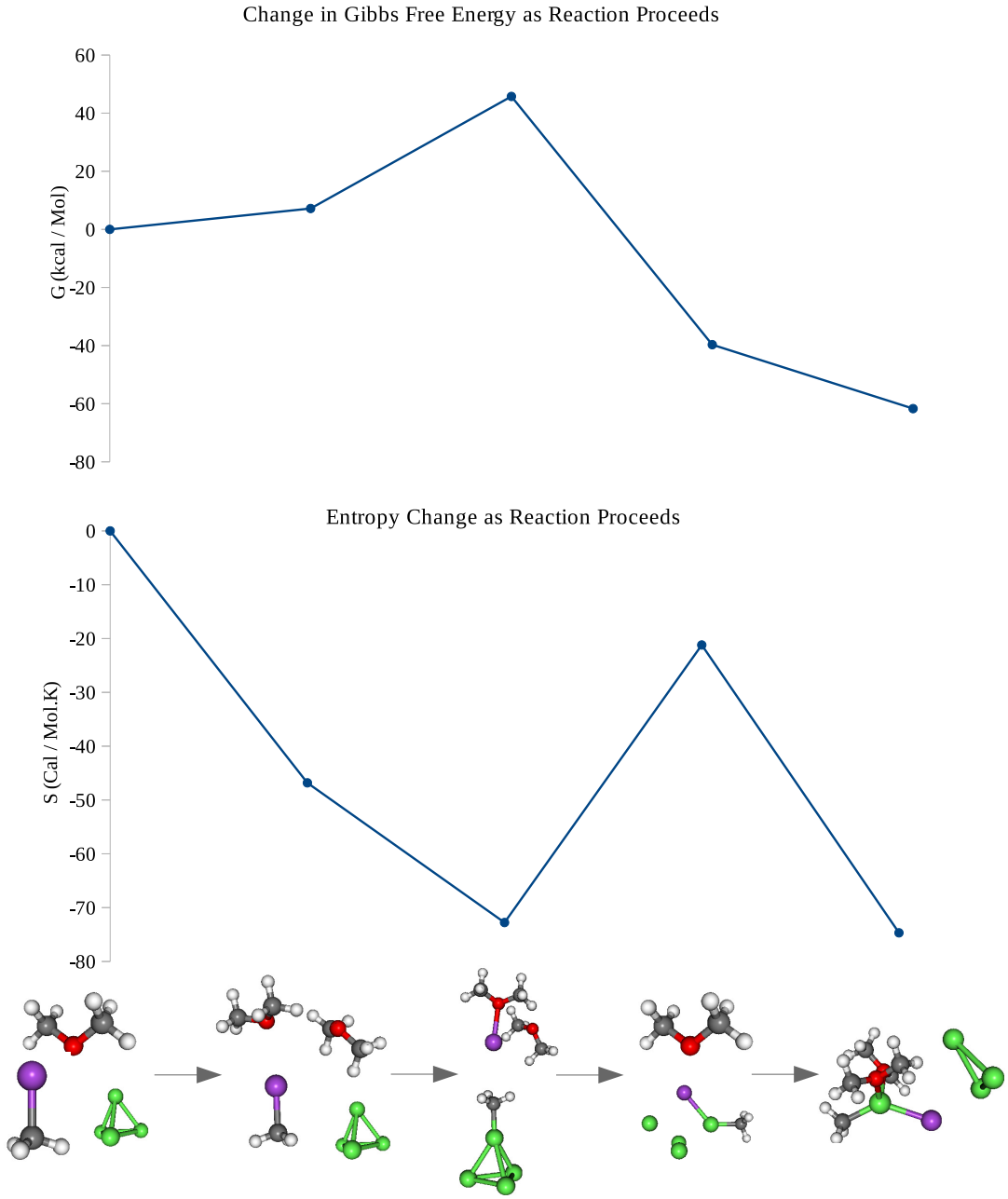

Figure 4.43: Gibbs free energy and entropy changes as the reaction progresses through TSHB. Images along the bottom of the image indicate the structure to which each data point corresponds.

Aside from the very obvious entropy change from transition state to local minimum in figure 4.43, which appears in the manner it does as a result of the solvent contribution being included as an afterthought from the optimised solvent geometry, the entropy profile is an interesting one. The entropy change seems to plateau at the transition state and remain almost constant between then and the product, indicating a seemingly spontaneous (from the Gibbs energy profile) process which is

hardly entropy driven at all despite involving so many molecules. Of course, this is a consequence of the solvent molecules remaining bound to the iodine throughout the reaction, but the thermodynamic changes are, as a result, very different from the other transition states we've seen so far. A noteworthy feature in the Gibbs energy profile of the reaction is the non-spontaneous nature of the solvation of the halogen-containing reactant.

Frontier orbital pictures are included for completeness and comparison with previous transition states.

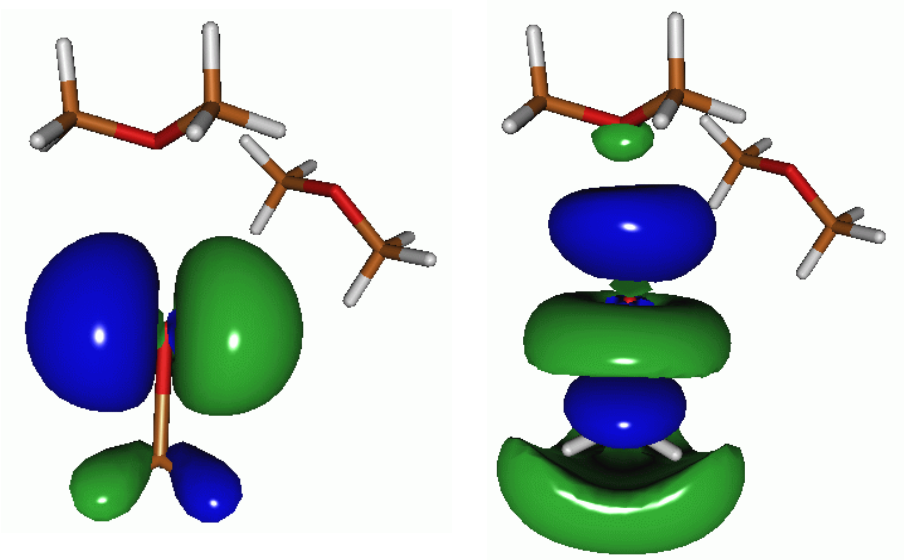

HOMO: -0.345540 Ha LUMO: -0.130620 Ha

Figure 4.44: Frontier orbitals of the solvated methyl iodide together with orbital energies.

Mulliken charges for the solvated methyl iodide indicate that there is charge on the carbon in the methyl group of +0.155. The introduction of easily polarizable magnesium atoms provides a source of electron density which as we see in figure 4.44, may find itself in the LUMO, specifically, through the part of the LUMO beneath the carbon atom. The result is electron density in an anti-bonding orbital which weakens the C-I bond, as one would expect. The HOMO is seen to be extremely similar to that of methyl bromide, presented in figure 4.19. Furthermore, the LUMO seen in figure 4.19 for methyl bromide supports the claim of the halogen bond weakening the C-I bond by providing a clear picture of how electron density may move into an anti-bonding orbital.

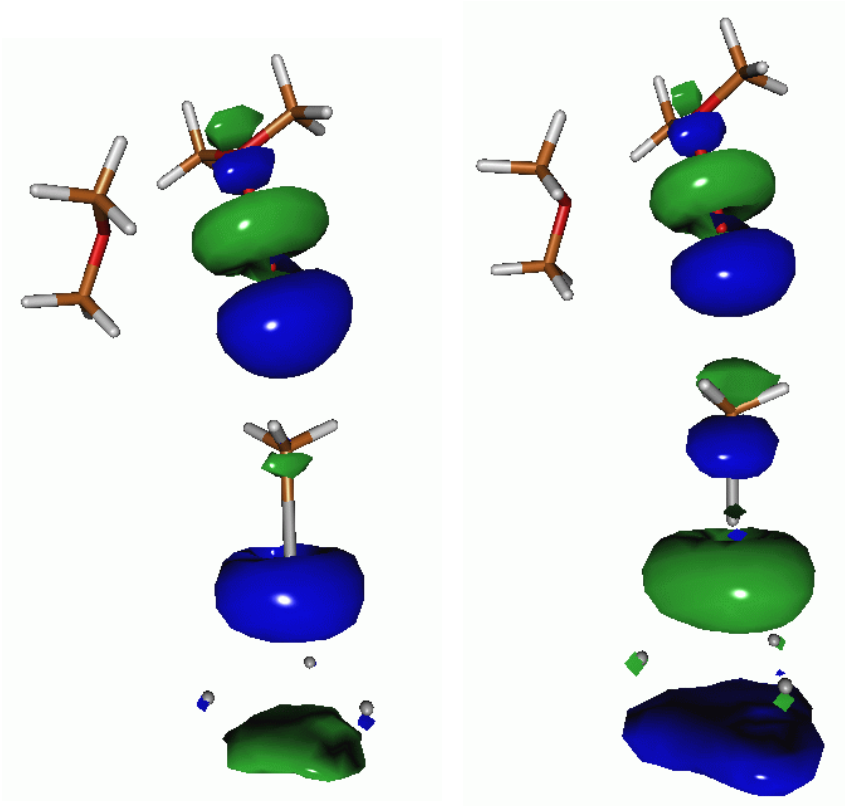

HOMO: -0.168400 Ha LUMO: -0.075160 Ha

Figure 4.45: Frontier orbitals of TSHB together with orbital energies.

The HOMO and LUMO for TSHB are extremely similar, and both have anti-bonding interactions between the carbon and iodine atoms. It is also noted that the DME molecule further from the iodine atom plays no part in either.

4.6 Comparing Transition States

Through a brief comparison of transition states and their thermodynamic quantities, it is possible to place the new transition state discussed in the previous section amongst its peers. It is also possible to decide which transition states are likely to be the most favourable within the Mg_4 cluster approximation.

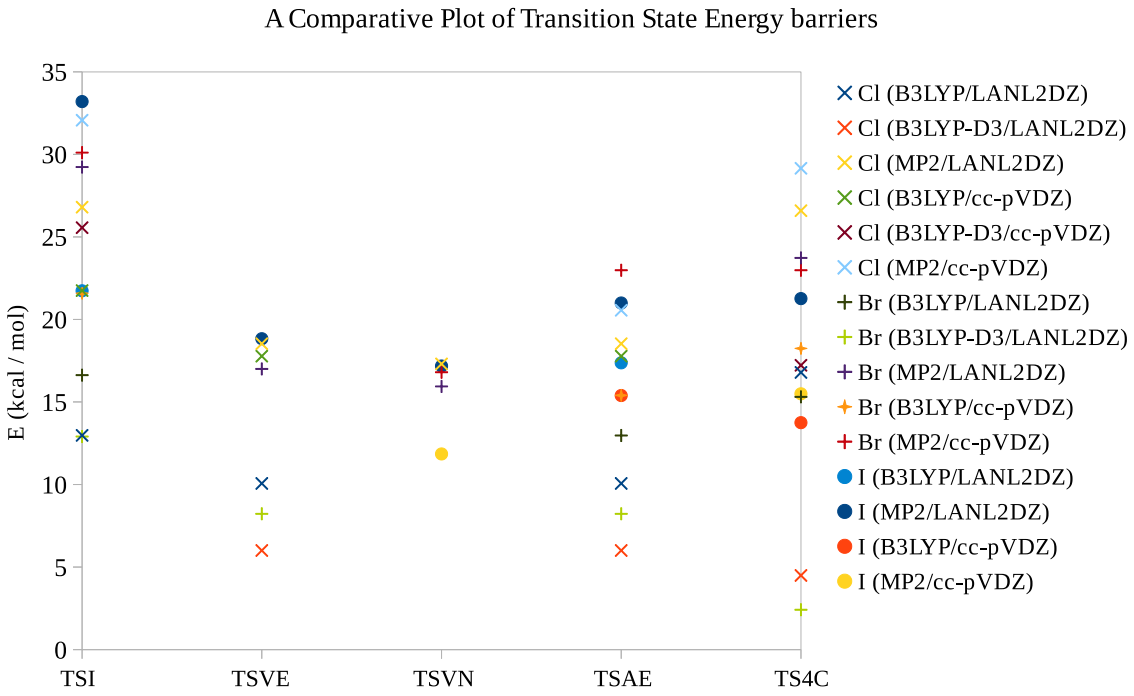

Figure 4.46: Energy barriers to the formation of transition states discussed in previous sections relative to the sum of the reactant energies.

It is seen in figure 4.46 that the transition states where R-X approaches a node vertically, or an edge vertically are, on average, the most favourable of those investigated. The transition state derived from the general oxidative addition mechanism is the highest in energy, the opposite to what is indicated by the series of calculations where the MP2/LANL2DZ method and basis set combination is used for transition states where X=Br, as was used to assign the order of presentation.

The spread of the calculated energy barriers is quite considerable. At the core of the inconsistency of the calculated energies is the smaller basis set and density functional theory methods, with the spread among higher level calculations significantly less exaggerated. Despite the discrepancy in energies, the methods chosen have provided higher level justification for those which are reported in the literature as having

only been optimised using lower level methods. It is acknowledged that to increase the cluster size and continue using high level calculations is extraordinarily costly computationally, but in some cases, as with the halogen bonded transition state, the high levels of theory are necessary for certain stationary points to exist on the PES.

Interestingly, there seems to be a trend developing in the energy barriers to transition state formation for different halogens. That is, in some cases, the barriers are consistently of lower energy for smaller halogens and for others, we see a preference for iodine. For instance, TSI and TSVE seem to show lower energy barriers for chlorine and bromine than iodine. TSVN shows a weak preference for iodine being the halogen present and very little difference in the chlorine and bromine energy barriers. TSAE seemingly shows very little of this trend at all, perhaps leaning ever so slightly towards the smaller halogens. TS4C perhaps shows a preference for iodine and bromine if the lower points for chlorine are removed as anomalous results. The transition state discussed in the previous section has an energy barrier of 22.55 kcal/mol. This places it in the lower half of those presented in figure 4.46, and brings justification to the idea that the transition states where a carbon-magnesium interaction is the first to form with the surface are very real possibilities which should be included in the discussion of possible mechanisms of GRF.

It is expected that were the study of these transition states to be repeated using larger clusters, the spread of the values presented would decrease significantly. The impact of changing the halogen on the structure of these transition states is quite obvious. In the case of iodine, Mg-Mg bonds within the cluster are lengthened to a much greater degree than the transition states containing chlorine. Moreover, the local minimum discussed in last sections varies with halogen, with the C-Mg-X bond angle increasing to an almost linear sequence as X is varied from chlorine to bromine to iodine. An extended lattice is needed to counteract the freedom of the cluster to modify itself so extensively and gain a truer picture of which pathway is most favourable for each halogen.

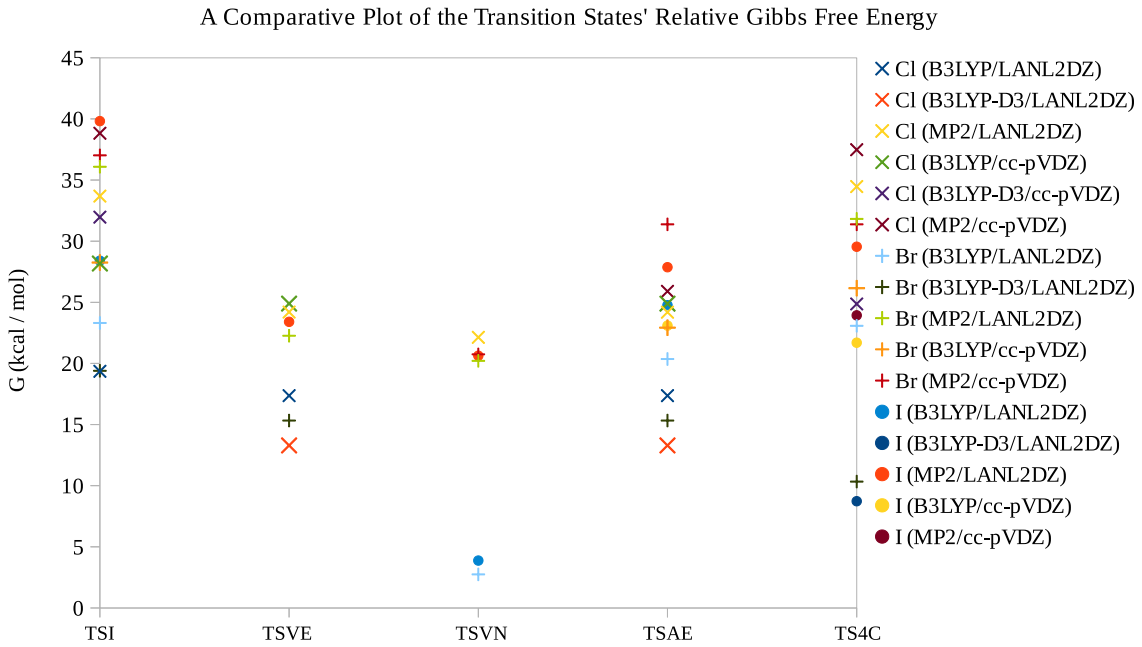

Figure 4.47: Gibbs free energy changes in the formation of transition states discussed in previous sections relative to the sum of the reactant free energies.

The Gibbs free energy profile of the transition states is very similar to the energy profile, with TSI being the least favourable over a number of calculations. TS4C and TSAE are similar in their unfavourabilities, and TSVE and TSVN are the least unfavourable of all. The observations of halogen dependence is carried forward here, to the extent that TS4C may be less unfavourable for iodine containing transition states than TSAE and similar to TSVE. Again, the impact of cluster size is likely to have an impact on the values for heavier halogens.

The Gibbs free energy change for the solvated transition state from the reactants is 45.75 kcal/mol, which is rather a large change in comparison with those seen in figure 4.43. Having said that, if we take the energy barrier to be from the solvated methyl iodide and magnesium cluster, the barrier is more in line with what we expect and sits at 38.5 kcal/mol and is lower than the value for TSI, X=I optimised at the MP2/LANL2DZ level.

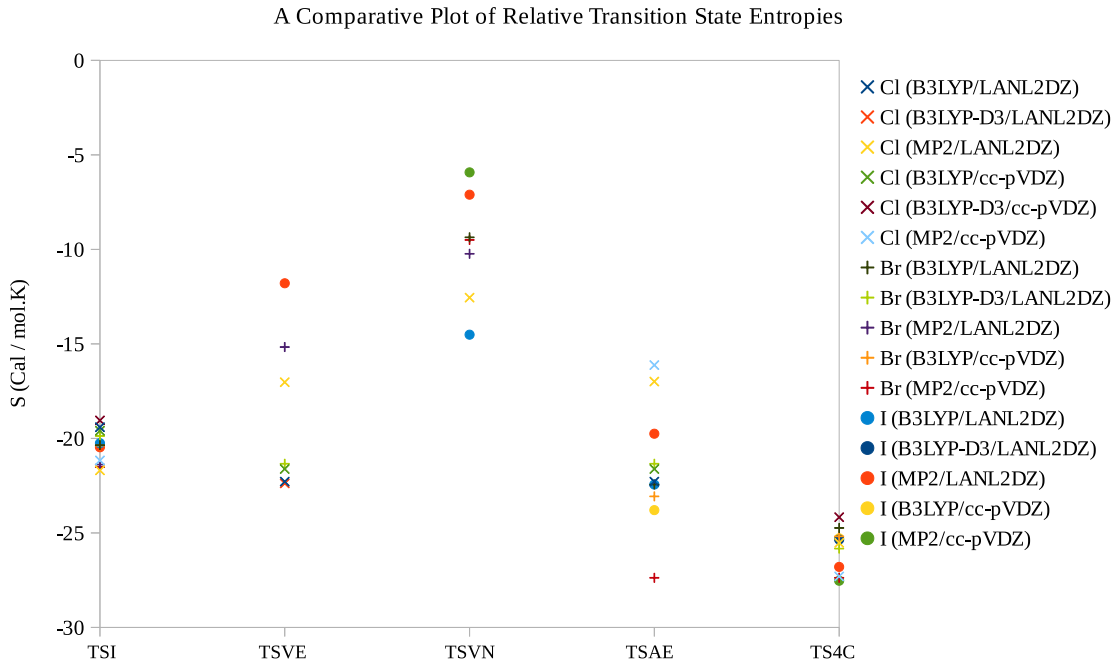

Figure 4.48: Entropy changes in the formation of transition states discussed in previous sections relative to the sum of the reactant entropies.

As may have been expected, the entropy profile for the transition states is reminiscent of an inverted plot of the Gibbs free energy, and shows that the TSVN transition state has an much smaller average entropy change than the rest, and is thus the least entropically unfavourable. The transition state where the solvent molecules are included is, of course, the most entropically unfavourable as order is imposed on two solvent molecules as opposed to them being included as free gaseous molecules. Of the transition states presented in figure 4.48, TS4C is the most unfavourable entropically, followed by TSAE, TSVE and TSI and finally TSVN.

5 Results from the Study of the Chemical Bond in C_2

The carbon-carbon bond in ethane is a single bond. The carbon atoms themselves are sp^3 hybridised centres. The carbon-carbon bond in ethene is a double bond as a result of the carbons being sp^2 hybridised. Finally, the carbon-carbon bond in acetylene is a triple bond, with the carbons being sp-hybridised centres. Dicarbon is another question altogether, with the orbital hybridisation being unclear. With the electronic structure of nitrogen being so similar to the electronic structure of carbon, it is not surprising that within the same model of hybridized orbitals, nitrogen shares the distribution of hybridised states discussed for carbon. The only difference between the two being that instead of single electrons occupying the sp^x as is the case with carbon atoms, one contains a lone pair instead. As was mentioned in section 1.2, the possibility of quadruple bonding in dicarbon is a topic for debate but the same cannot be said for any electronic state of dinitrogen. Here we explore the similarity between C_2 and $N_2{}^{2+}$ and the possibility that the so-called main group quadruple bond exists for dicarbon and if so, that it is not unique.

The method of investigation in this section is the modification of bond lengths and electronic states for a number of small carbon compounds and their nitrogen-containing analogues. All shielding data is captured using the MP2/cc-pVQZ method-/basis set combination. All planes of ghost atoms used to generate shielding plots are printed in a very fine grid (one ghost atom every 0.02 Å). All shielding data taken along the molecular axis was collected using the same level of theory, and ghost atoms placed every 0.01 Å.

A digression: It is worth noting that, despite chemists' reliance on their features, atomic and molecular orbitals do not exist in the way they are often pictured in literature and textbooks. They are an approximation to the true case, albeit a very good one. Certain assumptions are made about them, for instance, in theoretical chemistry the orthogonality of molecular orbitals is assumed for mathematical convenience. Worse than this, in organic chemistry, the orthogonality approximation is used to justify the selectivity of a plethora of reactions, most notably in reactions which substitute groups on phenyl rings. It seems that the definition of orthogonality is often forgotten and orthogonal orbitals are thought of in many undergraduate chemistry lectures as being orbitals which are at a right angle to one another. In

fact, it is the labelling of a result of the inner product of two functions belonging to the same function space being zero, which need not be true for all orbitals, though would inevitably be true for some (for instance 1s and 2s orbitals clearly overlap and are certainly not at right angles to one another, yet are said to be orthogonal so long as their inner product is zero). A good example of orthogonal functions existing over the same period are the sine and cosine functions. Showing this is a lengthy procedure and will not be performed here, but for the familiar function

$$\left\{cos\left(\frac{n\pi x}{L}\right)\right\}_{n=0}^{\infty} \qquad \text{on the interval } -L \leq x \leq L \tag{5.1}$$

it amounts to evaluating the integral

$$\int_{-L}^{L} cos\left(\frac{n\pi x}{L}\right) cos\left(\frac{m\pi x}{L}\right) dx = 2\int_{0}^{L} cos\left(\frac{n\pi x}{L}\right) cos\left(\frac{m\pi x}{L}\right) dx \tag{5.2}$$

over three cases; $n = m = 0$, $n = m \neq 0$ and $n \neq m$. Doing so shows that if $n \neq m$ the integral is is zero and if $n = m$ the integral is a positive constant and so the set is mutually orthogonal. This serves as a justification, of sorts, for mutually orthogonal orbital functions which are defined over the same interval in space and thus “overlap”.

5.1 Comparing chemical bonds in C_2, C_2H_2, C_2H_4, C_2^{2-}, N_2 and N_2^{2+}.

The first thing to consider in the bonding in dicarbon is the effect of shortening and lengthening the bond. If a kink appears in the PES for dicarbon but not for acetylene, then it is perhaps fair to say there is an additional bonding interaction valid. This is not observed here.

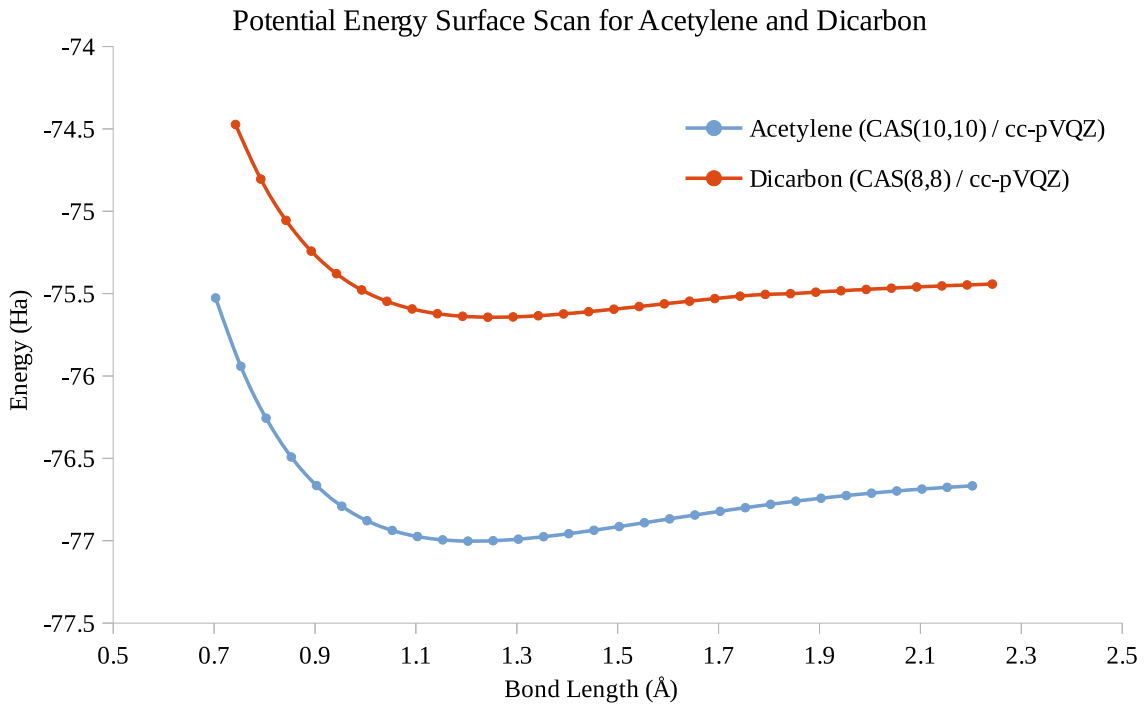

Figure 5.1: A stepwise scan of the potential energy surface for acetylene and dicarbon. Their experimental bond lengths are contracted by 0.5 Å (10 steps of 0.05 Å) and extended by 1.0 Å (20 steps of 0.05 Å).

Figure 5.1 features the PES scan carried out at CAS(8,8)/cc-pVQZ for dicarbon and CAS(10,10)/cc-pVQZ for acetylene. The shape of the curve is of a typical chemical bond breaking and features no kinks, thus dethroning the idea of interactions in dicarbon which are not range-specific and unseen elsewhere in chemistry.

Table 1: Experimental bond lengths of C_2, C_2H_2, C_2H_4 and N_2.

	C_2 (C-C)	C_2H_2 (C-C)	C_2H_4 (C-C)	N_2 (N-N)
Bond Length (Å)	1.2425	1.2030	1.3390	1.0980

Table 1 shows the tabulated bond lengths for the molecules under investigation for reference throughout the section.[45–48] In the opening pages of this thesis, a com-

ment was made about increasing bond strengths not necessarily correlating with decreasing bond lengths. While in the overwhelming majority of cases the correlation does exist, present in mind at the time of writing was the unexpected difference between C-C bond lengths in C_2 and C_2H_2. As we will see shortly, the C-C bond in C_2 is stronger than the C-C bond in C_2H_2, yet it is longer.

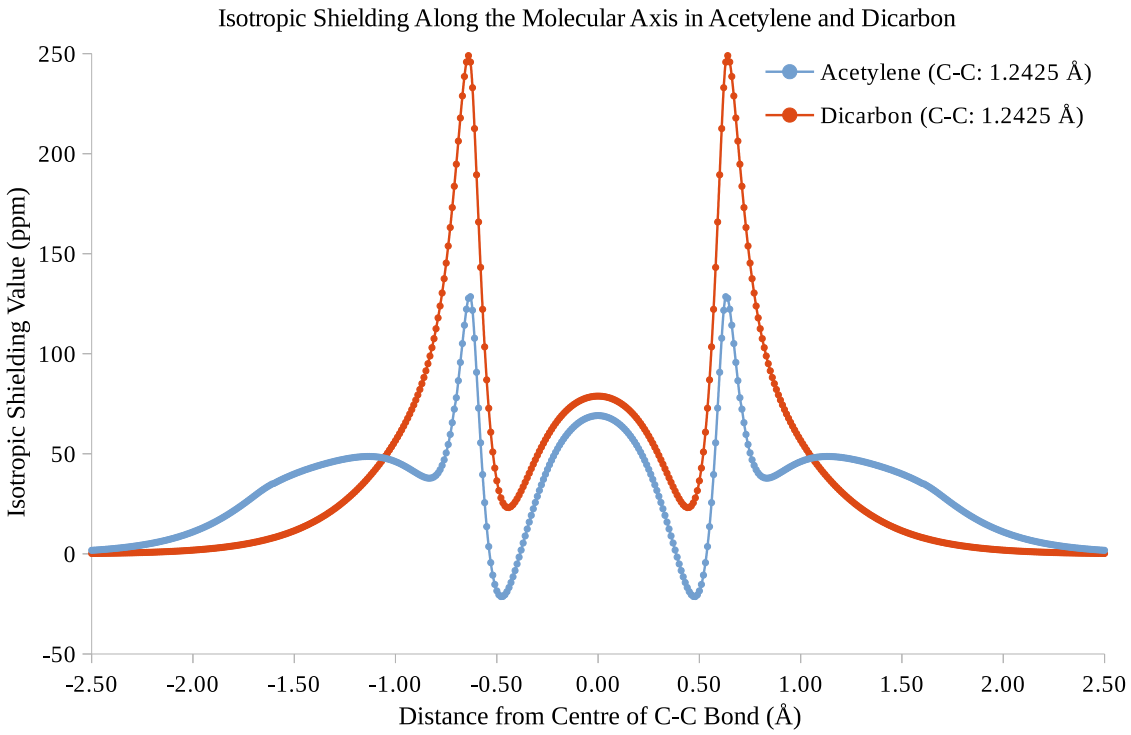

Figure 5.2: Isotropic shielding along the molecular axis of acetylene and dicarbon at the experimental bond length for dicarbon.

Figure 5.2 provides a clear image of the bond strengths of both acetylene and dicarbon at the experimental bond length of the latter. As has been discussed previously, a higher shielding value between the two carbons in indicative of a stronger bond. The picture could not be clearer. The shielding at the nuclei also differs significantly, with the sp-hybridised centres in C_2H_2 appearing to experience less isotropic shielding than the centres in dicarbon. The shoulders on the curve for acetylene are present as a result of the hydrogen atoms at -1.06 Å and +1.06 Å from the carbon centres. At no stage during these calculations are bond lengths optimised. To reduce the number of variables and isolate the bonds of interest, C-H lengths are always fixed at their experimental value. Were the geometry of acetylene to be optimised with a fixed C-C distance at an increased bond length, the only expected change in

figure 5.2 would be the contracting of the shoulders.

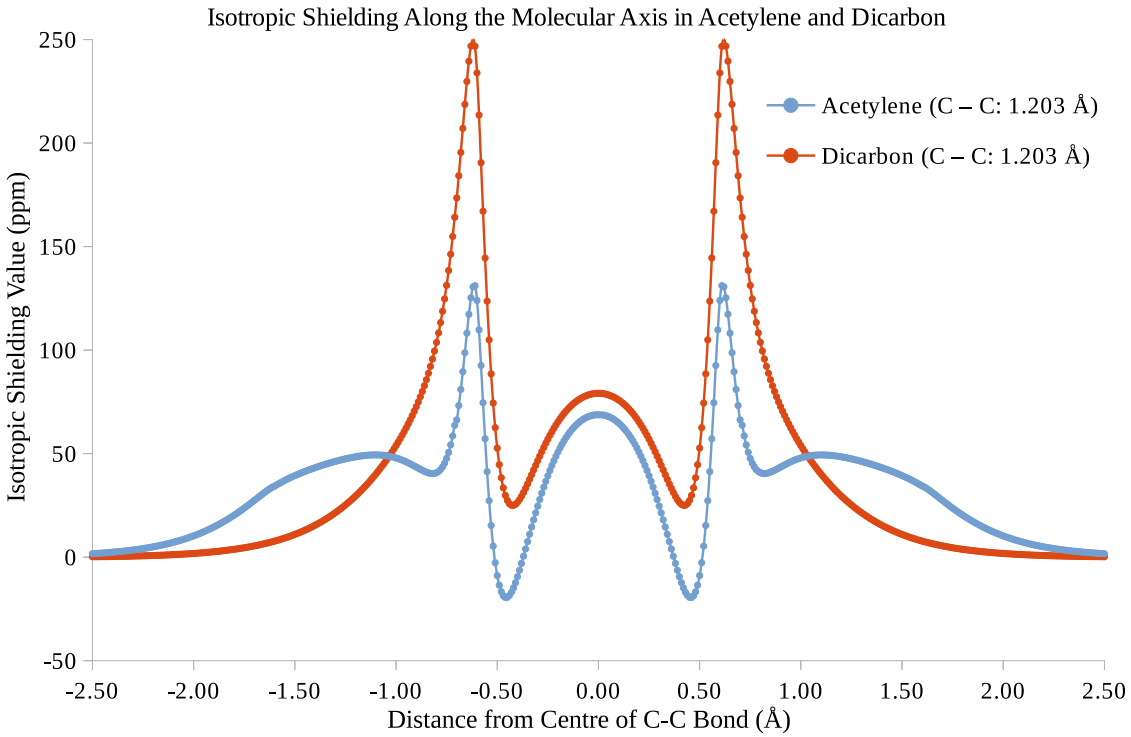

Figure 5.3: Isotropic shielding along the molecular axis of acetylene and dicarbon at both at the experimental bond length of acetylene.

Further justification of the increased bond strength in dicarbon is provided by setting the C-C distance equal to that seen in acetylene. Still, the shielding between the nuclei is significantly higher in dicarbon. A series of bond lengths were considered for acetylene, dicarbon and nitrogen (plots for this are included shortly), with the observation that at all bond lengths the C-C bond in dicarbon is significantly stronger than the bond in acetylene.

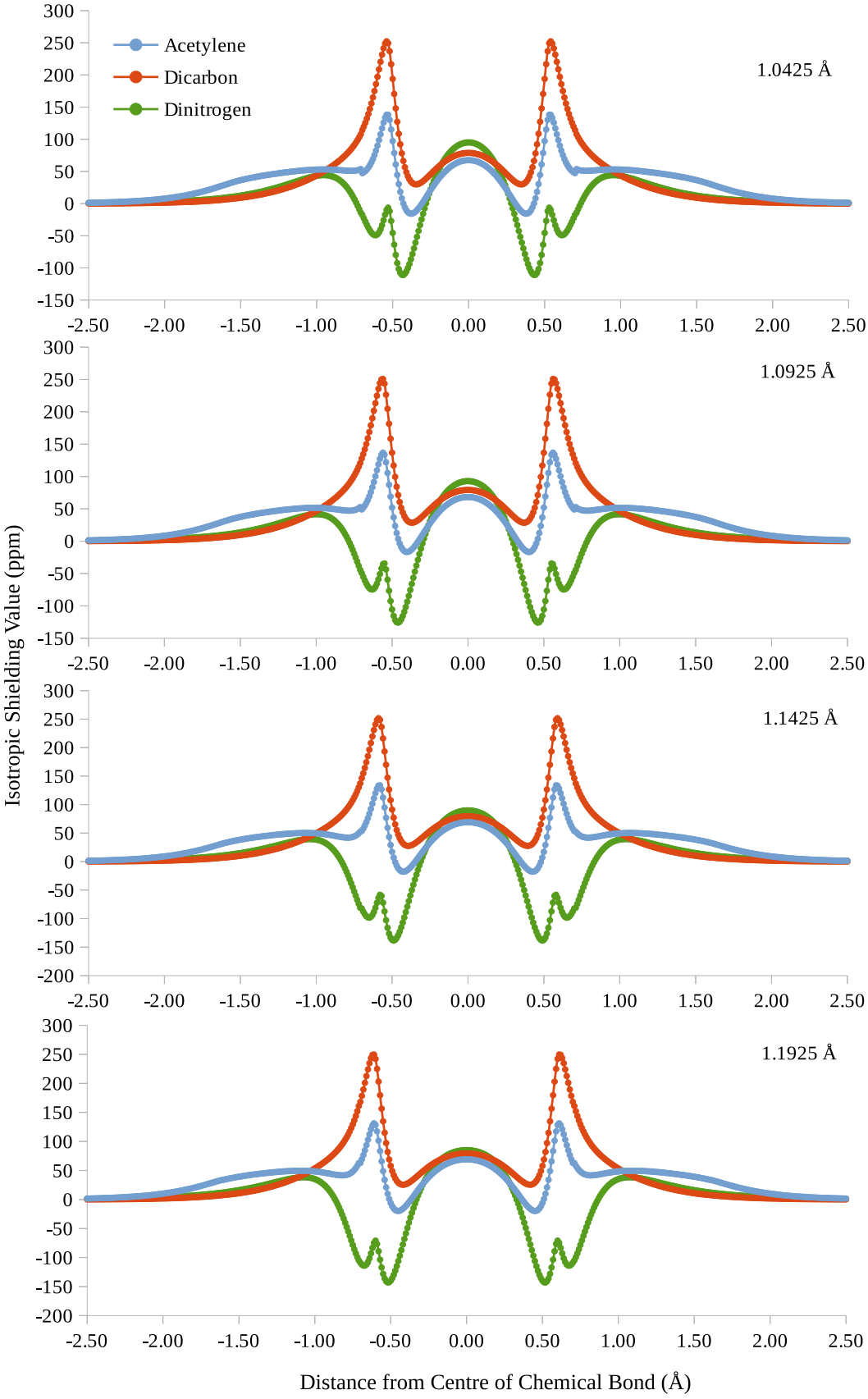

Figure 5.4: Isotropic shielding along the molecular axis of acetylene, dicarbon and dinitrogen over a selection of bond lengths generated by subtracting 0.05 Å from the experimental bond length of dicarbon.

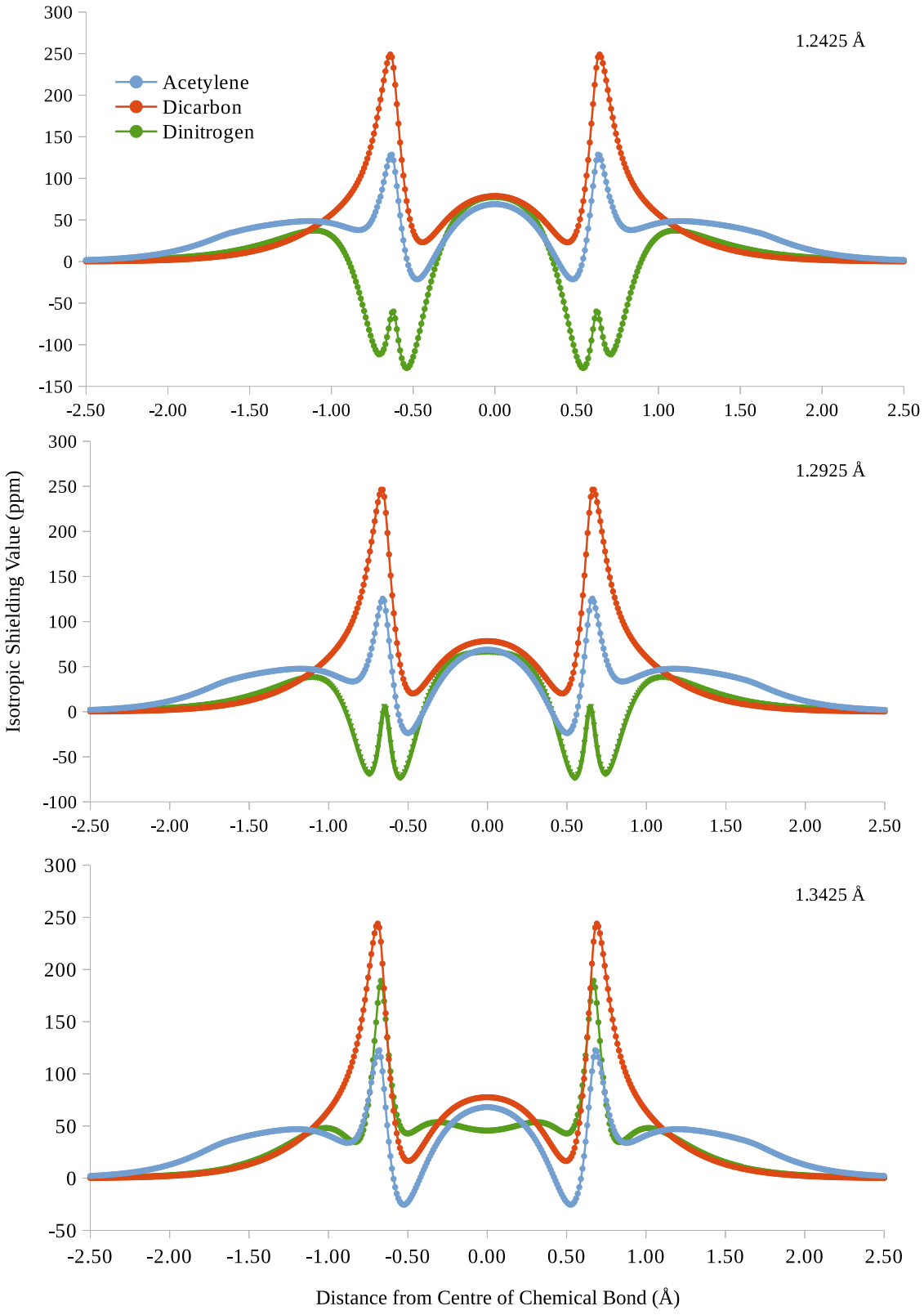

Figure 5.5: Isotropic shielding along the molecular axis of acetylene, dicarbon and dinitrogen over a selection of bond lengths generated by adding 0.05 Å to the experimental bond length of dicarbon.

Figures 5.4 and 5.5 show the changing bond strengths in acetylene, dinitrogen

and dicarbon as bond length is modified is reasonably predictable. The scan is stopped at 1.3425 Å, as the dinitrogen bond begins to break down, for which a CAS wave function would be needed to appropriately calculate shielding values which is not within the capabilities of the G09 package. It is immediately noticeable that the shielding between nitrogen atoms is much larger than the shielding between the carbon atoms. This should not be a surprise given the differences in electron withdrawing ability of the elements, along with the N-N triple bond being an extremely strong bond in its own right.

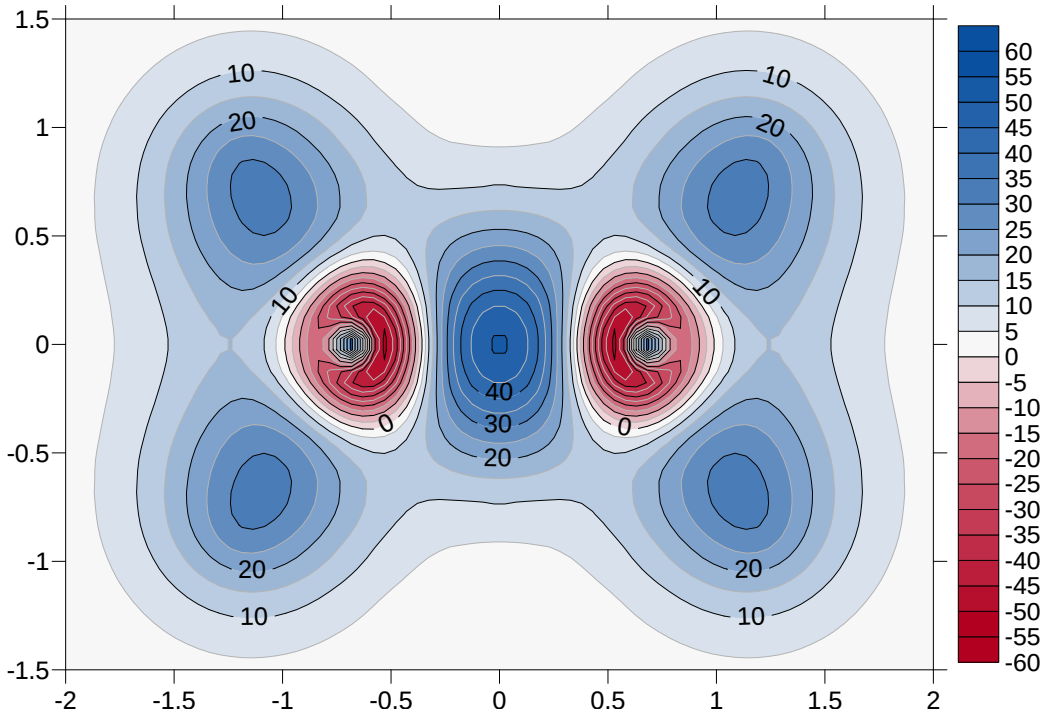

Figure 5.6: MP2 isotropic shielding (ppm) contour plot for ethene, at experimental bond length (1.339 Å), in the molecular plane. Distances in Å.

The maximum shielding between the carbons in ethene is seen to be less than 55 ppm at experimental bond length, with the shielding around the sp^2-hybridised carbons seen to be negative at all points, indicating heavily deshielded environment. Tracing along the bond, σ_{iso} increases, reaching its maximum at exactly the centre of the bond. The shielding patterns surrounding carbon nuclei, labelled "halos" by Karadakov and Horner, are a signature of sorts for the degree of s- and p-orbital hybridisation in modern valence bond theory.[34]

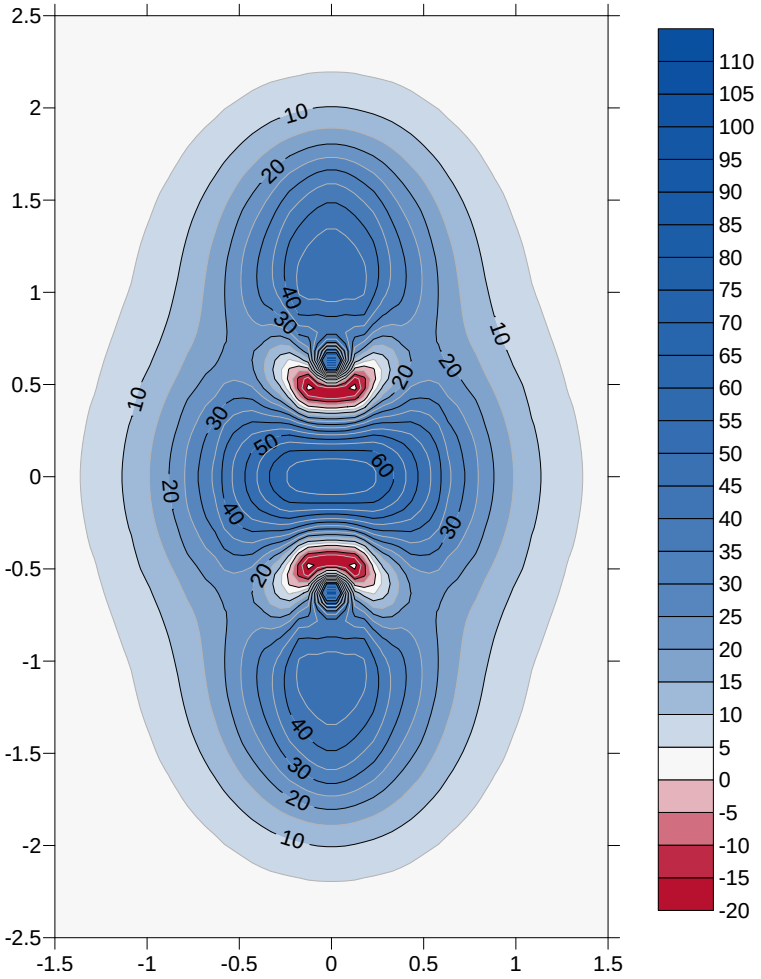

Figure 5.7: MP2 isotropic shielding (ppm) contour plot for acetylene, at experimental bond length (1.203 Å), in the molecular plane. Distances in Å

The shielding in the region surrounding the carbon nuclei is characteristic of, as one would expect, sp-hybridised centres, with a sharp decrease in σ_{iso} between each carbon nucleus and the centre of the C-C bond. Equivalently, a maximum is seen between the carbon and hydrogen nuclei. The shielding plots along the molecular axis in figures 5.4 and 5.5 give a clearer picture of this. Before the shielding in the molecular plane of dicarbon is presented, there are some features which need to be highlighted. In the case of the classical picture of sp-hybridised carbon centres, a lobe extends towards the hydrogen atom, and the π bonds are formed between the carbons from the remaining p-orbitals. In the case of dicarbon, where there are no hydrogens bound to the carbons, were the centre to be described using the usual sp^x descriptors, one should expect positively shielded lobes to appear. It was

seen in the early parts of this section that no such lobes exist. Additionally, were the carbon atoms in dicarbon to be sp-hybridised, the same shielding pattern around each nucleus should be observed, as is seen in figure 5.7. Justification of this observation is made available by considering the shielding in the molecular plane of N_2. While the differing electronegativities of the elements involved will mean characterising hybridisation by shielding patterns around the nuclei will not be possible by direct comparison, there is no doubt that, in N_2, the centres are sp-hybridised.

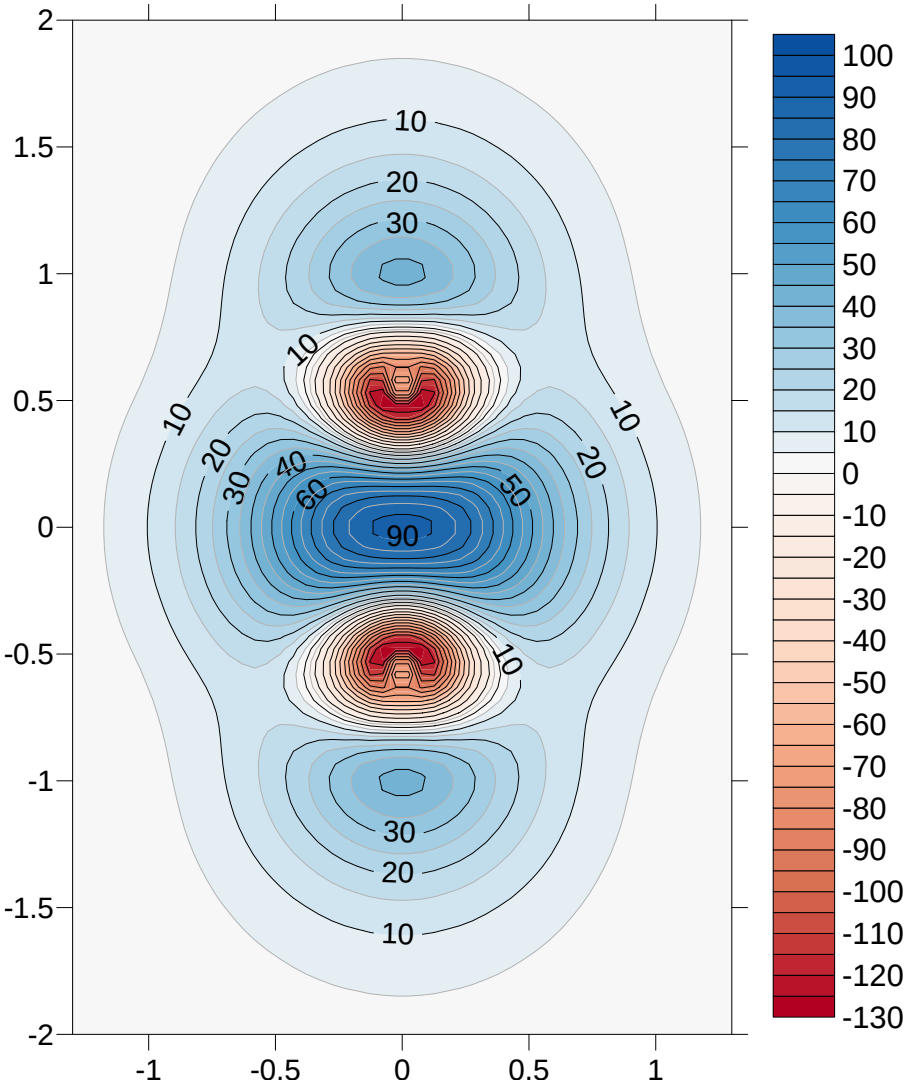

Figure 5.8: MP2 isotropic shielding (ppm) contour plot for dinitrogen, at experimental bond length (1.098 Å), in the molecular plane. Distances in Å.

It is immediately apparent that the lobes not seen for C_2 are present in the N_2 molecule. The shielding pattern around each of the nitrogen nuclei is more reminis-

cent of those seen for carbon in ethene than in dicarbon. However, the overall shape of the contour plot is more akin to the shape seen for acetylene in figure 5.7 than any other and given the increasing deshielding effect of nuclei moving across the periodic table (left to right), the shape of the plot is a more reliable descriptor of bond order and hybridisation than the "halos".

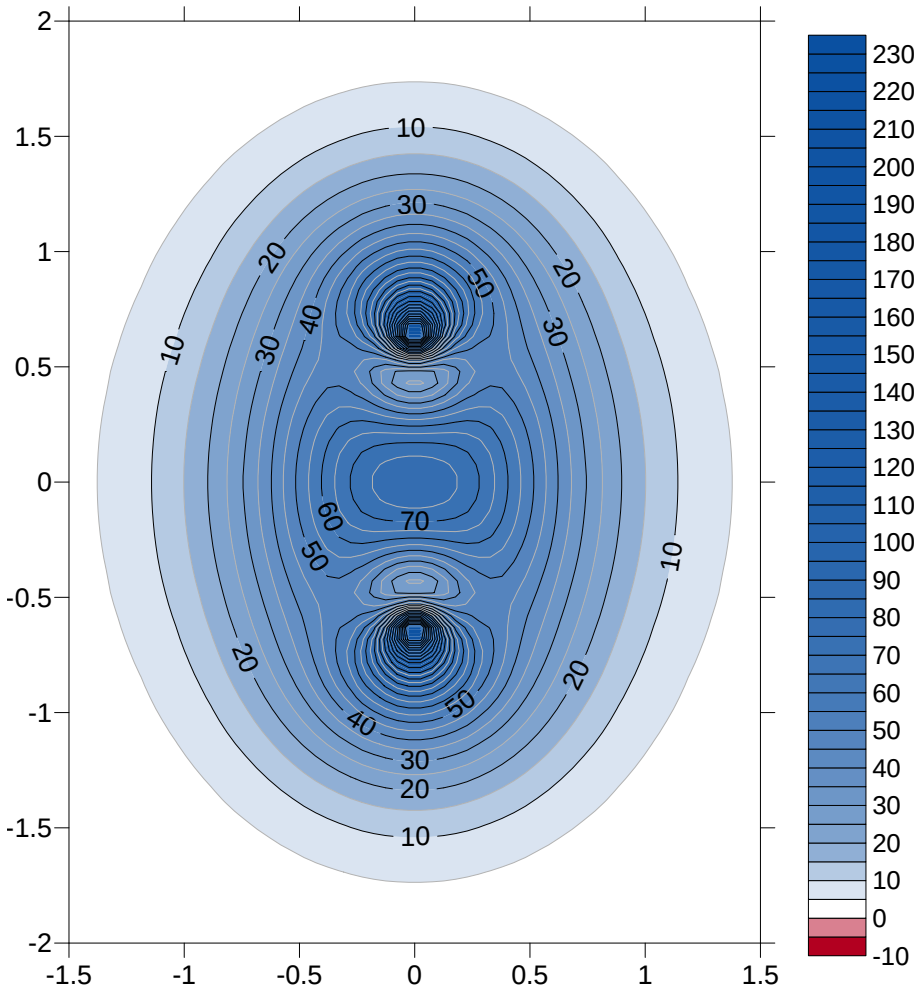

Figure 5.9: MP2 isotropic shielding (ppm) contour plot for dicarbon, at experimental bond length (1.2425 Å), in the molecular plane. Distances in Å.

Inspection of figure 5.9 reveals a lack of any lobes on the carbon centres, which is what one would expect were they to be sp-hybridised and bonded together by a triple bond. The maximum shielding value between the nuclei is >75 ppm. This is significantly greater than the maximum shielding observed between the carbon nuclei in acetylene (maximum shielding along the bond in ethene is $\sim$ 50 ppm, $\sim$ 65 ppm in acetylene and $\sim$ 75 ppm in dicarbon). Another noteworthy feature is the

width of the map where the shielding is greater than 5 ppm. The lack of any negative shielding values between the nuclei and peak of the bond is unique to C_2 within the series presented here. The patterns observed around the nuclear positions are also completely unique when compared to ethene and acetylene. This uniqueness, together with the bond in dicarbon being stronger than a carbon-carbon triple bond certainly suggests that the bond order is greater than 3 and it is, in fact, a quadruple bond.

Further evidence for the bond in dicarbon being of order greater than 3 is provided by considering the case where two C^- ions are brought together to form C_2^{2-}.

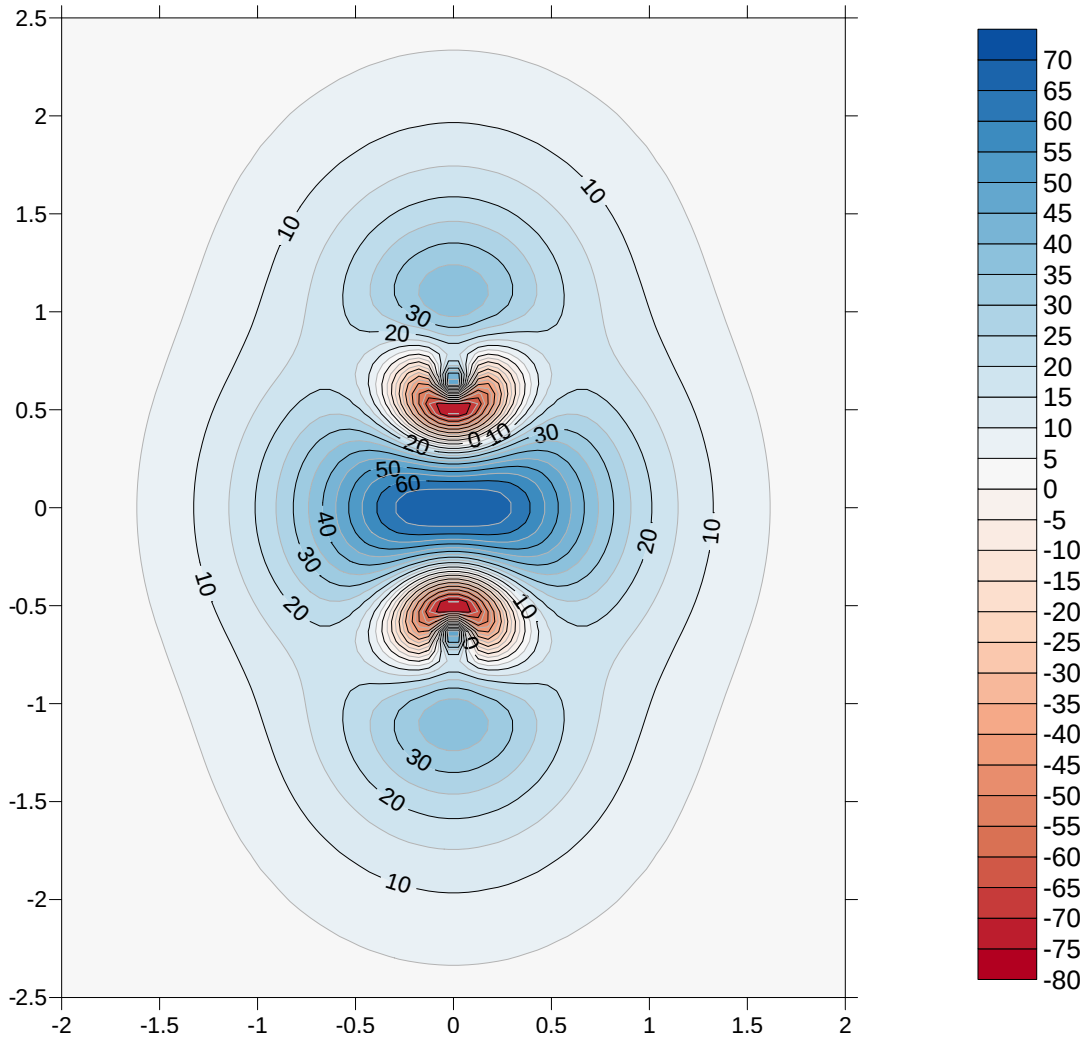

Figure 5.10: MP2 isotropic shielding (ppm) contour plot for C_2^{2-}, at dicarbon's experimental bond length (1.2425 Å), in the molecular plane. Distances are in Å.

We observe in figure 5.10 a decrease in isotropic shielding between the two car-

bons despite the introduction of two electrons to the system. So, the bond is weaker in C_2^{2-} then in dicarbon. Additionally, the shielding pattern around the nuclei is almost identical to the shielding in acetylene, providing evidence for the carbon centres being sp-hybridised. The lobes not seen in dicarbon are present in C_2^{2-} almost to the same extent as in N_2.

Now, as a response to the accusation made by Grunenberg that a bond order which is greater than 3 in the main group has yet to "jump from the test bench", we examine N_2^{2+} and show that the chemical bond therein is of the same order as the bond in dicarbon.[50]

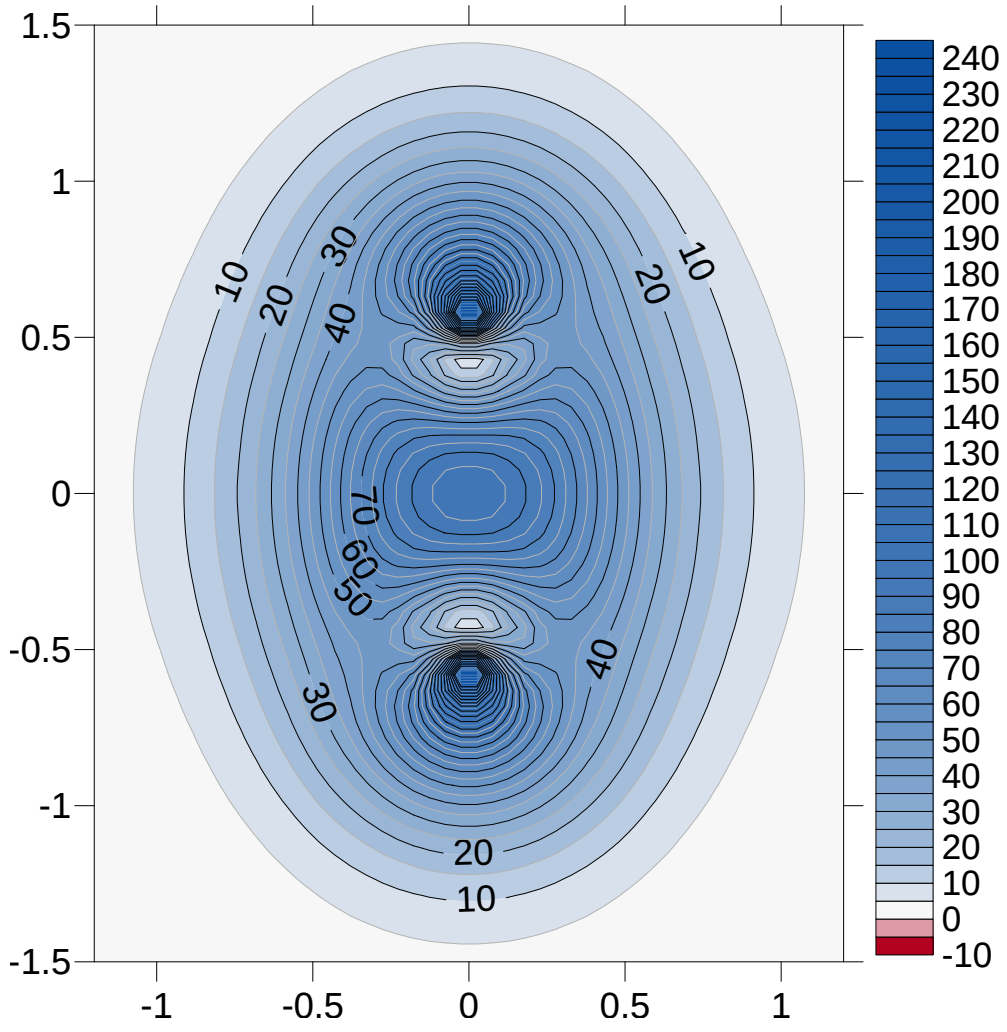

Figure 5.11: MP2 isotropic shielding (ppm) contour plot for N_2^{2+}, at dinitrogen's experimental bond length (1.098 Å), in the molecular plane. Distances are in Å.

Fascinatingly, upon the removal of two electrons from N_2 the shielding between

the two nuclei increases (the bond strengthens), the lobes disappear and the shielding pattern observed at the nuclei is almost identical to that seen in dicarbon. So, if the enigmatic main group quadruple bond exists for C_2, it certainly exists for N_2^{2+}. This provides a means of justification for other approaches which have sought to prove the existence of a carbon-carbon bond of order 4.

Two more isotropic shielding surfaces are presented for completeness and to show that the bond lengths used for the two charged diatomic molecules has little influence over the shielding surfaces discussed thus far.

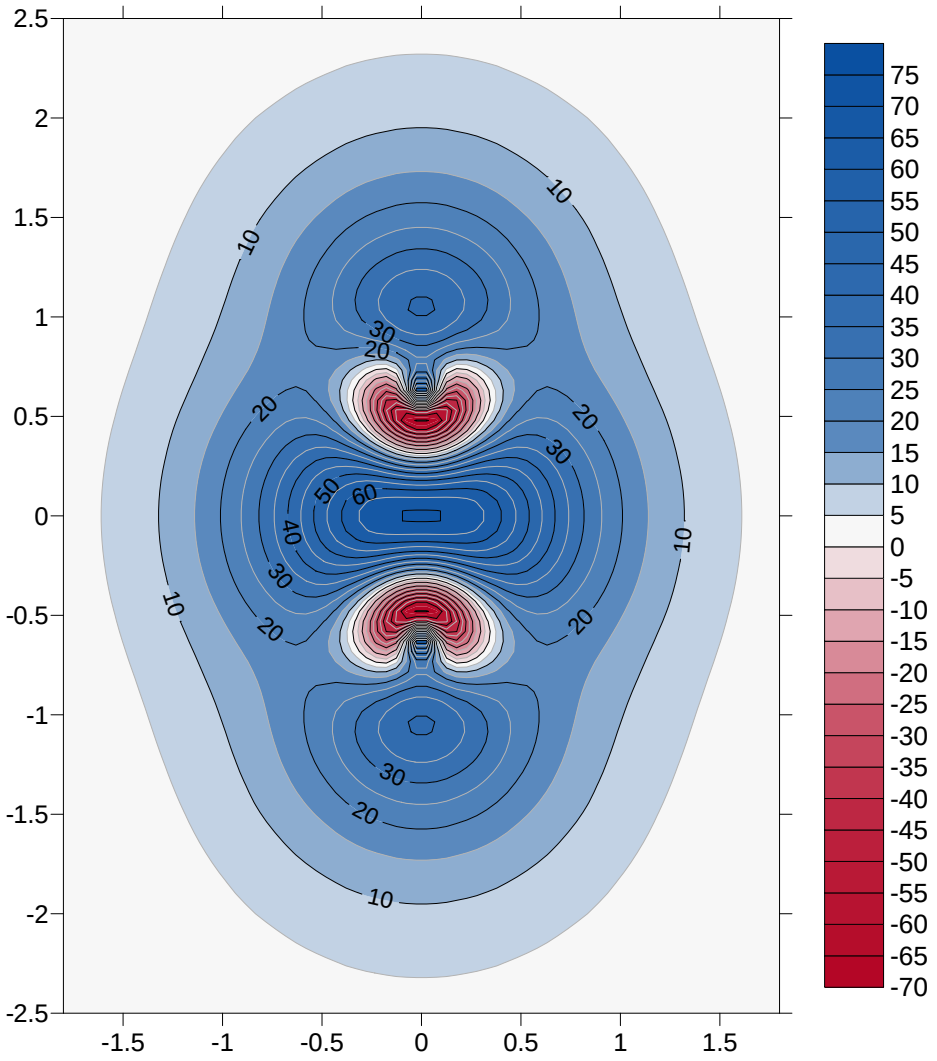

Figure 5.12: MP2 isotropic shielding (ppm) contour plot for C_2^{2-}, at acetylene's experimental bond length (1.203 Å), in the molecular plane. Distances are in Å.

Figure 5.12 shows that the shielding around the nuclei and along the bond as the bond length is decreased remains unchanged and mirrors almost perfectly, those

seen in acetylene.

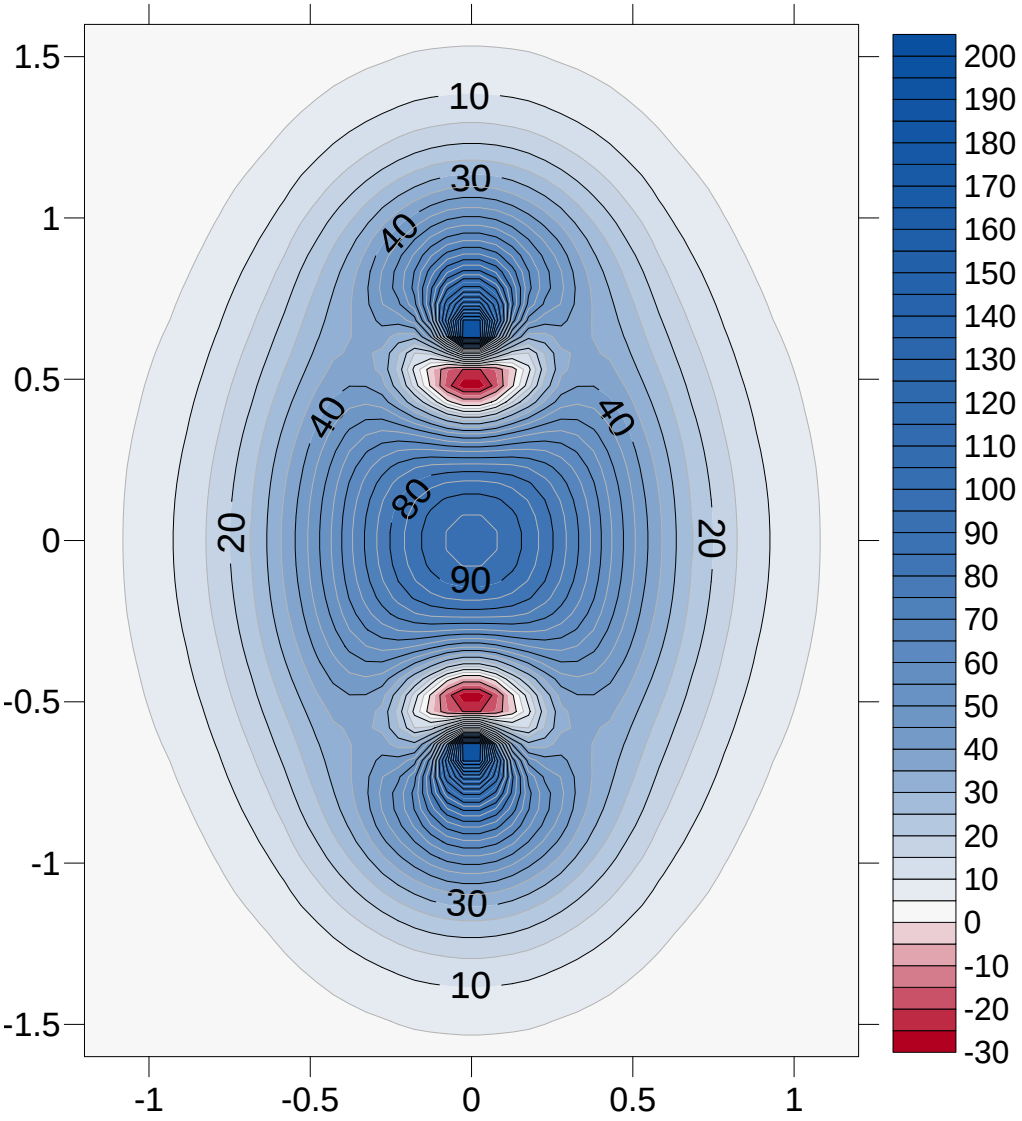

Figure 5.13: MP2 isotropic shielding (ppm) contour plot for N_2^{2+}, at dicarbon's experimental bond length (1.2425 Å), in the molecular plane. Distances are in Å.

Figure 5.13 shows that the shielding around the nuclei and along the bond as the bond length is increased remains unchanged and mirrors almost perfectly, those seen in dicarbon.

A number of other planes as bond length is modified in the molecules presented here are included in Appendix 7.3 for completeness and has been omitted from this section of the thesis as there is little to be discussed; over all bond lengths studied there is no observed change in the shielding patterns, only to the extent of shielding at the middle point of the bond.

6 Conclusions

6.1 Grignard Reagent Formation

The investigation of GRF has yielded some interesting results, and a large number of results which corroborate with and confirm a number of pathways studied at lower levels of theory.

Solvent and halogen effects have been studied in greater detail than ever before. Solvents with strong electron donating character have been shown to have a greatest influence the carbon-magnesium bond. For the first time, isotropic shielding data taken along bonds in organometallic species such as those explored in the study of GRF are presented as a qualitative measure of bond strength. They have been shown to elucidate information with reasonable success across sytems containing three different halogens and in vastly different geometries. They have been done so with reasonable success, and agreement between bond length observations and relative shielding plots, even as the halogen is modified throughout the study.

Reactant-solvent interactions have been considered for the first time and provide interesting results. The co-ordination of two ether molecules to the iodine lengthens the carbon-iodine bond in methyl iodide, serving as the prelude to the formation of a transition state geometry which maintains the halogen bonding interaction. The stationary point corresponding to this transition state is only present in MP2/cc-pVDZ level calculations, and has never been seen before, with halogen bonding playing a vital role in stabilising the first of what is expected to be a series of transition states. As a result, the assumption that the only possible transition states for GRF are those in which the halogen comes into contact with the magnesium solid first is shown to be poor. Furthermore, the role of solvents in GRF beyond the removal of the nascent Grignard reagent from the magnesium surface should not continue to go unstudied. The importance of a large set of basis functions cannot be understated for future investigations of transition states of this kind, along with increasing the size of the magnesium cluster to test energy differences (typically one would expect the transition state energy to decrease).

Overall, the GRF study has provided the starting point for higher level calculations and new interactions. Were more time available, the next actions would be to take the magnesium-halogen transition states and test their magnesium-carbon analogues

while using solvent molecules to stabilise the halogen atoms.

6.2 The Chemical Bond in C_2

The isotropic shielding surfaces presented in this thesis show some fascinating results. The PES for acetylene and dicarbon as bond length is modified shows no noticeable differences between the two molecules, so rules out any range-specific interactions in dicarbon. Isotropic shielding plots along the molecular axis of both molecules indicate that the C-C bond in dicarbon is stronger than the triple C-C bond in acetylene. The difference in shielding at the middle of the bonds is shown to be approximately 10 ppm. This is rather a large difference. It is observed as one increases the bond order from 2 to 3, going from ethene to acetylene, that the shielding increases at the centre of the bond by approximately 15 ppm. There may be no doubt placed upon the orders of the C-C bonds in ethene and acetylene, and thus the preliminary results suggest that the bond in dicarbon is, if one is forced to stick to integer bond orders, of order 4.

The isotropic shielding surfaces calculated using an extremely fine, regular grid (0.02 Å) only offer support to this observation. The shielding patterns around the nuclei in dicarbon are unique among ethene, acetylene and dicarbon and so indicates that the orbitals responsible for the bonds are not the sp-hybrids some may have expected. When 2 electrons are added to dicarbon to form C_2^{2-}, the shielding is near-identical to the shielding in acetylene and certainly contains two sp-hybridised carbon centres, showing that the bond in dicarbon is truly different to the others. The nature of the bonding in the ionic N_2^{2+}, wherein the bond is both stronger than the N-N bond in dinitrogen and has a shielding pattern very similar to dicarbon, provides investigators with a means of testing the true bond order of dicarbon by definitively showing not that the bond is of order 4 in N_2^{2+}, but that the bond order is equal to that of the C-C bond in dicarbon, which the data suggests is a quadruple bond, and thus giving a basis for comparison.

7 Appendices

7.1 FORTRAN program for printing ghost atom co-ordinates along bonds.

```
      program bondvector
      double precision PF(1,3),PI(1,3),x,y,z,REF(1,3),length,step
      double precision refcoeff,nsteps,GhostPos(1,3)
      integer AI,AF,i,isteps
      Character*1 runup,impale,main,char0,BrI
      Character*2 A,NProc,mem,charge,spin,specbasis
      Character*50 input, output, output2, output3,title,method,basis
      Character*50 mandb,cands,atoms

      nsteps=40. !Input as real
      isteps=40 !Input as integer
      input="input"
      output="output"
      AI=1
      AF=11
      NProc='2'
      mem='2Gb'
      title='test'
      method='HF'
      basis='Gen Pseudo=Read'
      charge='0'
      spin='1'

      open(unit=3,file=output,status='new')

      open(unit=2,file=input)
      i=0
      char0='0'
      do while(.true.)
         read(2,*,end=10)A,x,y,z
         i=i+1
         if (i.eq.AI) then
            PI(1,1)=x
            PI(1,2)=y
            PI(1,3)=z
            print *, 'Atom selected: ',A
         end if
         if (i.eq.AF) then
            PF(1,1)=x
            PF(1,2)=y
            PF(1,3)=z
            print *, 'Atom selected: ',A
         end if
       end do
10     close(2)
```

```
      print *, 'initial number of atoms: ',i

      open(2,file=input,status='old')

      write(3, *) '%NProc=',trim(NProc)
      write(3, *) '%mem=',trim(mem),'Gb'
      mandb=trim(method)//'/'//basis
      write(3, *) '#',mandb
      write(3, *) '#NMR SCF(Tight)'
      write(3, *)
      write(3, *) title
      write(3, *)
      cands=charge//' '//spin
      write(3, *) cands

      do while (.true.)
         read(2,*,end=20)A,x,y,z
         write(3, 15)A,x,y,z
15       format(a2,3F10.6)
      end do
20    close(2)

      print *, 'initial position: ',PI
      print *, 'final position: ',PF

      do i=1,3
         REF(1,i)=PF(1,i)-PI(1,i)
      end do

     print *, 'reference vector defined as: ',REF

      length=sqrt((REF(1,1)*REF(1,1))+(REF(1,2)*REF(1,2))+(REF(1,3)*
     . REF(1,3)))

     print *, 'calculated bond length: ',length
     print *, 'number of steps requested: ',nsteps

     step=length/nsteps

     print *, 'Step size along bond (Angstroms): ',step

     refcoeff=1./nsteps

     print *, 'reference vector coefficient: ',refcoeff
     print *, 'Begin line before nucleus of start atom? (Y/N)'
     read(*,*) runup
     print *, 'Continue line though nucleus of final atom? (Y/N)'
     read(*,*) impale
     print *, 'include main bond? (Y/N)'
     read(*,*) main
     print *, 'printing ghost atoms... '
```

7.1 FORTRAN program for printing ghost atom co-ordinates along bonds.

```
      if ((runup.eq."Y").and.(impale.eq."Y").and.(main.eq."Y")) then
      go to 100
      end if

      if ((runup.eq."N").and.(impale.eq."Y").and.(main.eq."Y")) then
      go to 200
      end if

      if ((runup.eq."Y").and.(impale.eq."N").and.(main.eq."Y")) then
      go to 300
      end if

      if ((runup.eq."N").and.(impale.eq."N").and.(main.eq."Y")) then
      go to 400
      end if

      if ((runup.eq."Y").and.(impale.eq."Y").and.(main.eq."N")) then
      go to 500
      end if

      if ((runup.eq."N").and.(impale.eq."N").and.(main.eq."N")) then
      go to 600
      end if

      if ((runup.eq."Y").and.(impale.eq."N").and.(main.eq."N")) then
      go to 700
      end if

      if ((runup.eq."N").and.(impale.eq."Y").and.(main.eq."N")) then
      go to 800
      end if

  100 do i=isteps,0,-1
         do j=1,3
            GhostPos(1,j)=(PI(1,j)-(REF(1,j)))+(REF(1,j)*refcoeff*i)
         end do
         write(3, '(''Bq '' 3F10.6)')GhostPos
      end do
      do i=1,isteps
         do j=1,3
            GhostPos(1,j)=PI(1,j)+(REF(1,j)*refcoeff*i)
         enddo
         write(3, '(''Bq '' 3F10.6)')GhostPos
      end do
      do i=1,isteps
         do j=1,3
            GhostPos(1,j)=PF(1,j)+(REF(1,j)*refcoeff*i)
         enddo
         write(3, '(''Bq '' 3F10.6)')GhostPos
      end do
      go to 1000
```

```
200  do i=1,isteps
        do j=1,3
           GhostPos(1,j)=PI(1,j)+(REF(1,j)*refcoeff*i)
        enddo
        write(3, '(''Bq '' 3F10.6)')GhostPos
     end do
     do i=1,isteps
        do j=1,3
           GhostPos(1,j)=PF(1,j)+(REF(1,j)*refcoeff*i)
        enddo
        write(3, '(''Bq '' 3F10.6)')GhostPos
     end do

     go to 1000

300  do i=1,isteps
        do j=1,3
           GhostPos(1,j)=PI(1,j)-(REF(1,j)*refcoeff*i)
        end do
        write(3, '(''Bq '' 3F10.6)')GhostPos
     end do
     do i=1,isteps
        do j=1,3
           GhostPos(1,j)=PI(1,j)+(REF(1,j)*refcoeff*i)
        enddo
        write(3, '(''Bq '' 3F10.6)')GhostPos
     end do

     go to 1000

400  do i=1,isteps
        do j=1,3
           GhostPos(1,j)=PI(1,j)+(REF(1,j)*refcoeff*i)
        enddo
        write(3, '(''Bq '' 3F10.6)')GhostPos
     end do

     go to 1000

500  do i=isteps,1,-1
        do j=1,3
           GhostPos(1,j)=PI(1,j)-(REF(1,j)*refcoeff*i)
        end do
        write(3, '(''Bq '' 3F10.6)')GhostPos
     end do
     do i=1,isteps
        do j=1,3
           GhostPos(1,j)=PF(1,j)+(REF(1,j)*refcoeff*i)
        enddo
        write(3, '(''Bq '' 3F10.6)')GhostPos
     end do
```

7.1 FORTRAN program for printing ghost atom co-ordinates along bonds.

```
      go to 1000

600   print *, 'Well, that was a waste of time...'
      close(3)
      go to 1000

700   do i=0,isteps
         do j=1,3
            GhostPos(1,j)=(PI(1,j)-(REF(1,j)))+(REF(1,j)*refcoeff*i)
         end do
         write(3, '(''Bq '' 3F10.6)')GhostPos
      end do

      go to 1000

800   do i=1,isteps
         do j=1,3
            GhostPos(1,j)=PF(1,j)+(REF(1,j)*refcoeff*i)
         enddo
         write(3, '(''Bq '' 3F10.6)')GhostPos
      end do

      go to 1000

      open (unit=3,file=output,status='old')

1000  continue
      print *, 'Done'
      print *, 'write cc-pvdz-PP basis for Br/I to file? (Y/N)'
      read (*,*) BrI
      if (BrI.eq."Y") then
      go to 2000
      end if

      write (3, *)
      write (3, '(''!'')')
      close(3)
      print *, 'No special basis printed'
      go to 10000

2000  print *, 'Which? (Br/I)'
      read (*, *)specbasis

      if (specbasis.eq."Br") then
      write (3, *)
      print *, 'Other atoms present? (input format example: "C H O")'
      read (*, *) atoms
      write(3, *) trim(atoms)//' '//char0
      write(3, '(''cc-pvdz'')')
      print *, 'Writing Br cc-pVDZ-PP to file...'
      write (3, '(''****'')')
```

```
write (3, '(''Br   0 '')')
write (3, '(''S 6   1.00'')')
write (3, '('' 2808.6000000           0.0016060  '')')
write (3, '('' 421.1800000            0.0083930  '')')
write (3, '('' 50.3457000             0.0695780  '')')
write (3, '('' 17.9133000            -0.3899080  '')')
write (3, '('' 3.8053100              0.6944970  '')')
write (3, '('' 1.7496800              0.4913540  '')')
write (3, '(''S 6   1.00    '')')
write (3, '('' 2808.6000000          -0.0006350  '')')
write (3, '('' 421.1800000           -0.0034920  '')')
write (3, '('' 50.3457000            -0.0251950  '')')
write (3, '('' 17.9133000             0.1501130  '')')
write (3, '('' 3.8053100             -0.3662260  '')')
write (3, '('' 1.7496800             -0.3834220  '')')
write (3, '(''S 1   1.00    '')')
write (3, '('' 0.4485550              1.0000000  '')')
write (3, '(''S 1   1.00    '')')
write (3, '('' 0.1644980              1.0000000  '')')
write (3, '(''P 6   1.00    '')')
write (3, '('' 105.7520000            0.0053410  '')')
write (3, '('' 27.6368000            -0.0830840  '')')
write (3, '('' 6.5965600              0.4477660  '')')
write (3, '('' 2.7852200              0.5506170  '')')
write (3, '('' 1.0781200              0.1235000  '')')
write (3, '('' 0.3935370             -0.0037710  '')')
write (3, '(''P 6   1.00    '')')
write (3, '('' 105.7520000           -0.0013080  '')')
write (3, '('' 27.6368000             0.0229210  '')')
write (3, '('' 6.5965600             -0.1450290  '')')
write (3, '('' 2.7852200             -0.2090370  '')')
write (3, '('' 1.0781200              0.0937300  '')')
write (3, '('' 0.3935370              0.6050210  '')')
write (3, '(''P 1   1.00    '')')
write (3, '('' 0.1274690              1.0000000  '')')
write (3, '(''D 6   1.00    '')')
write (3, '('' 143.8650000            0.0102370  '')')
write (3, '('' 46.1163000             0.0760830  '')')
write (3, '('' 17.3694000             0.2298070  '')')
write (3, '('' 6.9510700              0.4033470  '')')
write (3, '('' 2.7560700              0.4097280  '')')
write (3, '('' 1.0117800              0.1627900  '')')
write (3, '(''D 1   1.00    '')')
write (3, '('' 0.4291000              1.0000000  '')')
write (3, '(''****       '')')
write (3, '('' '')')
write (3, '(''BR   0        '')')
write (3, '(''BR-ECP   4    10      '')')
write (3, '(''g-ul potential '')')
write (3, '('' 1        '')')
write (3, '(''2    1.0000000           0.0000000 '')')
write (3, '(''s-ul potential '')')
```

7.1 FORTRAN program for printing ghost atom co-ordinates along bonds.

```
write (3, '('' 3        '')')
write (3, '(''2   70.0242570          49.9628340 '')')
write (3, '(''2   31.1784120         370.0142050 '')')
write (3, '(''2    7.1565930          10.2414390 '')')
write (3, '(''p-ul potential    '')')
write (3, '('' 4         '')')
write (3, '(''2   46.7734710          99.1122440 '')')
write (3, '(''2   46.1841200         198.2530460 '')')
write (3, '(''2   21.7138580          28.2617400 '')')
write (3, '(''2   20.9417920          56.6233660 '')')
write (3, '(''d-ul potential    '')')
write (3, '('' 6        '')')
write (3, '(''2   50.6988390         -18.6058530 '')')
write (3, '(''2   50.6447640         -27.9232800 '')')
write (3, '(''2   15.4475090          -0.3796930 '')')
write (3, '(''2   15.5002590          -0.7805830 '')')
write (3, '(''2    2.8003910           0.0359680 '')')
write (3, '(''2    1.0774800           0.0943970 '')')
write (3, '(''f-ul potential'')')
write (3, '('' 2'')')
write (3, '(''2   14.4656060          -1.0912690 '')')
write (3, '(''2   21.2340650          -2.8876910 '')')
write (3, *)
write (3, *) '!'
write (3, *)
Close(3)
print *, 'Done'
go to 10000
end if

if (specbasis.eq."I") then
write (3, *)
print *, 'What other atoms are present?'
read (*, *) atoms
write(3, *) trim(atoms)//' '//char0
write(3, '(''cc-pvdz'')')
print *, 'Writing I cc-pVDZ-PP to file...'
write (3, '(''****    '')')
write (3, '(''I   0        '')')
write (3, '(''S 6   1.00    '')')
write (3, '('' 2.449790E+03        4.190000E-04  '')')
write (3, '('' 3.598080E+02        2.240000E-03  '')')
write (3, '('' 1.440580E+01        3.972230E-01  '')')
write (3, '('' 9.076320E+00       -9.322490E-01  '')')
write (3, '('' 2.088100E+00        9.371380E-01  '')')
write (3, '('' 1.034980E+00        3.920860E-01  '')')
write (3, '(''S 6   1.00      '')')
write (3, '('' 2.449790E+03        1.750000E-04  '')')
write (3, '('' 3.598080E+02        1.057000E-03  '')')
write (3, '('' 1.440580E+01        1.690000E-01  '')')
write (3, '('' 9.076320E+00       -4.217930E-01  '')')
write (3, '('' 2.088100E+00        6.388640E-01  '')')
```

```
write (3, '('' 1.034980E+00 3.201150E-01 '')')
write (3, '(''S 1 1.00 '')')
write (3, '('' 3.162840E-01 1.0000000 '')')
write (3, '(''S 1 1.00 '')')
write (3, '('' 1.217190E-01 1.0000000 '')')
write (3, '(''P 5 1.00 '')')
write (3, '('' 1.953010E+01 5.893400E-02 '')')
write (3, '('' 1.108820E+01 -2.309300E-01 '')')
write (3, '('' 2.715630E+00 6.648010E-01 '')')
write (3, '('' 1.204300E+00 4.506730E-01 '')')
write (3, '('' 3.399450E-01 2.898000E-02 '')')
write (3, '(''P 5 1.00 '')')
write (3, '('' 1.953010E+01 -1.883600E-02 '')')
write (3, '('' 1.108820E+01 8.000600E-02 '')')
write (3, '('' 2.715630E+00 -3.066520E-01 '')')
write (3, '('' 1.204300E+00 -1.475940E-01 '')')
write (3, '('' 3.399450E-01 6.075060E-01 '')')
write (3, '(''P 1 1.00 '')')
write (3, '('' 1.108810E-01 1.0000000 '')')
write (3, '(''D 5 1.00 '')')
write (3, '('' 4.547650E+01 4.266000E-03 '')')
write (3, '('' 1.319280E+01 -1.362500E-02 '')')
write (3, '('' 4.227410E+00 3.097560E-01 '')')
write (3, '('' 1.942800E+00 5.097720E-01 '')')
write (3, '('' 8.397710E-01 2.974610E-01 '')')
write (3, '(''D 1 1.00 '')')
write (3, '('' 3.000000E-01 1.0000000 '')')
write (3, '(''**** '')')
write (3, '('' '')')
write (3, '(''I 0 '')')
write (3, '(''I-ECP 4 28 '')')
write (3, '(''g-ul potential '')')
write (3, '('' 1 '')')
write (3, '(''2 1.00000000 0.00000000 '')')
write (3, '(''s-ul potential '')')
write (3, '('' 3 '')')
write (3, '(''2 40.03337600 49.98964900 '')')
write (3, '(''2 17.30057600 281.00655600 '')')
write (3, '(''2 8.85172000 61.41673900 '')')
write (3, '(''p-ul potential '')')
write (3, '('' 4 '')')
write (3, '(''2 15.72014100 67.41623900 '')')
write (3, '(''2 15.20822200 134.80769600 '')')
write (3, '(''2 8.29418600 14.56654800 '')')
write (3, '(''2 7.75394900 28.96842200 '')')
write (3, '(''d-ul potential '')')
write (3, '('' 4 '')')
write (3, '(''2 13.81775100 35.53875600 '')')
write (3, '(''2 13.58780500 53.33975900 '')')
write (3, '(''2 6.94763000 9.71646600 '')')
write (3, '(''2 6.96009900 14.97750000 '')')
write (3, '(''f-ul potential '')')
```

```
      write (3, '('' 4          '')')
      write (3, '(''2   18.52295000         -20.17661800   '')')
      write (3, '(''2   18.25103500         -26.08807700   '')')
      write (3, '(''2    7.55790100          -0.22043400   '')')
      write (3, '(''2    7.59740400          -0.22164600   '')')
      write (3, *)
      write (3, *) '!'
      write (3, *)
      Close(3)
      print *, 'Done'
      go to 10000
      end if

10000 STOP
      end program bondvector
```

7.2 Supporting Data: Bond length Changes on Solvation of R-Mg-X

Table 2: Internuclear distances for C-Mg and Mg-X for all method/basis set combinations in the unsolvated species, where X=Cl, Br and I.

X=Cl				
Basis set:	LANL2DZ		cc-pVDZ(-PP)	
	C-Mg (Å)	Mg-X (Å)	C-Mg (Å)	Mg-X (Å)
B3LYP	2.06519	2.26187	2.07736	2.21629
B3LYP-D3	2.06331	2.26053	2.07527	2.21508
MP2	2.09322	2.26042	2.08952	2.21443
X=Br				
Basis set:	LANL2DZ		cc-pVDZ(-PP)	
	C-Mg (Å)	Mg-X (Å)	C-Mg (Å)	Mg-X (Å)
B3LYP	2.06791	2.42960	2.07869	2.36547
B3LYP-D3	2.06589	2.42768	2.07640	2.36375
MP2	2.09450	2.42420	2.09044	2.35752
X=I				
Basis set:	LANL2DZ		cc-pVDZ(-PP)	
	C-Mg (Å)	Mg-X (Å)	C-Mg (Å)	Mg-X (Å)
B3LYP	2.06917	2.62469	2.07987	2.57916
B3LYP-D3	2.06695	2.62184	2.07740	2.57662
MP2	2.09485	2.62049	2.09148	2.57538

Table 3: Internuclear distances for C-Mg, Mg-X and Mg-O for all method and basis set combinations, where X=Cl, Br and I in species solvated by DME

X=Cl								
Basis:	LANL2DZ				cc-pVDZ(-PP)			
	C-Mg (Å)	Mg-X (Å)	Mg-O (Å)	Mg-O (Å)	C-Mg (Å)	Mg-X (Å)	Mg-O (Å)	Mg-O (Å)
B3LYP	2.12055	2.36644	2.07687	2.07687	-	-	-	-
B3LYP-D3	-	-	-	-	2.11326	2.30405	2.10626	2.10626
MP2	2.14401	2.35426	2.09238	2.09011	2.13263	2.29569	2.12182	2.12182
X=Br								
Basis:	LANL2DZ				cc-pVDZ(-PP)			
	C-Mg (Å)	Mg-X (Å)	Mg-O (Å)	Mg-O (Å)	C-Mg (Å)	Mg-X (Å)	Mg-O (Å)	Mg-O (Å)
B3LYP	2.12035	2.55401	2.07763	2.07763	2.11889	2.47148	2.13557	2.13557
B3LYP-D3	-	-	-	-	-	-	-	-
MP2	2.14144	2.53276	2.08778	2.09016	2.13209	2.44895	2.12271	2.12271
X=I								
Basis:	LANL2DZ				cc-pVDZ(-PP)			
	C-Mg (Å)	Mg-X (Å)	Mg-O (Å)	Mg-O (Å)	C-Mg (Å)	Mg-X (Å)	Mg-O (Å)	Mg-O (Å)
B3LYP	2.11914	2.77235	2.07814	2.07814	2.11831	2.70310	2.13698	2.13698
B3LYP-D3	2.10697	2.75226	2.05091	2.04698	2.10435	2.68992	2.09632	2.11777
MP2	2.13945	2.74438	2.08885	2.08885	2.12457	2.68227	2.13014	2.11437

Table 4: Internuclear distances for C-Mg, Mg-X and Mg-O for all method and basis set combinations, where X=Cl, Br and I in species solvated by DEE.

X=Cl								
Basis:	LANL2DZ				cc-pVDZ(-PP)			
	C-Mg (Å)	Mg-X (Å)	Mg-O (Å)	Mg-O (Å)	C-Mg (Å)	Mg-X (Å)	Mg-O (Å)	Mg-O (Å)
B3LYP	2.11666	2.37061	2.08228	2.07187	2.11956	2.31139	2.13443	2.13098
B3LYP-D3	2.10699	2.35792	2.04107	2.03806	-	-	-	-
MP2	2.14210	2.35594	2.08366	2.07685	2.13011	2.29750	2.11443	2.12124
X=Br								
Basis:	LANL2DZ				cc-pVDZ(-PP)			
	C-Mg (Å)	Mg-X (Å)	Mg-O (Å)	Mg-O (Å)	C-Mg (Å)	Mg-X (Å)	Mg-O (Å)	Mg-O (Å)
B3LYP	2.11586	2.55885	2.08169	2.07081	2.11671	2.47439	2.12665	2.13326
B3LYP-D3	-	-	-	-	2.10863	2.46380	2.09917	2.09505
MP2	2.14189	2.53447	2.08323	2.07575	2.12917	2.44919	2.11267	2.10702
X=I								
Basis:	LANL2DZ				cc-pVDZ(-PP)			
	C-Mg (Å)	Mg-X (Å)	Mg-O (Å)	Mg-O (Å)	C-Mg (Å)	Mg-X (Å)	Mg-O (Å)	Mg-O (Å)
B3LYP	2.11395	2.77721	2.07295	2.06626	2.11546	2.70934	2.13489	2.12807
B3LYP-D3	2.10440	2.75427	2.04139	2.03489	-	-	-	-
MP2	-	-	-	-	-	-	-	-

7.3 Misc. Isotropic Shielding Surfaces for C_2, N_2, C_2H_2 ,C_2H_4, C_2^{2-} and N_2^{2+}

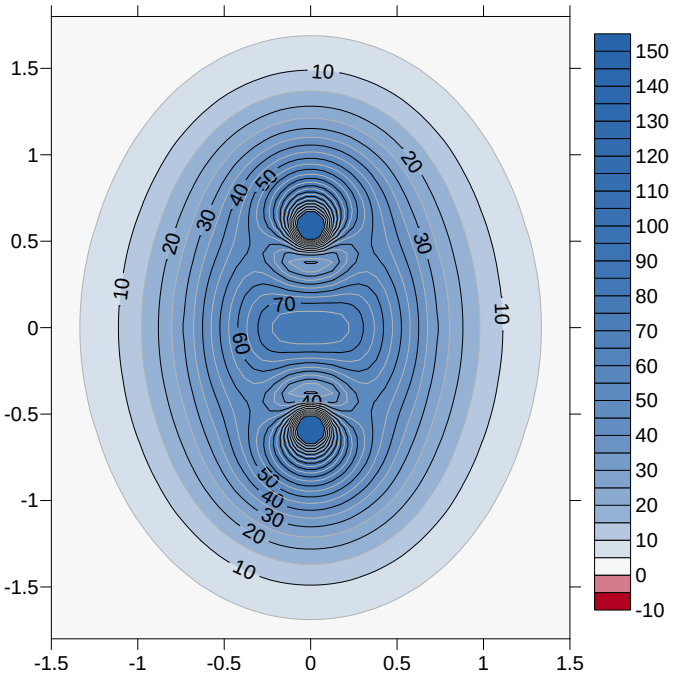

Figure 7.1: MP2 isotropic shielding (ppm) contour plot for dicarbon at the experimental bond length of dinitrogen (1.098 Å), in the molecular plane. Distances in Å.

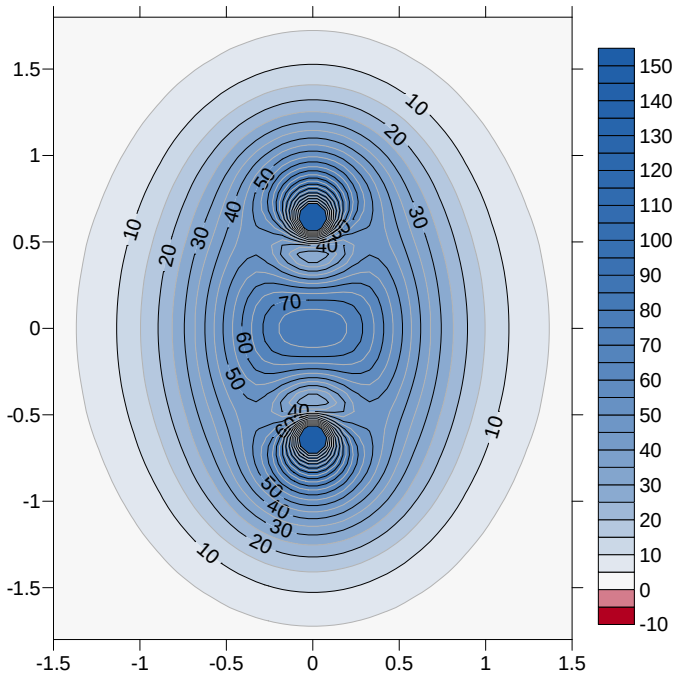

Figure 7.2: MP2 isotropic shielding (ppm) contour plot for dicarbon at the experimental bond length of acetylene (1.203 Å), in the molecular plane. Distances in Å.

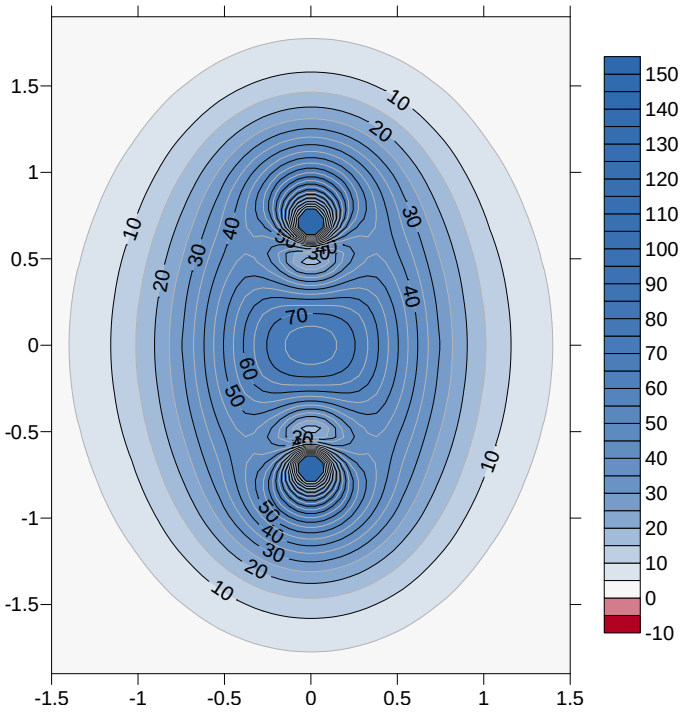

Figure 7.3: MP2 isotropic shielding (ppm) contour plot for dicarbon at the experimental bond length of ethene (1.339 Å), in the molecular plane. Distances in Å.

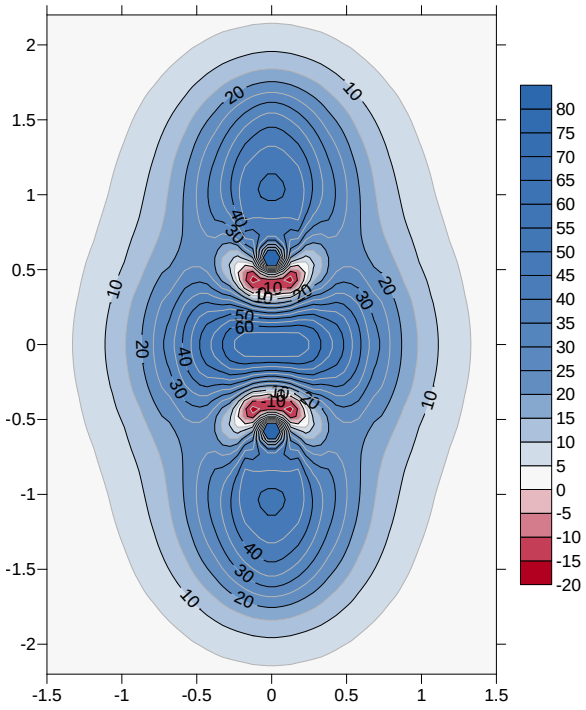

Figure 7.4: MP2 isotropic shielding (ppm) contour plot for acetylene at the experimental bond length of dinitrogen (1.098 Å), in the molecular plane. Distances in Å.

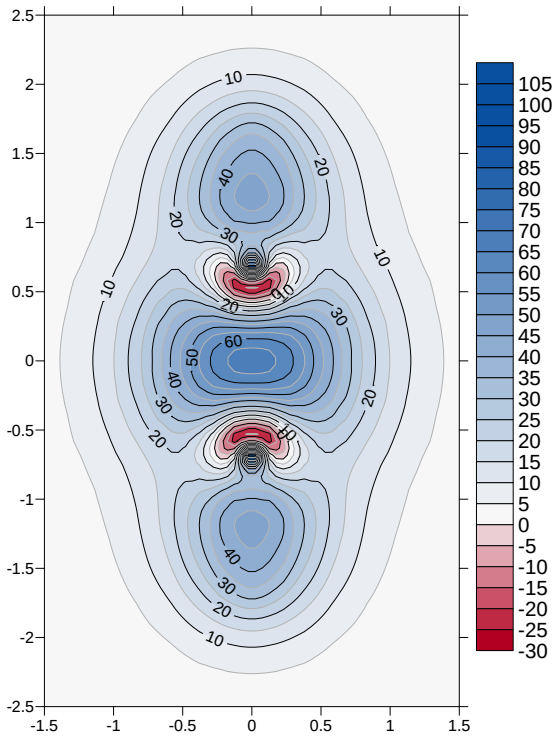

Figure 7.5: MP2 isotropic shielding (ppm) contour plot for acetylene at the experimental bond length of ethene (1.339 Å), in the molecular plane. Distances in Å.

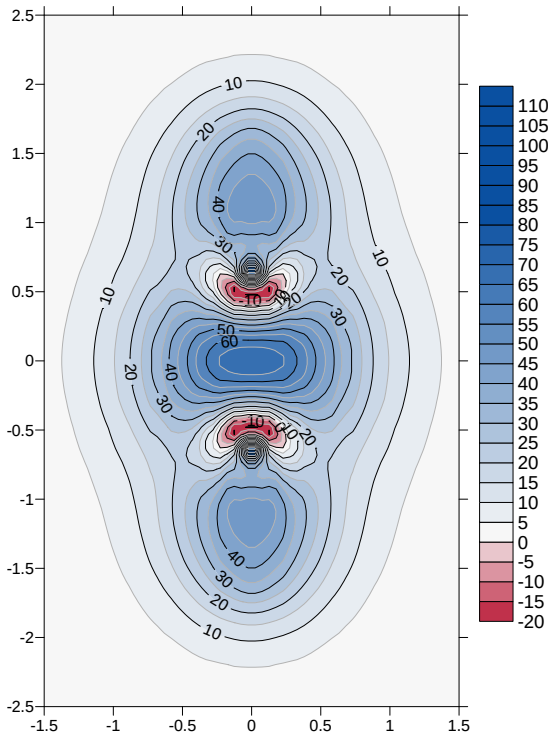

Figure 7.6: MP2 isotropic shielding (ppm) contour plot for acetylene at the experimental bond length of dicarbon (1.2425 Å), in the molecular plane. Distances in Å.

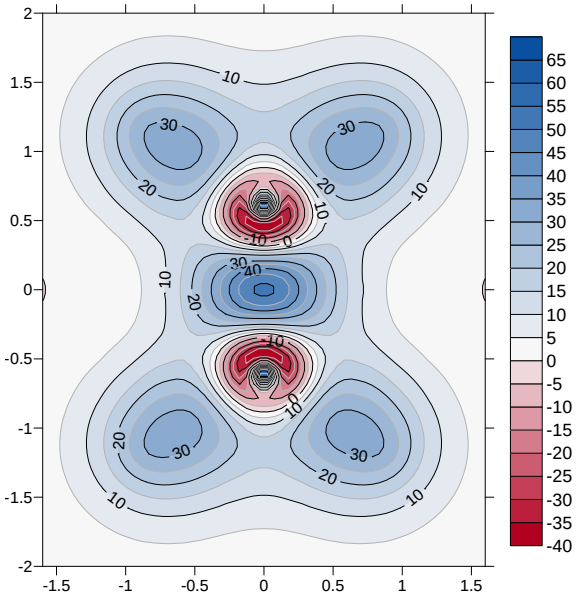

Figure 7.7: MP2 isotropic shielding (ppm) contour plot for acetylene at the experimental bond length of dicarbon (1.203 Å), in the molecular plane. Distances in Å.

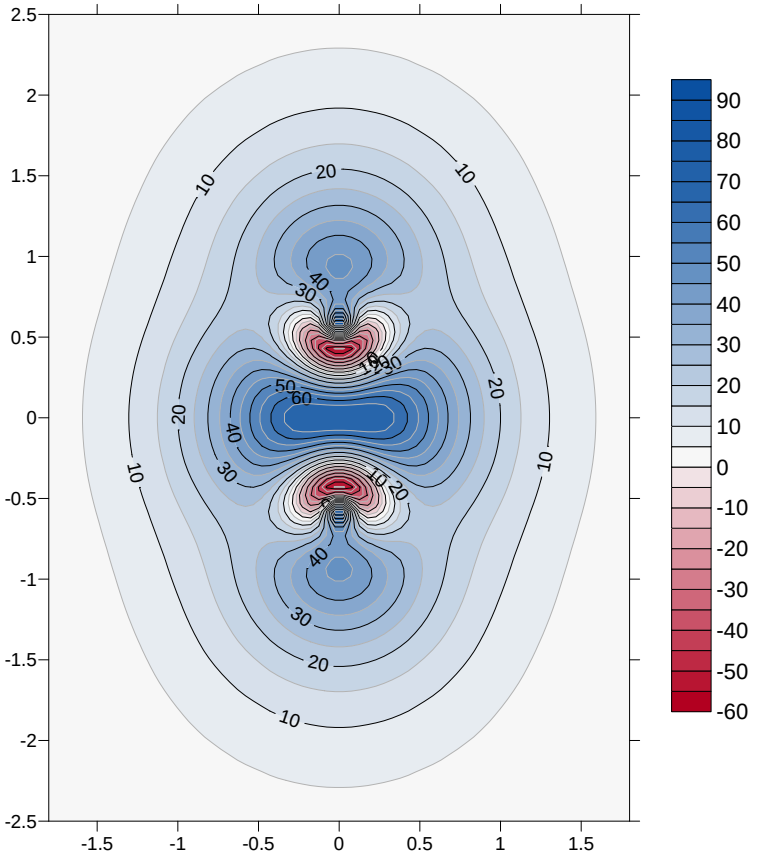

Figure 7.8: MP2 isotropic shielding (ppm) contour plot for C_2^{2-} at the experimental bond length of dinitrogen (1.098 Å), in the molecular plane. Distances in Å.

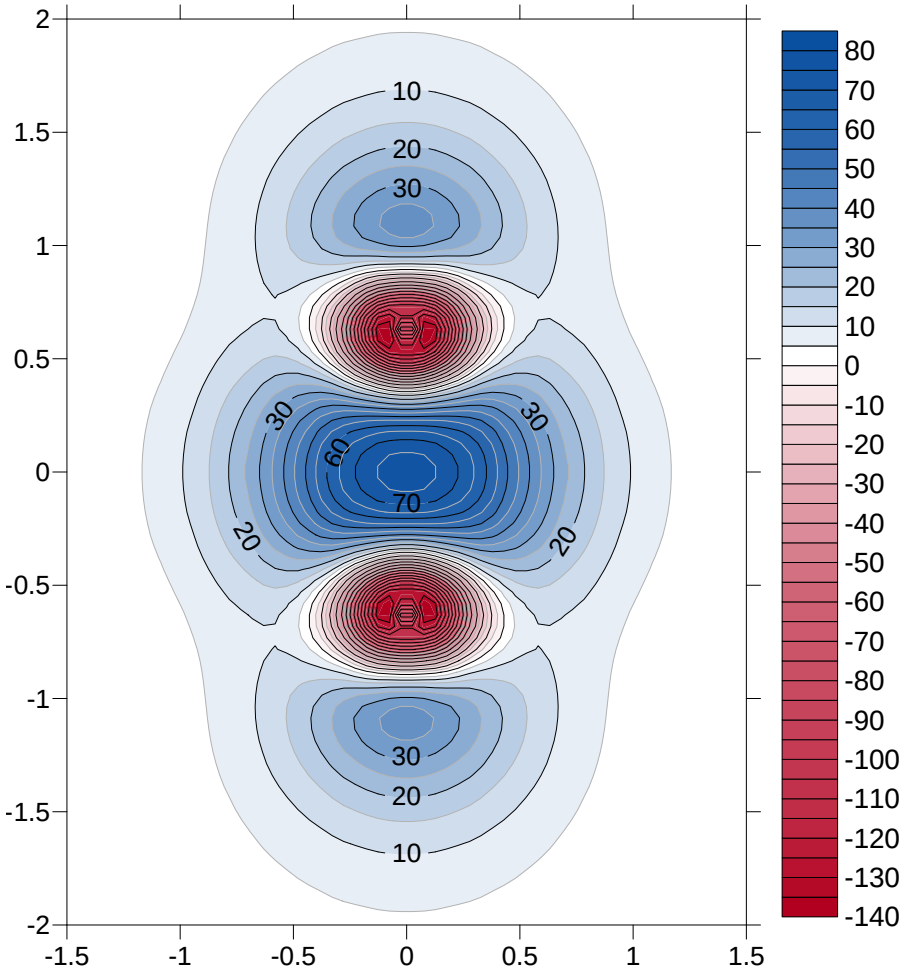

Figure 7.9: MP2 isotropic shielding (ppm) contour plot for dinitrogen at the experimental bond length of dicarbon (1.2425 Å), in the molecular plane. Distances in Å.

8 Bibliography

[1] Grignard V. Sur quelques nouvelles combinaisons organometalliques du magnésium et leur application à des synthèses dalcools et dhydrocarbures. CR Acad Sci Paris. 1900;130:1322–1324.

[2] Walborsky HM, Aronoff M. Cyclopropanes: XXXII. The mechanism of Grignard formation. Journal of Organometallic Chemistry. 1973;51:31–53.

[3] Garst JF, Swift BL. Mechanism of Grignard reagent formation. Comparisons of D-model calculations with experimental product yields. Journal of the American Chemical Society. 1989;111(1):241–250.

[4] Walborsky H, Young A. Cyclopropanes. XVI. An optically active Grignard reagent and the mechanism of Grignard formation. Journal of the American Chemical Society. 1964;86(16):3288–3296.

[5] Rachon J, Walborsky H. Mechanism of grignard reagent formation. Further evidence for the surface nature of the reaction. Tetrahedron letters. 1989;30(52):7345–7348.

[6] Garst JF, Soriaga MP. Grignard reagent formation. Coordination chemistry reviews. 2004;248(7):623–652.

[7] Porsev V, Barsukov YV, Tulub A. Systematic quantum chemical research of the reaction of magnesium clusters with organic halides. Computational and Theoretical Chemistry. 2012;995:55–65.

[8] Porsev V, Tulub A. Cluster quantum-chemical study of Grignard reagent formation. Doklady Physical Chemistry. 2006;409(2):237–241.

[9] Porsev V, Tulub A. Generation of radicals in Grignard reagent formation in the framework of the cluster model. Doklady Physical Chemistry. 2008;419(1):53–58.

[10] Chen ZN, Fu G, Xu X. Theoretical studies on Grignard reagent formation: radical mechanism versus non-radical mechanism. Organic & biomolecular chemistry. 2012;10(47):9491–9500.

[11] Frenking G. Building a quintuple bond. Science. 2005;310(5749):796–797.

[12] Gagliardi L, Roos BO. Quantum chemical calculations show that the uranium molecule U2 has a quintuple bond. Nature. 2005;433(7028):848–851.

[13] Xu B, Li QS, Xie Y, King RB, Schaefer III HF. Metal- Metal Quintuple and Sextuple Bonding in Bent Dimetallocenes of the Third Row Transition Metals. Journal of chemical theory and computation. 2010;6(3):735–746.

[14] Fischer RC, Power PP. π-Bonding and the lone pair effect in multiple bonds involving heavier main group elements: developments in the new millennium. Chemical reviews. 2010;110(7):3877–3923.

[15] de Sousa DWO, Nascimento MAC. Is There a Quadruple Bond in C2? Journal of chemical theory and computation. 2016;12(5):2234–2241.

[16] Xu LT, Dunning Jr TH. Insights into the perplexing nature of the bonding in C2 from generalized valence bond calculations. Journal of chemical theory and computation. 2013;10(1):195–201.

[17] Shaik S, Danovich D, Wu W, Su P, Rzepa HS, Hiberty PC. Quadruple bonding in C2 and analogous eight-valence electron species. Nature chemistry. 2012;4(3):195–200.

[18] Su P, Wu J, Gu J, Wu W, Shaik S, Hiberty PC. Bonding conundrums in the C2 molecule: A valence bond study. Journal of chemical theory and computation. 2010;7(1):121–130.

[19] von RaguéSchleyer P, Maslak P, Chandrasekhar J, Grev RS. Is a CC quadruple bond possible? Tetrahedron letters. 1993;34(40):6387–6390.

[20] Cooper DL, Penotti FE, Ponec R. Why is the bond multiplicity in C 2 so elusive? Computational and Theoretical Chemistry. 2015;1053:189–194.

[21] Matxain JM, Ruipérez F, Infante I, Lopez X, Ugalde JM, Merino G, et al. Communication: Chemical bonding in carbon dimer isovalent series from the natural orbital functional theory perspective. The Journal of chemical physics. 2013;138(15):151102.

[22] Hay PJ, Hunt WJ, Goddard III WA. Generalized valence bond description of simple alkanes, ethylene, and acetylene. Journal of the American Chemical Society. 1972;94(24):8293–8301.

[23] Johnson Jr C, Bovey F. Calculation of nuclear magnetic resonance spectra of aromatic hydrocarbons. The Journal of Chemical Physics. 1958;29(5):1012–1014.

[24] Schleyer PvR, Maerker C, Dransfeld A, Jiao H, Hommes NJvE. Nucleus-independent chemical shifts: a simple and efficient aromaticity probe. Journal of the American Chemical Society. 1996;118(26):6317–6318.

[25] von Ragué Schleyer P, Manoharan M, Wang ZX, Kiran B, Jiao H, Puchta R, et al. Dissected nucleus-independent chemical shift analysis of π-aromaticity and antiaromaticity. Organic letters. 2001;3(16):2465–2468.

[26] Steiner E, Fowler PW, Jenneskens LW. Counter-Rotating Ring Currents in Coronene and Corannulene. Angewandte Chemie International Edition. 2001;40(2):362–366.

[27] Wolinski K. Magnetic shielding surface in molecules. Neutron as a probe in the hypothetical magnetic resonance spectroscopy. The Journal of chemical physics. 1997;106(14):6061–6067.

[28] Kleinpeter E, Klod S, Koch A. Visualization of through space NMR shieldings of aromatic and anti-aromatic molecules and a simple means to compare and estimate aromaticity. Journal of Molecular Structure: THEOCHEM. 2007;811(1):45–60.

[29] Kleinpeter E, Koch A. Are lithium and sodium salts of N-(2-hydroxyphenyl)-salicylaldimine aromatic metalla-hetero [10] annulenes? An answer given by spatial magnetic properties (through space NMR shieldingsTSNMRS). Physical Chemistry Chemical Physics. 2012;14(24):8742–8746.

[30] Kleinpeter E, Koch A. Antiaromaticity Proved by the Anisotropic Effect in 1H NMR Spectra. The Journal of Physical Chemistry A. 2012;116(23):5674–5680.

[31] Karadakov PB, Horner KE. Magnetic shielding in and around benzene and cyclobutadiene: a source of information about aromaticity, antiaromaticity, and chemical bonding. The Journal of Physical Chemistry A. 2013;117(2):518–523.

[32] Horner KE, Karadakov PB. Chemical bonding and aromaticity in furan, pyrrole, and thiophene: a magnetic shielding study. The Journal of organic chemistry. 2013;78(16):8037–8043.

[33] Horner KE, Karadakov PB. Shielding in and around Oxazole, Imidazole, and Thiazole: How Does the Second Heteroatom Affect Aromaticity and Bonding? The Journal of organic chemistry. 2015;80(14):7150–7157.

[34] Karadakov PB, Horner KE. Exploring Chemical Bonds through Variations in Magnetic Shielding. Journal of chemical theory and computation. 2016;12(2):558–563.

[35] Szabo A, Ostlund NS. Modern quantum chemistry: introduction to advanced electronic structure theory. Courier Corporation; 1989.

[36] Raimes S. Many-electron theory. 1972;.

[37] Helgaker T, Jorgensen P, Olsen J. Molecular electronic-structure theory. John Wiley & Sons; 2014.

[38] Dunning Jr TH. Gaussian basis sets for use in correlated molecular calculations. I. The atoms boron through neon and hydrogen. The Journal of chemical physics. 1989;90(2):1007–1023.

[39] Frisch MJ, Trucks GW, Schlegel HB, Scuseria GE, Robb MA, Cheeseman JR, et al.. Gaussian09 Revision E.01;. Gaussian Inc. Wallingford CT 2009.

[40] Davis SR. Ab initio study of the insertion reaction of magnesium into the carbon-halogen bond of fluoro-and chloromethane. Journal of the American Chemical Society. 1991;113(11):4145–4150.

[41] Garst JF, Lawrence KE, Batlaw R, Boone JR, Ungváry F. Magnesium bromide in Grignard reagent formation. Inorganica Chimica Acta. 1994;222(1):365–375.

[42] Garst JF, Ungváry F, Baxter JT. Definitive Evidence of Diffusing Radicals in Grignard Reagent Formation. Journal of the American Chemical Society. 1997;119(1):253–254.

[43] Jasien PG, Abbondondola JA. A quantum mechanical study of the reactivity of methyl chloride on magnesium clusters. Journal of Molecular Structure: THEOCHEM. 2004;671(1):111–118.

[44] Beals BJ, Bello ZI, Cuddihy KP, Healy EM, Koon-Church SE, Owens JM, et al. Absolute kinetic rate constants and activation energies for the formation of Grignard reagents. The Journal of Physical Chemistry A. 2002;106(3):498–503.

[45] Irikura KK. Experimental vibrational zero-point energies: Diatomic molecules. Journal of physical and chemical reference data. 2007;36(2):389–397.

[46] Graner G, Hirota E, Iijima T, Kuchitsu K, Ramsay D, Vogt J, et al.. Structure data of free polyatomic molecules. Basic data. Springer, Berlin; 1998.

[47] Herzberg G. Molecular spectra and molecular structure. Vol. 3: Electronic spectra and electronic structure of polyatomic molecules. New York: Van Nostrand, Reinhold, 1966. 1966;1.

[48] Huber KP. Molecular spectra and molecular structure: IV. Constants of diatomic molecules. Springer Science & Business Media; 2013.

[49] Carlotti M, Johns J, Trombetti A. The ν5 Fundamental Bands of N2H2 and N2D2. Canadian Journal of Physics. 1974;52(4):340–344.

[50] Grunenberg J. Quantum chemistry: Quadruply bonded carbon. Nature chemistry. 2012;4(3):154–155.